Functional Ionic Liquids and Related Porous Materials for Gas Capture and Catalysis

A Dissertation Presented for the

Doctor of Philosophy

Degree

The University of Tennessee, Knoxville

Nanqing Chen

May 2018

ACKNOWLEDGMENTS

First and foremost, I would like to express my sincere gratitude to my advisor, Dr. Sheng Dai, for his support, guidance, patience, motivation, enthusiasm and broad knowledge throughout my time at UTK. Besides my advisor, I would like to thank Dr. Pengfei Zhang for his academic help in my last year at UTK.

In addition, I would like to thank the rest of my thesis committee: Dr. Bin Zhao, Dr. Michael Douglas Best, and Dr. Robert M Counce, for their encouragement, insightful comments, and hard questions.

ABSTRACT

Ionic liquids are a class of promising materials that show potential as electrolytes, solvents, and absorbents. Designing and synthesizing task-specific ionic liquids for specific purposes are required for the further development of this technology. We designed and synthesized a series of functionalized ionic liquids for applications such as gas absorption, electrolyte, and catalysis. Guanidine-derived ionic liquids were successfully synthesized as an extension of our group's previous research. However, this ionic liquid showed no response towards CO_2. An amidine-functionalized ionic liquid was then designed. A new method, a modified Pinner reaction, was developed for the synthesis of amidines under basic conditions, side reactions were utterly avoided. An α-oximehydrazone zwitterion type ionic liquid was the ionic liquid that had an excellent activity towards CO_2. However, it suffers from a vital drawback that it decomposes during gas desorption process. Polymerized viologen-type ionic materials were discovered to have catalytic activities in selective oxidizing thioanisoles and benzoyl alcohols. The mechanism of this process is unclear so far. In this thesis, a non-ionic liquid project- "*A Linear Crystalline Porous Organic Polymer*" is discussed. So far, none of a polymer was found to have linearity, crystallinity and porosity three properties at the same time.

TABLE OF CONTENTS

1.Chapter 1 Introduction 1
1.1.Ionic liquids 2
1.2.Preparation of ionic liquids 4
1.3.Physical properties 5
1.3.1.Densities 5
1.3.2.Viscosities 6
1.3.3.Vapor pressures 6
1.3.4.Melting points 7
1.4.Chemical properties 7
1.5.Dissolution of metal oxides in ionic liquids 8
1.6.Task-specific ionic liquids 9
1.7.Catalysis 9
1.8.Support carrier for reactions 11
1.9.Magnetism and Luminescence 11
1.10.Analysis applications 12
1.11.Electrochemical applications 12
1.12.Gas adsorption 13
1.13.References 14
2.Chapter 2 Objectives and Motivations 17
2.1.Background 18
2.1.1.CO_2 catastrophe 19
2.1.2.Task-specific ionic liquids in capturing CO_2 20
2.2.Objectives and motivations 22
2.3.Project 1- α-oximehydrazone functionalized ionic liquid 23

2.4.Project 2- guanidine tethered ionic liquids 25
2.5.Project 3- amidine functionalized ionic liquids 27
2.6.Project 4- ultra-pure ionic liquid as electrolyte 29
2.7.Project 5- heterogenous viologen catalysts for metal-free and selective oxidations. 30
2.8.Project 6- mesoporous carbon derived from propargylic ionic liquids 32
2.9.Project 7- linear crystalline porous organic polymer 33
2.10.References 35
3.Chapter 3 α-Oximehydrazone Functionalized Ionic Liquid 36
3.1.Abstract 37
3.2.Introduction 37
3.3.Results and discussion 41
3.3.1.Oximehydrazone functionalized ionic liquid 41
3.4.Experimental 47
3.4.1.Chemicals and materials 47
3.5.Summary 50
3.6.Abbreviates 50
3.7.References 51
4.Chapter 4 Guanidine Tethered Ionic Liquids 52
4.1.Abstract 53
4.2.Introduction 53
4.3.Results and Discussions 54
4.4.Experimental 59
4.4.1.Chemicals and materials 59
4.5.Summary 67

4.6.Abbreviates..... 67
4.7.References..... 68
5.Chapter 5 Amidine Functionalized Ionic Liquids..... 69
5.1.Abstract..... 70
5.2.Introduction..... 70
5.2.1.Acidic strategy..... 73
5.2.2.Basic strategy..... 77
5.3.Experimental..... 77
5.3.1.Experiment chemicals and materials..... 77
5.4.Summary..... 80
5.5.Abbreviates..... 80
5.6.References..... 81
6.Chapter 6 Ultra-pure Ionic Liquid as An Electrolyte..... 82
6.1.Abstract..... 84
6.2.Introduction..... 84
6.3.Results and discussion..... 85
6.4.Experimental..... 98
6.4.1.Chemicals and materials..... 99
6.5.Summary..... 101
6.6.Abbreviations..... 101
6.7.References..... 103
7.Chapter 7 Heterogenous Viologen Catalysts for Metal-free and Selective Oxidations..... 104
7.1.Abstract..... 105
7.2.Introduction..... 105
7.3.Results and Discussion..... 109

7.4.Experiment 117
7.4.1.Chemicals and materials 117
7.5.Summary 120
7.6.References 122
8.Chapter 8 Mesoporous Carbon Derived from Propargylic Ionic Liquids……..124
8.1.Abstract 125
8.2.Introduction 125
8.3.Results and discussion 129
8.3.1.Carbon yields of TSILs 129
8.4.Experimental 135
8.4.1.Chemicals and materials 135
8.4.2.Ion exchange 138
8.5.Summary 139
8.6.Abbreviates 139
8.7.References 140
9.Chapter 9 Linear Crystalline Porous Organic Polymer 141
9.1.Abstract 142
9.2.Introduction 142
9.3.Results and discussion 146
9.4.Future work 151
9.5.Experimental 151
9.5.1.Chemicals and reagents 151
9.5.2.Synthesis of polyimine 151
9.6.Summary 154
9.7.Abbreviates 154

9.8.References 155
10.Chapter 10 Conclusions 157
10.1.α-Oximehydrazone Functionalized Ionic Liquid 157
10.2.Guanidine Tethered Ionic Liquids 157
10.3.Amidine Functionalized Ionic Liquids 158
10.4.Ultra-pure Ionic Liquid as Electrolyte 158
10.5.Heterogenous Viologen Catalysts for Metal-free and Selective Oxidations. 159
10.6.Mesoporous Carbon Derived from Propargylic Ionic Liquids 160
10.7.Linear Crystalline Porous Organic Polymer 160
10.8.References 162
11.Vita…… ……..……...163

LIST OF TABLES

Table 1.1 Melting points and onset points of some ionic liquids..... 8
Table 6.1 The carbon recovery after electrolysis carbon black in $CaCl_2$ at 1093 K. 92
Table 7.1 Selective oxidation of methyl phenyl sulfide by PINs-based catalysts. 110
Table 7.2 Selective oxidation of various sulfides by the PIN-1/H_2O_2 system. 114
Table 7.3 Selective oxidation of benzyl alcohols by PIN-1-Br/H_2O_2 system. 116
Table 8.1 Surface area and CO_2 uptake and fraction of micropore 133
Table 9.1 Surface area of Polymer. 147

LIST OF FIGURES

Figure 1.1 Common cations and anions. 3
Figure 1.2 Metal hybridized ionic liquids. 5
Figure 1.3 Phosphonium sulfonate. 11
Figure 2.1 Oximehydrazone functionalized ionic liquid. 23
Figure 2.2 Guanidine functionalized ionic liquids. 25
Figure 2.3 Amidine ionic liquid. 27
Figure 2.4 Structure of Pyr14TFSI 29
Figure 2.5 The viologen-type ionic liquid. 30
Figure 2.6 Polymeric ionic viologen. 31
Figure 2.7 Propargylic ionic liquids. 32
Figure 3.1 Oximehydrazone functionalized ionic liquid. 41
Figure 3.2 H^{1}-NMR of ILs and ILs-CO_2 abduct 43
Figure 3.3 C^{13}-NMR of ILs and ILs-CO_2 abduct 44
Figure 4.1 Target guanidine functionalized ionic liquids. 54
Figure 4.2 Single crystal structure of guanidine zwitterion. 57
Figure 4.3 Kugelrohr distillation. 57
Figure 5.1 a), NMR spectrum of **3** without any purification. b), the reaction of **2** after 60 hours. c), the reaction of **2** after 24 hours. d), starting material **1**. 75
Figure 6.1 Cycle voltammograms (CVs) at a scan rate of 10 mVs^{-1}. 86
Figure 6.2 Left amorphous carbon, Right graphite. 86
Figure 6.3 Thickness of graphite. 87
Figure 6.4 TEM of flake like graphite. 87

Figure 6.5 TGA curves of Carbon Black (CB), and graphitized carbon black. 88
Figure 6.6 XPS patterns of CB before and after a constant voltage at 2.6 V for 1 h and 2h. Reveal a deoxygenation process ... 88
Figure 6.7 SEM of graphitized carbon black. 88
Figure 6.8 SEM of Carbon Black (CB). 88
Figure 6.9 Raman- spectrum of graphitization process. 89
Figure 6.10 CVs of the molybdenum cavity electrode, and MCEs loaded with carbon black (CB) and graphite powder in $CaCl_2$ at 1093 K (20 mVs@1)..... 90
Figure 6.11 XRD patterns of CB after cathodic polarization at different potentials for the times indicated. 91
Figure 6.12 The 2nd CVs (10 mVs^{-1}). 93
Figure 6.13 Electrochemical performance of the commercial graphite in Pyr14TFSI. 94
Figure 6.14 Electrochemical performance of the EGN in Pyr14TFSI. 94
Figure 6.15 Electrochemical performance of the graphite powder in Pyr14TFSI. 94
Figure 6.16 Specific discharge capacity and coulombic efficiency during the long-term cycling. 95
Figure 6.17 The 150th CVs in Pyr14TFSI. 95
Figure 6.18 Rate performances. 95
Figure 6.19 SEM image of the commercial graphite nanosheet..... 96
Figure 6.20 Electrochemical window of the Pyr_{14}TFSI ionic liquid ... 97

Figure 6.21 The charge/discharge curves for between 2.25V and 5.25 V 97
Figure 6.22 Specific discharge capacities and coulombic efficiencies at 1800 mA while the upper limit charging potential is increased to 5.25 V after the rate performance tests. 97
Figure 7.1 Paraquat..... 107
Figure 7.2 Pictures of PIN-1 in the dark or UV conditions. 108
Figure 7.3 The conversion and selectivity vs. time plots for the oxidation by PIN-1/H_2O_2 at different temperatures. Reaction conditions: thioanisole 1 mmol, PIN-1 20 mg, 30%H_2O_2 2 mmol, 4mL CH_3CN, 30-60 ℃. Temperature dependence of the rate parameter in the Arrhenius coordinates for the PIN-1/H_2O_2 system. 112
Figure 8.1 TGA of Ionic Liquids. 129
Figure 8.2 IR Spectrum of ionic liquid before and after the heat at 300 ℃. 131
Figure 8.3 nitrogen sorption isotherms 131
Figure 8.4 SEM image of carbon. Top), BpHIm- Beti500. Bottom), BpMIm-Beti500. 134
Figure 9.1 Polymerization occurred in DMF solvent (1mmol 4,4'-(9-fluorenylidene)dianiline with 1mmol terephthalaldehyde per trial)..... 146
Figure 9.2 ^{1}H-NMR of the soluble polymer and terephthalaldehyde 149
Figure 9.3 FTIR of starting materials and polymer..... 149

Figure 9.4 XRD pattern of starting materials and non-soluble polymer. 149
Figure 9.5 SEM image of the polymer.....150
Figure 9.6 Single crystal structure of the model molecule..... 152

Chapter 1 Introduction

Ionic liquids

Ionic liquids are a kind of promising environmental-friendly materials with negligible vapor pressure, favorable recyclability and low to moderate liquidity. Another advantage is the stability at high temperature, and even in the existence of air.[1] Ionic liquids can be classified by terms of melting points or functions.

Being different to the “molten salts’’, ionic liquids have a much lower melting point. The melting points of ionic compounds are determined by the electrostatic potential that exists between cations and anions. For conventional inorganic salts such as NaCl, this electrostatic potential is high. An equation (Equation **1.1**) expresses the lattice energy, which is related to melting points of salts.

$$E = k\frac{Q2Q1}{d} \qquad \text{Equation } \mathbf{1.1}$$

In Equation **1.1**, *k* represents the Madelung constant, *Q*1 and *Q*2 are the charges of the cation and anion, respectively. *d* is the distance between charge centers. With a larger ion, the larger *d* could result in the small lattice energy and a low melting point. Ionic organic compounds with lower melting points below 100℃ are considered as ionic liquids. Figure **1.1** lists the most common types of ionic liquids. $[Et_3NH_3]$ $[NO_3]$ is believed to be the first room temperature ionic liquid, which was reported in 1914.[2]

Ionic liquids can be used as solvents for the dissolution of some materials such as cellulose,[3] chitin[4], etc. The excellent solubility of organic/inorganic compounds in ionic liquids and a wide range of ionic liquids as the liquid state make them good solvents for some reactions. Moreover, they showed competitive yields when compared with

conventional organic solvents.[5, 6] Thermodynamic parameters of these ionic liquids were investigated by chromatographic techniques.[7, 8] Generally speaking, ionic liquids could be considered to be polar solvents in terms of the ability of the salt to act as a hydrogen-bond acceptor or donor with the degree of delocalization of the charge on anions. Positive charges on ammonium and phosphonium salts do not delocalize, and this is a primary difference compared with aromatic ionic liquids such as pyridinium and imidazolium-based ionic liquids. Besides, it was investigated that the length of alkyl substituents on both cations and anions have an enormous impact on lipophilicities of ionic liquids. Ionic liquids with longer chains will perform better lipophilicities.[8, 9] Anions in ionic liquids can be fluorinated to avoid hydrogen bonding.[10] Ionic liquids are based on the various system, and the most widely studied are N'N-dialkylimidazolium, alkylammonium, alkylphosphonium, and N-alkylpyridinium (Figure **1.1**).

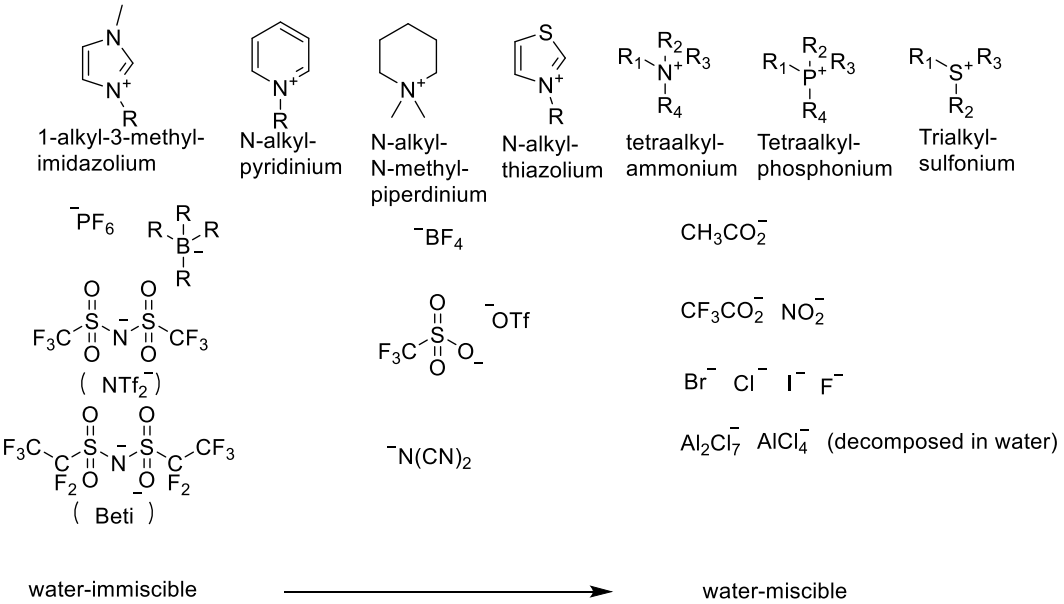

Figure 1.1 Common cations and anions.

Preparation of ionic liquids

Ionic liquids at least consist of one part of an organic ion. There are three basic methods for the synthesis of ionic liquids (Scheme **1.1**). One is displacement reaction of alkyl halides with corresponding nucleophiles such as N-alkylimidazole, pyridine, pyrrolidine, phosphine, or sulfide.

Typically, reactions with nucleophiles can be carried out neatly or in polar solvents such as acetone, acetonitrile, N'N-dimethylformamide, and alcohol. Nonpolar solvents such as petroleum ether, hexane, ethyl acetate rarely reported and are not favored.

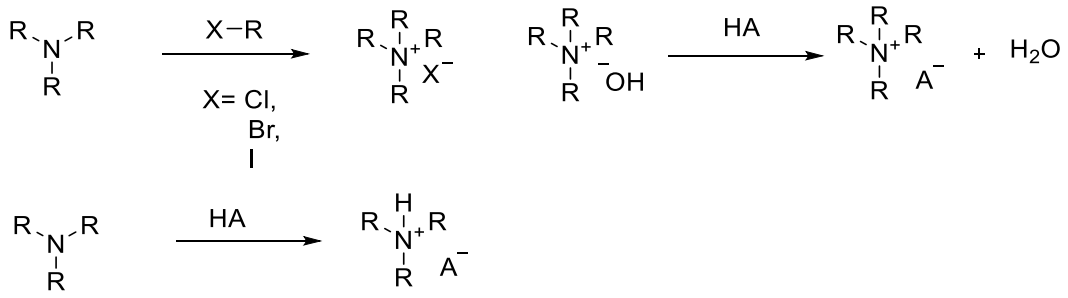

Scheme 1.1 Three synesthetic strategies for ionic liquids.

Another approach is ion metathesis method, which utilizes acid-base neutralization reaction or by mixing metal salts and organic salts. Monoalkylammoniums are readily prepared by mixing primary amines with nitric acid[11] or other acids. Tetraalkylammonium sulfate was reported by mixing tetraalkylammonium hydroxide and sulfonic acid.[7]

There is another family of ionic liquids consisting of a metal core such as halogenoaluminate(III),[12] halogenoironate(III),[13] halogenocuprate(I)

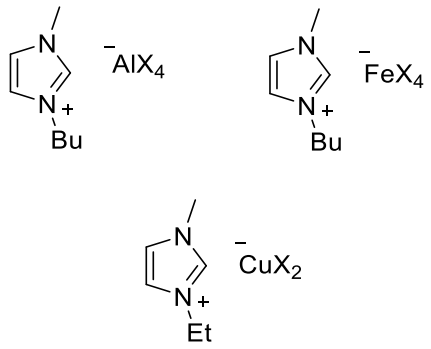

Figure 1.2 Metal hybridized ionic liquids.

(Figure **1.2**).[14] Applications of those metal hybridized ionic liquids have drawn much attention.[15, 16] They were made by mixing metal halides and the corresponding ionic liquids that bearing halide anions.

These metal hybridized ionic liquids exhibit excellent catalytic activities such as for aryl Grignard cross-coupling of alkyl halides,[13] oligomerization of butene.[17]

Physical properties

Densities

The length of alkyl chain slightly affects the density of the ionic liquids. The density decreases with an increasing chain length.[18]Anions also contribute to the densities following the order of DCA^- < SCN^- < TFA^-< TfO^- < SAC^- < NTf_2^- . This suggests that densities of the ionic liquids will increase with an increase in anion size.[19] As same as other

conventional solvents, the densities of ionic liquids decrease as temperature increase.[20]

Viscosities

An increase in chain length will result in an increase in viscosity because of the increased Van der Waals interaction.[20-23] Imidazoliums have lower viscosities than pyridiniums and pyrrolidiniums. Anions also affect the viscosities of ionic liquids. The viscosities of the imidazolium-based ionic liquids are increased in the order of NTf_2^-< $CF_3SO_3^-$< BF_4^- < $EtSO_4^-$< $MeSO_4^-$< PF_6^-< CH_3COO^-.[24] In the [C_nMIM] [NTf_2] type ionic liquids, an increase in the viscosity was found almost linearly as the function of the length of alkyl groups.[25] However, in ethylene glycol functionalized ionic liquids, an increase in chain length was accompanied by a decrease in viscosity was also observed.[26] The ionic liquids with alkoxy chains have lower viscosities than the alkyl chain with the same length.[27]

Vapor pressures

It is well known that ionic liquids have the negligible vapor pressures. However, this was proved not to be the case at lower pressure.[28] The vaporization of some thermal stable ionic liquids such as [$C_n$mim][NTf_2] was achieved by Kugelrohr distillation at 200-300℃. Some imidazolium-based ionic liquids were observed to evaporating as ion pairs, which indicated the Coulombic interaction was the primary interaction in the gas-phase ion pairs, and ionic liquids can be distilled without decomposition. The vapor pressures and vaporization enthalpies of ionic liquids were measured by a thermogravimetric

method,[29] ultraviolet absorption spectroscopy, [30] transpiration method,[31] and integral effusion Knudsen method.[32]

Melting points

The melting points of ionic liquids are not predictable. But by reducing the numbers of carbon in the alkyl chain will result in a lower melting point. Here is the table of the melting points of alkylmethylimidazoliums, which indicates a longer chain length will result in a lower melting point. Counter ions play an important role in melting points and even solubilities. Ionic liquids can be designed with the even lower melting point to room temperature. Ionic liquids bearing tetrafluoroborate (BF_4^-), hexafluorophosphate (PF_6^-), bis(trifluoromethylsulfonyl)imide (Tf_2N^-) and bis(pentafluoroethylthyl-sulfonyl) imide ($Beti^-$) show a weak solubility in water, which enables the metathesis method in making these water immiscible ionic liquids. However, halide residues can be detected after ion exchange; the halide residues might significantly affect the catalytic properties of ionic liquids. These water immiscible ionic liquids have drawn much attention from scientists because the bad solubility of these ionic liquids in water enables the biphasic separation.

Table 1.1 Melting points and onset points of some ionic liquids.

Salt	T_{mp} (℃)	T_{onset}
EMImCl	89	285
EMImBr	79	311
PMImCl	60	282
$EMImPF_6$	62	375
$PMImPF_6$	40	335
EMImBeti	-1	423
$EMImBF_4$	11	450

Chemical properties

Some ionic liquids are chemically stable in air and highly durable at high temperature. Table **1.1** shows the onset temperature (decomposition temperature) of some ionic liquids. By summarizing data from the table, the stabilities of ionic liquids can be ranked in the order of PF_6>Beti>BF_4>halogens. The decomposition behavior shows no difference in the presence of oxygen.[1] Imidazolium-based ionic liquids are not stable in the presence of strong base because of the acidity of the proton in position 2. This property also enables the capture of carbon dioxide in the presence of strong bases (Scheme **1.2**).

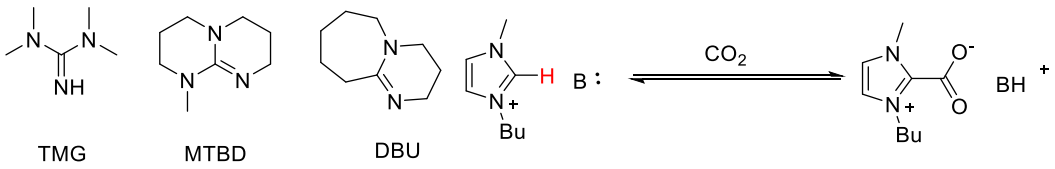

Scheme 1.2 Deprotonation of imidazolium occurs in position 2.

Dissolution of metal oxides in ionic liquids

Some functionalized ionic liquids such as the protonated betaine were designed to dissolve metal oxides. [Hbet][NTf_2] can dissolve the stoichiometric amount of metal oxides such as the rare earth metal oxide and uranium oxide.[33] The crystal structure shows that metal-ionic liquids complexes are dimers by coordinating with the zwitterionic

carboxylate group.[34.35] In hydrophobic ionic liquids, the Cs^+-18-crown-6 coordination was studied by utilizing NMR spectroscopy.[36]

Task-specific ionic liquids

Classified by functionalities, task-specific ionic liquids are another prominent group. The concept of task-specific ionic liquids was first proposed by Davis's group in 2002.[37] In their work, the utility of an amine functionalized ionic liquid in absorbing CO_2 was described. ^{13}C NMR was applied to investigate the mechanism, which was clarified by going through the formation of a carbamate salt. The amine scrubs, which was used in the industry for the capture of CO_2 from natural gas. However, when compared with the scrubbing agents, task-specific ionic liquids perform well without the loss of any active ingredients.

In term of application, the chloroaluminate salt of pyridinium is regarded as the first task-specific ionic liquid. It was intentionally developed for the battery applications. It was found to have catalytic activities for a variety of essential processes, including the Friedel–Crafts reaction (Scheme **1.3**).

Scheme 1.3 Friedel–Crafts reaction

Catalysis

Ionic liquids were found to have the catalytic activities toward many reactions, and it turned out that the trace amount of halogens had made a tremendous contribution to the chemical properties. To achieve catalytic activities, scientists introduced functional groups with

the known catalytic activities to ionic liquids, which made it the task-specific ionic liquids.[38]

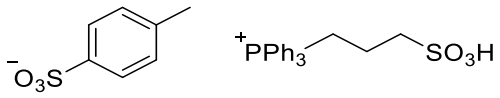

Figure 1.3 Phosphonium sulfonate.

The phosphonium sulfonate (Figure **1.3**) is believed to be the first ionic liquid[39] and exhibits catalytic activities for some acid-catalyzed reactions, such as esterification reactions, rearrangement reactions, and dehydration reactions.

Another compelling example is the ion pairing effect in the hydrogenation of chiral cation[40]. As in Scheme **1.4**, the enantiomeric excess is over 80%.

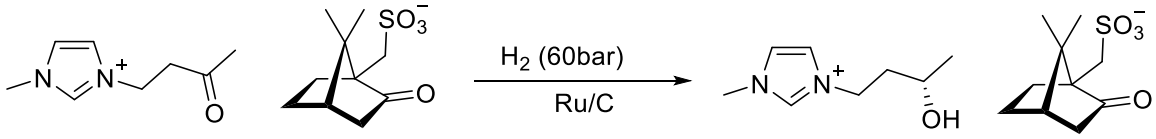

Scheme 1.4 Ionic liquid in asymmetric synthesis.

1-N-butyl-3-methylimidazolium tetra-fluoroborate offers almost 100% conversion in catalyzing the cycloaddition of carbon dioxide to propylene oxide without the solvent (Scheme **1.5**), and the ionic liquid was recyclable.[41]

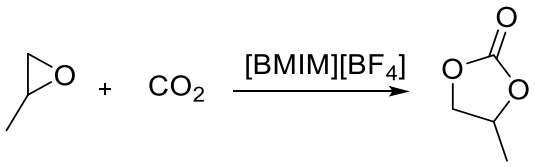

Scheme 1.5 cycloaddition of carbon dioxide to propylene oxide

Ionic liquids also have the accelerative effects of some reactions such as the Diels-Alder reactions, (Scheme **1.6**) which is catalyzed by scandium triflate, with (BMIM)BF_4 as the solvent.[42]

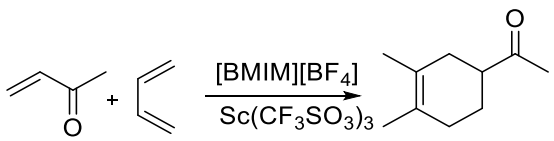

Scheme 1.6 Diels-Alder reactions catalyzed by scandium triflate.

These ionic liquids catalytic system achieved a much higher regioselectivity and reaction rate than the parallel experiments which were conducted in conventional organic solvents. Another advantage is that these ionic liquids can be reused up to 10 times without the loss of catalytic activities and regioselectivities.

Support carrier for reactions

The peptide synthesis can be carried out in a solid phase by bonding starting chemicals to materials such as resin, soluble polyethylene glycols (PEG), polyvinyl alcohols, and other polymers.[43] This greatly simplified the purification process by merely washing with appropriate solvents. The overall yield up to 86% was achieved by Fraga-Dubreuil and Bazureau in which the three components reaction was tested.[44] This is believed to be a promising method that can be applied to the industry.

Magnetism and Luminescence

The magnetism and luminescence properties have been found in some ionic liquids. Okuno et al.[45] reported a magnetic ionic liquid with formula [BMIM][$FeCl_4$]. In this magnetic ionic liquid, non-magnetic materials can be transported with the help of magnetic field.

Analysis applications

Ionic liquids were found to have strong intermolecular forces toward polar molecules, which enables the application as the stationary phase in gas chromatography.[46] After that, ionic liquids were found to be useful in liquid chromatography[47] as the stationary phase or mobile phase[48] by bonding with hydroxyl groups in silica gel. Ionic liquids with a chiral center were used as the stationary phase to purify chiral compounds.[49]

Electrochemical applications

Ionic liquids are ionic compounds and consisted of a cation and anion, which result in the ion conductivities. The existence of the trace amount of organic solvents and water have a severe impact on the conductivity of ionic liquids. By reducing the amount of water from 8.98×10^{-3} to 1×10^{-5} at 298.15 K, the conductivity of $[C_6mim][NTf_2]$ was decreased by 40%.[28] The conductivity of the aqueous ionic liquid solution is decreased as the ion concentration increased because the mobility of ions is disproportionate to the ion concentration.[50] This effect can be ascribed to the increase in viscosity, which reduced the mobility and aggregation of ions.[51]

Bis(trifluoromethylsulphonyl)amide, as an anion, combining with imidazolium cations resulted in a water-immiscible room temperature ionic liquid. This ionic liquid has a good conductivity when compared with organic electrolyte solutions.[52] Ionic liquids can overcome the potential limitation in aqueous or organic media, in ionic liquids, a wide electrochemical window up to 6V can be reached.[53] A quasi-solid-state

material with the combination of the ionic liquid, 1-Methyl-3-propylimidazolium Iodide, and polymers had been employed as the electrolytes for electrochemical devices and membranes. [54] Very recently, an ionic liquid made from aluminum chloride and urea was discovered to be the high-efficiency electrolyte in Al-ion battery,[55] approximate 99.7% coulombic efficiency with a cathode capacity of 73mA/g at 100mA/g.[56]

Gas adsorption

It is known that CO_2 has good solubility in imidazolium ionic liquids based on numerous studies. CO_2 has physical interactions with ionic liquids, which enables the application of ionic liquids in the gas adsorption field. [57-61] For example, at 5 Mpa pressure, one mole of the ionic liquid can dissolve half a mole of CO_2. Some studies revealed that anions and functional groups on cations have some impact on the CO_2 solubility. 1-Alkyl-3-methyimidazolium bis(trifluoromethylsulfonyl)-imide were discovered to have the highest CO_2 solubility among non-functionalized ionic liquids.[62] By switching the anion from Tf_2N^- to BF_4^-, imidazolium-based ionic liquids will have a decrease in the capacity of CO_2 by 31%.[63]

References

1. H. L. Ngo, K. LeCompte, L. Hargens and A. B. McEwen, *Thermochimica Acta*, 2000, **357-358**, 97-102.
2. P. Walden, *Bull. Acad. Imper. Sci. (St. Petersburg)*, 1914, **1800**.
3. S. Zhu, Y. Wu, Q. Chen, Z. Yu, C. Wang, S. Jin, Y. Ding and G. Wu, *Green Chemistry*, 2006, **8**, 325-327.
4. H. Xie, S. Zhang and S. Li, *Green Chemistry*, 2006, **8**, 630-633.
5. D. W. Morrison, D. C. Forbes and J. H. Davis, *Tetrahedron Letters*, 2001, **42**, 6053-6055.
6. T. Welton, *Chemical Reviews*, 1999, **99**, 2071-2084.
7. S. K. Poole, P. H. Shetty and C. F. Poole, *Analytica Chimica Acta*, 1989, **218**, 241-264.
8. P. H. Shetty, P. J. Youngberg, B. R. Kersten and C. F. Poole, *Journal of Chromatography A*, 1987, **411**, 61-79.
9. K. G. Furton and R. Morales, *Analytica Chimica Acta*, 1991, **246**, 171-179.
10. R. M. Pomaville and C. F. Poole, *Journal of Chromatography A*, 1989, **468**, 261-278.
11. S. Sugden and H. Wilkins, *Journal of the Chemical Society (Resumed)*, 1929, 1291-1298.
12. C. Hussey, *Pure Appl. Chem*, 1988, **60**, 1763.
13. K. Bica and P. Gaertner, *Organic Letters*, 2006, **8**, 733-735.
14. S. A. Bolkan and J. T. Yoke, *Journal of Chemical and Engineering Data*, 1986, **31**, 194-197.
15. H. Zhao, J. E. Holladay, H. Brown and Z. C. Zhang, *Science*, 2007, **316**, 1597-1600.
16. I. J. Lin and C. S. Vasam, *Journal of organometallic chemistry*, 2005, **690**, 3498-3512.
17. J. D. Holbrey and K. R. Seddon, *Clean Products and Processes*, 1999, **1**, 223-236.
18. E. Rilo, J. Pico, S. García-Garabal, L. Varela and O. Cabeza, *Fluid Phase Equilibria*, 2009, **285**, 83-89.
19. P. S. Kulkarni, L. C. Branco, J. G. Crespo, M. C. Nunes, A. Raymundo and C. A. Afonso, *Chemistry-A European Journal*, 2007, **13**, 8478-8488.
20. U. Domańska and M. Laskowska, *Journal of solution chemistry*, 2009, **38**, 779-799.
21. J. Kagimoto, S. Taguchi, K. Fukumoto and H. Ohno, *Journal of Molecular Liquids*, 2010, **153**, 133-138.
22. P. Bonhote, A.-P. Dias, N. Papageorgiou, K. Kalyanasundaram and M. Grätzel, *Inorganic chemistry*, 1996, **35**, 1168-1178.
23. B. D. Fitchett, T. N. Knepp and J. C. Conboy, *Journal of the Electrochemical Society*, 2004, **151**, E219-E225.
24. R. L. Gardas and J. A. Coutinho, *Fluid Phase Equilibria*, 2008, **266**, 195-201.
25. S. V. Dzyuba and R. A. Bartsch, *ChemPhysChem*, 2002, **3**, 161-166.

26. E. Kuhlmann, S. Himmler, H. Giebelhaus and P. Wasserscheid, *Green Chemistry*, 2007, **9**, 233-242.
27. Z. B. Zhou, H. Matsumoto and K. Tatsumi, *Chemistry-A European Journal*, 2005, **11**, 752-766.
28. M. J. Earle, J. M. Esperança, M. A. Gilea, J. N. C. Lopes, L. P. Rebelo, J. W. Magee, K. R. Seddon and J. A. Widegren, *Nature*, 2006, **439**, 831.
29. Y. Chen, Y. Cao, Y. Shi, Z. Xue and T. Mu, *Industrial & Engineering Chemistry Research*, 2012, **51**, 7418-7427.
30. A. Stark, P. Behrend, O. Braun, A. Müller, J. Ranke, B. Ondruschka and B. Jastorff, *Green chemistry*, 2008, **10**, 1152-1161.
31. V. N. Emel'yanenko, S. P. Verevkin and A. Heintz, *Journal of the American Chemical Society*, 2007, **129**, 3930-3937.
32. D. H. Zaitsau, G. J. Kabo, A. A. Strechan, Y. U. Paulechka, A. Tschersich, S. P. Verevkin and A. Heintz, *The Journal of Physical Chemistry A*, 2006, **110**, 7303-7306.
33. P. Nockemann, B. Thijs, S. Pittois, J. Thoen, C. Glorieux, K. Van Hecke, L. Van Meervelt, B. Kirchner and K. Binnemans, *The Journal of Physical Chemistry B*, 2006, **110**, 20978-20992.
34. P. Nockemann, B. Thijs, K. Lunstroot, T. N. Parac‐Vogt, C. Görller‐Walrand, K. Binnemans, K. Van Hecke, L. Van Meervelt, S. Nikitenko and J. Daniels, *Chemistry-A European Journal*, 2009, **15**, 1449-1461.
35. P. Nockemann, R. Van Deun, B. Thijs, D. Huys, E. Vanecht, K. Van Hecke, L. Van Meervelt and K. Binnemans, *Inorganic chemistry*, 2010, **49**, 3351-3360.
36. A. G. Vendilo, D. I. Djigailo, H. Rönkkömäki, M. Lajunen, E. A. Chernikova, L. H. Lajunen, I. V. Pletnev and K. I. Popov, *Mendeleev Communications*, 2010, **2**, 122-124.
37. E. D. Bates, R. D. Mayton, I. Ntai and J. H. Davis, *Journal of the American Chemical Society*, 2002, **124**, 926-927.
38. R. Giernoth, *Angewandte Chemie International Edition*, 2010, **49**, 2834-2839.
39. A. C. Cole, J. L. Jensen, I. Ntai, K. L. T. Tran, K. J. Weaver, D. C. Forbes and J. H. Davis, *Journal of the American Chemical Society*, 2002, **124**, 5962-5963.
40. P. S. Schulz, N. Müller, A. Bösmann and P. Wasserscheid, *Angewandte Chemie*, 2007, **119**, 1315-1317.
41. J. Peng and Y. Deng, *New Journal of Chemistry*, 2001, **25**, 639-641.
42. C. E. Song, W. H. Shim, E. J. Roh, S.-g. Lee and J. H. Choi, *Chemical Communications*, 2001, 1122-1123.
43. R. B. Merrifield, *Angewandte Chemie*, 1985, **97**, 801-812.
44. J. Fraga-Dubreuil and J. P. Bazureau, *Tetrahedron*, 2003, **59**, 6121-6130.
45. M. Okuno, H.-o. Hamaguchi and S. Hayashi, *Applied physics letters*, 2006, **89**, 132506.
46. D. W. Armstrong, L. He and Y.-S. Liu, *Analytical Chemistry*, 1999, **71**, 3873-3876.

47. M. P. Marszałł and R. Kaliszan, *Critical Reviews in Analytical Chemistry*, 2007, **37**, 127-140.
48. L. He, W. Zhang, L. Zhao, X. Liu and S. Jiang, *Journal of Chromatography A*, 2003, **1007**, 39-45.
49. J. Ding, T. Welton and D. W. Armstrong, *Analytical Chemistry*, 2004, **76**, 6819-6822.
50. P.-Y. Lin, A. N. Soriano, R. B. Leron and M.-H. Li, *The Journal of Chemical Thermodynamics*, 2010, **42**, 994-998.
51. D. Wu, B. Wu, Y. M. Zhang and H. P. Wang, *Journal of Chemical & Engineering Data*, 2009, **55**, 621-624.
52. M. Armand, F. Endres, D. R. MacFarlane, H. Ohno and B. Scrosati, *Nature materials*, 2009, **8**, 621.
53. F. Endres, A. Abbott and D. R. MacFarlane, *Electrodeposition from ionic liquids*, John Wiley & Sons, 2017.
54. P. Wang, S. M. Zakeeruddin, P. Comte, I. Exnar and M. Grätzel, *Journal of the American Chemical Society*, 2003, **125**, 1166-1167.
55. M.-C. Lin, M. Gong, B. Lu, Y. Wu, D.-Y. Wang, M. Guan, M. Angell, C. Chen, J. Yang and B.-J. Hwang, *Nature*, 2015, **520**, 324.
56. M. Angell, C.-J. Pan, Y. Rong, C. Yuan, M.-C. Lin, B.-J. Hwang and H. Dai, *Proceedings of the National Academy of Sciences*, 2017, **114**, 834-839.
57. L. A. Blanchard, D. Hancu, E. J. Beckman and J. F. Brennecke, *Nature*, 1999, **399**, 28.
58. L. A. Blanchard, Z. Gu and J. F. Brennecke, *The Journal of Physical Chemistry B*, 2001, **105**, 2437-2444.
59. J. L. Anthony, E. J. Maginn and J. F. Brennecke, *The Journal of Physical Chemistry B*, 2002, **106**, 7315-7320.
60. Á. Pérez-Salado Kamps, D. Tuma, J. Xia and G. Maurer, *Journal of Chemical & Engineering Data*, 2003, **48**, 746-749.
61. R. Babarao, S. Dai and D.-e. Jiang, *The Journal of Physical Chemistry B*, 2011, **115**, 9789-9794.
62. D. Camper, C. Becker, C. Koval and R. Noble, *Industrial & Engineering Chemistry Research*, 2006, **45**, 445-450.
63. J. E. Bara, T. K. Carlisle, C. J. Gabriel, D. Camper, A. Finotello, D. L. Gin and R. D. Noble, *Industrial & Engineering Chemistry Research*, 2009, **48**, 2739-2751.

Chapter 2 Objectives and Motivations

Background

CO_2 catastrophe

CO_2 has caused great environmental problems such as greenhouse effect, and ocean acidification. The atmospheric CO_2 level increased by 40% in the past 250 years. The rising amount of CO_2, mainly from human activities such as the fuel combustion, increases the average temperature and a decrease the ocean pH. Scientists are working on the sequestration of CO_2 in a large scale and reducing the emission of CO_2. There are two basic strategies to achieve the storage and capture of CO_2. One is the capture of CO_2 directly from industry sources. An alternative way is to fix CO_2 from the atmosphere by natural biological processes such as marine sediments, soils, and plants.

Many materials were developed for the capture of CO_2 such as amine scrubbing, porous frameworks (e.g., metal organic frameworks,[64] covalent organic frameworks, [65] zeolite-imidazolate frameworks.[66]) and amine modified silicas (e.g., molecular basket sorbents,[67] hyperbranched aminosilica.[68]) and carbonaceous materials (e.g., the pyrolysis of ILs,[69] coals[70], and natural materials.[71,72]) and task-specific ionic liquids. The amine scrubbing has been used for the capture of CO_2 in natural gas and gaseous hydrogen since 1930. However, this method suffered some drawbacks including the solvent loss, corrosions, and high energy costs for the regeneration.

Task-specific ionic liquids were designed to overcome the disadvantages that the amine scrubbing suffered. With negligible vapor pressures and good stabilities, ionic liquids can be reused without the loss of activities and active ingredients, which is favored in the industry.

Task-specific ionic liquids in capturing CO_2

Task-specific ionic liquids were found to have a better capability for CO_2 by chemical interactions.

Davis's group proposed the concept of task-specific ionic liquids (TSILs) and designed the first amine-tethered task-specific ionic liquid, the absorption of CO_2 was investigated(Scheme **2.1**).[37]

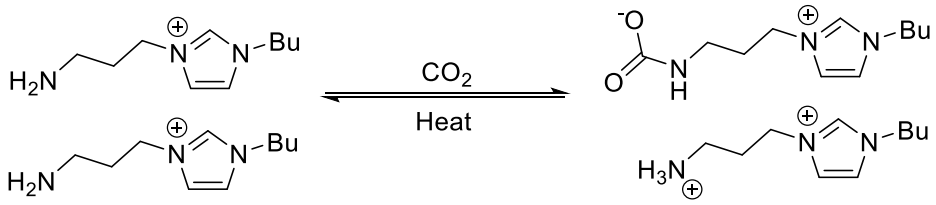

Scheme 2.1 Task-specific ionic liquid in CO_2 capture.

Amine groups react with CO_2 to form a carbamate, which results in a maximum 0.5 mole of CO_2 being captured by a mole ionic liquid. Another half of amine groups stabilized carbamates by capturing protons. The desorption of CO_2 was conducted in vacuum at 80℃-100℃.

An anion functionalized ionic liquid with the stoichiometric CO_2 capture was studied(Scheme **2.2**).[73]

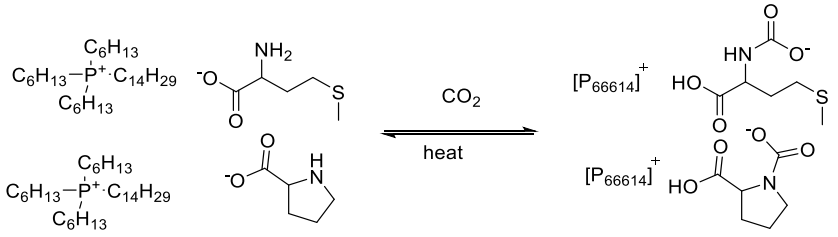

Scheme 2.2 Equimolar CO_2 absorption by amino acid ionic liquids.

An anion functionalized ionic liquid was designed to have a multi-molar capacity for CO_2. (Scheme **2.3**)

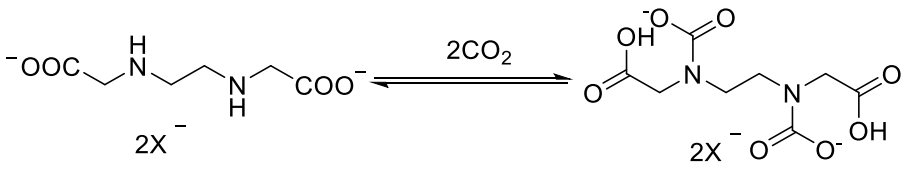

Scheme 2.3 Multimolar CO_2 capture process.

Dai et al. investigated bases assisted CO_2 absorption process by mixing organic super-bases with ionic liquids (Scheme **2.4**). In these cases, organic bases stabilized CO_2-ILs adducts by capturing free protons.

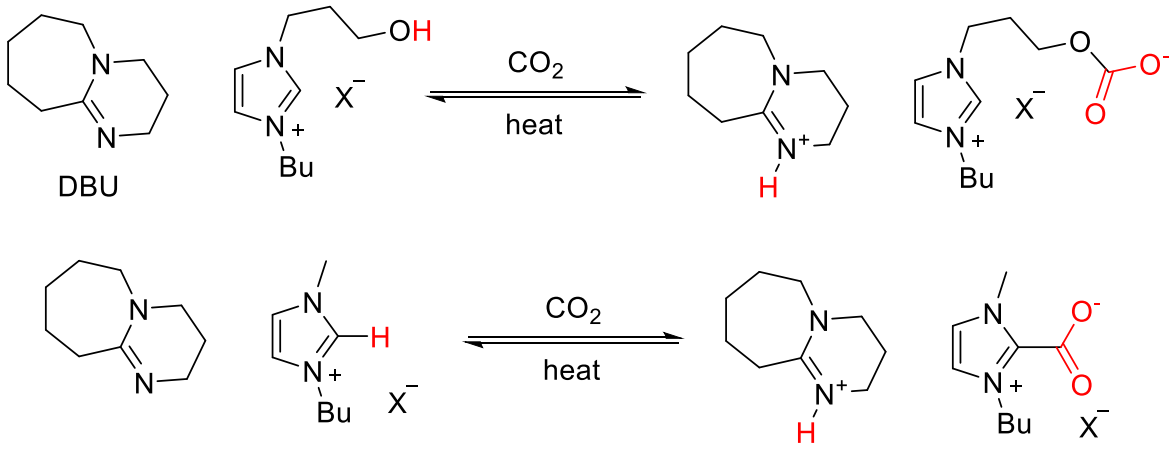

Scheme 2.4 Base assisted CO_2 capture.

Anion functionalized ionic liquids bearing strong basic anions were also studied by Dai et al. The deprotonated imidazole, pyrazole and triazole

anion were found to directly react with CO_2 and form adducts without the presence of stabilizer agents. (Scheme **2.5**)

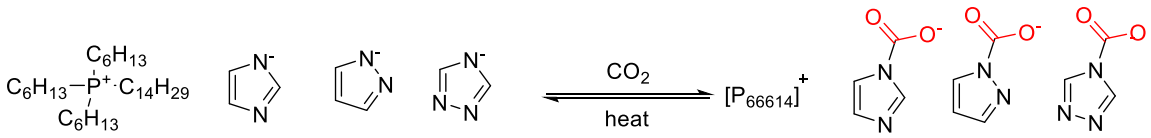

Scheme 2.5 Anion functionalized ionic liquid for CO_2 capture.

SO_2 has even stronger interactions with ionic liquids, and the absorption of SO_2 in BF_4^- based ionic liquids were reported. In ambient conditions, at the room temperature and atmospheric pressure, up to 2 moles of SO_2 can be absorbed by one mole of an ionic liquid. Vacuum or heat was required for the desorption of SO_2.[74] No significant loss of performance was found after several cycles.

Some other findings showed the solubility of poisonous gases such as CO,[75] BF_3, PH_3[76] in some specific ionic liquids. PH_3 and BH_3 can form a complex and stored without high pressure in a regular cylinder, which is a considerable improvement in safety.

Objectives and motivations

Ionic liquids have been reported can act as absorbents with functionalized anions or cations. Noteworthily, a strategy by mixing organic super-bases with ionic liquids was investigated and showed a good capacity towards CO_2. This method has a crucial problem that basic additives will be lost during the cycling run, which is not favored in the industry. Meanwhile, a cation bearing a strong basic group was barely investigated. So, my goals are to design and synthesize basic

groups functionalized ionic liquids by attaching basic groups onto ionic liquid cations for equimolar CO_2 capture. Beti was selected as an anion, because of the big size, the melting points of ionic liquids will be decreased below room temperature. A low melting point enables the applications of these ionic liquids at room temperature. Ideally, a reversible CO_2 capture in mild conditions and good stabilities are the final criterions.

In addition, task-specific ionic liquids in the field of catalysis, and as precursors for high-surface-area materials were also studied.

Project 1- α-oximehydrazone functionalized ionic liquid

In this project, an α-oximehydrazone functionalized ionic liquid (Figure **2.1**) was designed.

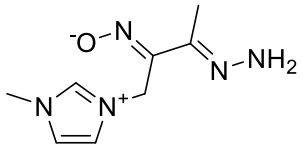

Figure 2.1 Oximehydrazone functionalized ionic liquid.

This zwitterion-type of ionic liquid contains a nucleophilic part and an electron acceptor part, which might have a synergic process in capturing CO_2.

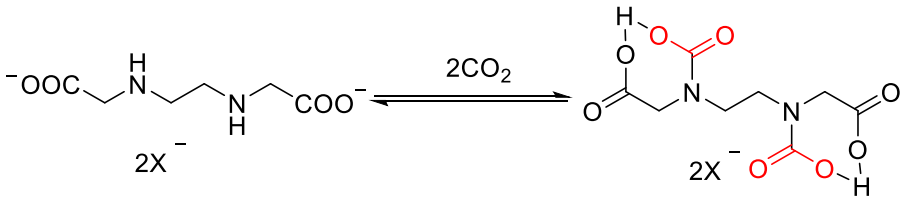

Scheme 2.6 Synergic process in the capture of CO_2.

As shown in Scheme **2.6**, CO_2 is fixed in the amino-functionalized ionic liquid as the form of carbamate. Anionic carboxylic groups take part in the stabilization of the carbamate by forming a seven-member-ring. With the help of this process, ionic liquids can capture CO_2 up to the equal mole.

This seven-members-ring mechanism is crucial for the CO_2 capture, and the distance between the amine group and the carboxylic group is critical to the form of the seven members-ring. Ionic liquids with similar structure but disparate result confirmed this mechanism. (Scheme **2.7**) In this case, only half a mole of CO_2 was captured by one mole of an ionic liquid.

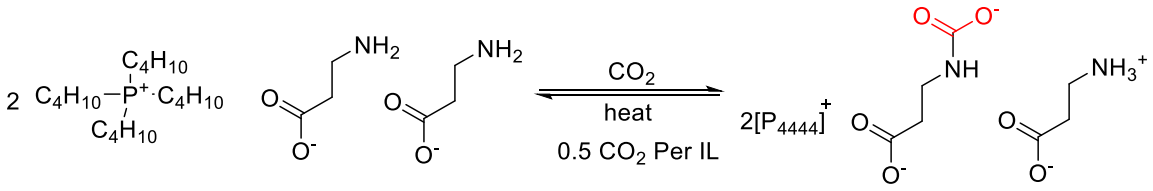

Scheme 2.7 Amino-acids capture CO_2 without the synergic process.

Herein, to investigate the distance between anion and amine, and the possible ring-dominant mechanism, I designed an α-oximehydrazone-

type ionic liquid. I proposed a possible mechanism for the CO_2 capture. (Scheme **2.8**)

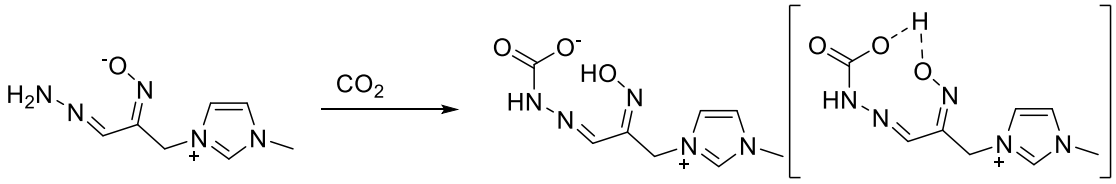

Scheme 2.8 A nine-members-ring synergic process.

There are nine atoms involved in this synergic process. However, the conjugated oximehydrazone system might greatly limit the freedom of the movement.

Project 2- guanidine tethered ionic liquids

In this project, to attach a strong basic group to the ionic liquid, I designed some guanidine functionalized ionic liquids (Figure **2.2**).

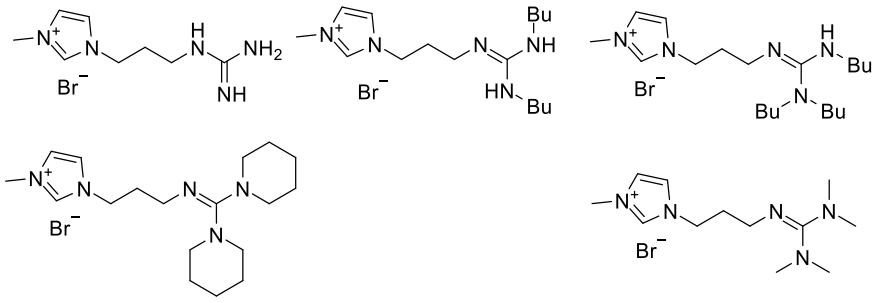

Figure 2.2 Guanidine functionalized ionic liquids.

Guanidines, with the p*K*a value of 13.6 in DMSO, are considered as strong organic bases. In the presence of guanidines, ionic liquids in capturing CO_2 were reported.

As shown in Scheme **2.9**, with the help of MTBD, an equimolar CO_2 capture was achieved by the alcoholic ionic liquid.

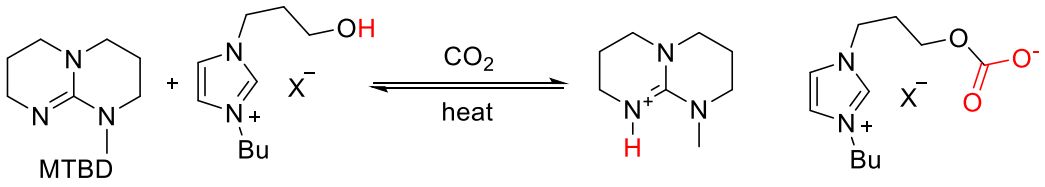

Scheme 2.9 Alcoholic ionic liquid capture CO_2 with the assistance of MTBD.

In another case, owing to the acidity of the proton in the position two of imidazoliums. The introduction of strong bases will deprotonate imidazoliums and followed by the occurrence of CO_2 capture in the position two. (Scheme **2.10**)

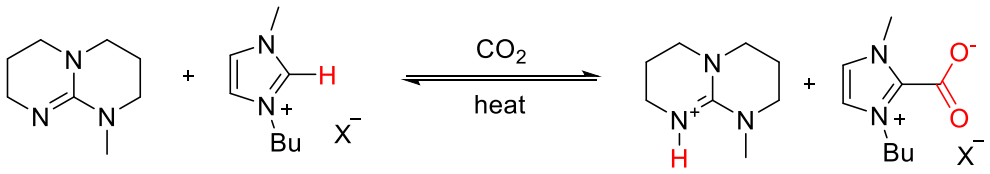

Scheme 2.10 Equimolar CO2 capture by imidazolium-based ionic liquids and super-base systems.

However, these strong-bases were added as an additive. It suffered from a drawback that additives will escape from the system.

So, in this project, the synthesis of guanidine ionic liquids will be illustrated, and a CO_2 uptake experiment will be conducted at room temperature.

Project 3- amidine functionalized ionic liquids

Similar to the project 2-*guanidines functionalized ionic liquids*, amidines functionalized ionic liquids was designed. (Figure **2.3**) In this project, the synthetic route will be more focused on a linear strategy.

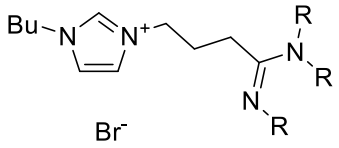

Figure 2.3 Amidine ionic liquid.

Amidines, with p*K*a value of 13.6 in DMSO, are considered as strong organic bases. In the presence of amidines, ionic liquids capturing CO_2 was reported. (Scheme **2.11**)

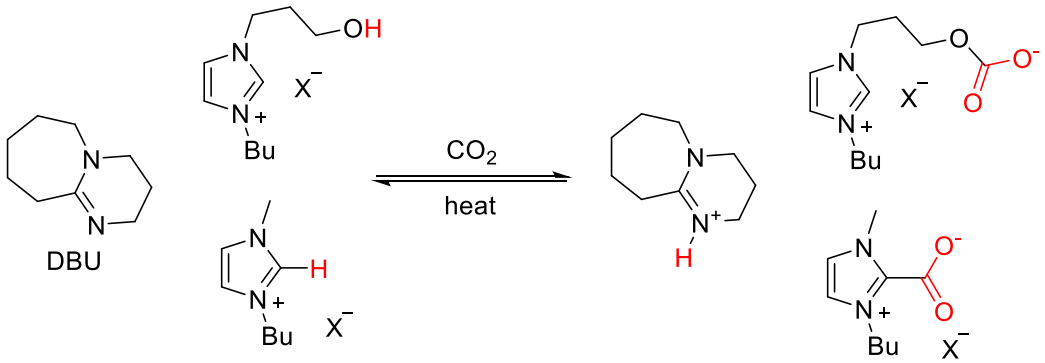

Scheme 2.11 Amidine assisted CO_2 capture.

In this work, a linear strategy was applied in the synthesis of amidine-type ionic liquids.

There are two basic methods for synthesizing functional ILs, the linear and convergent method. (Scheme **2.12**) Especially, F_2 group is a nucleophilic group.

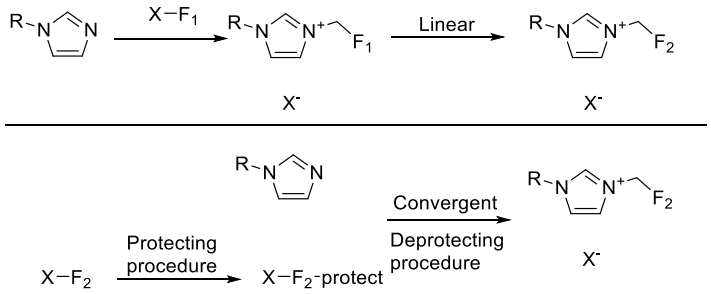

Scheme 2.12 The linear and the convergent approaches.

The convergent strategy is more favored in the synthesis of functionalized ionic liquids. However, two additional steps are needed in linear strategy, the protect and deprotect steps, which is not the atomic economy. The linear strategy is more straightforward than convergent strategy. However, it suffered some purification issues, which made the selection of reactions and reaction conditions more restricted. Reactions must have a 100% conversion in the last step for pure ionic liquids.

Herein, the Pinner reaction was employed to convert nitriles to amidines.

The Pinner reaction can be conducted in either acidic or basic conditions. (Scheme **2.13**)

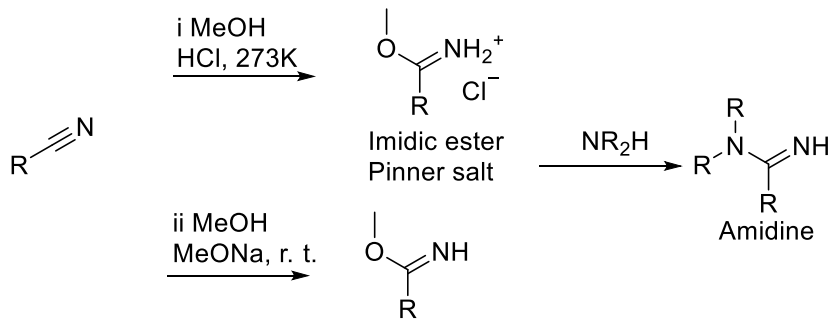

Scheme 2.13 The Pinner reaction in acidic or basic condition.

In this work, the reaction conditions of the Pinner reaction will be studied to meet the required conversion.

Project 4- ultra-pure ionic liquid as electrolyte

In this project, N-butyl-N-methylpyrrolidinium bistrifluoromethanesulfonylimide ($Pyr_{14}TFSI$) was synthesized as an electrolyte. (Figure **2.4**)

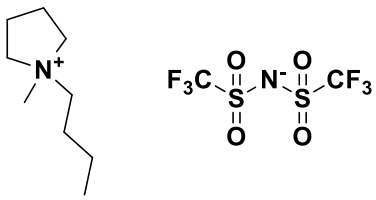

Figure 2.4 Structure of Pyr14TFSI

Because of the electrochemical window of this ionic liquid is up to 5.75V, which enables a comprehensive study of carbonaceous materials.

The purity of this ionic liquid is crucial to electric experiments. With even trace amount of impurities, some extra peaks will be observed in cyclic voltammetry, which greatly affects the analysis of materials.

Classic purification method in purifying ionic liquids is to wash ionic liquids by organic solvents in which ionic liquids have solubilities.

In this project, the purification method of this ionic liquid will be studied.

Project 5- heterogenous viologen catalysts for metal-free and selective oxidations.

Viologen-type ionic liquids were studied in this work because viologen-type ionic compounds (Figure **2.5**) can form radicals and can be reduced reversibly, which enabled the occurrence of single electron transformation process. The oxidation of thiols to sulfoxides is believed to go through a single electron transformation process. However, a metal-free process in the oxidation of sulfoxides has rarely been seen.

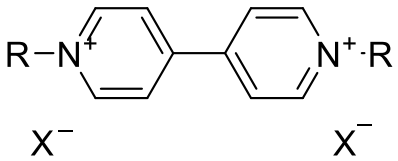

Figure 2.5 viologen-type ionic compounds

A preliminary experiment indicated that viologen-type ionic liquids have catalytic properties in selectively oxidizing thioanisoles to sulfoxides.

So, my goal is to investigate the reaction conditions and activities of the viologen ionic liquids as a catalyst in thiols oxidation.

Heterogeneous catalysis is favored in the industry because the recycling of catalysts can be simply achieved by the filtration. However, the most viologen-type ionic liquids have good solubility in organic solvents, and they are highly toxic. So, I synthesized the polymerized viologen-type ionic compound. (Figure **2.6**)

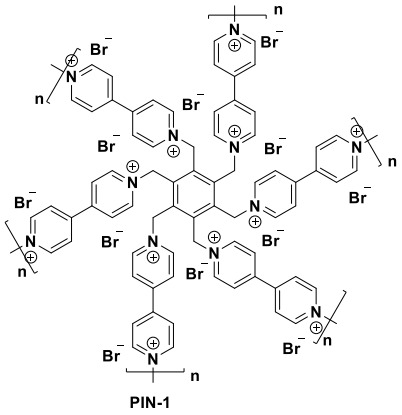

Figure 2.6 Polymeric ionic viologen.

The activities of this catalyst will be tested in the aspect of conversions, stabilities, and selectivities. Hydrogen peroxide will be employed as the oxidizing reagent, because it is a green chemical, with water as the only byproduct.

Reaction conditions will be carefully studied by changing the solvent, catalyst amount, and reaction temperature.

Project 6- mesoporous carbon derived from propargylic ionic liquids

In this project, to synthesize porous carbon materials, we designed some propargylic ionic liquids precursors.

A previous study of our group indicated nitrile groups underwent a trimerization process at high temperature, and eventually produced porous carbon materials. These porous carbon materials have a high capacity toward carbon dioxide. Some other studies showed alkyne groups could be oligomerized in the presence of catalysts. This inspired us to design and synthesize alkyne functionalized ionic liquids and to study the behavior of this ionic liquid at high temperature.

A preliminary experiment indicated that the alkyne functionalized ionic liquids formed microporous carbon under thermal treatment, and the length of carbon bridge that connecting two cations will have a great impact on the fraction of mesopores.

Series propargylic ionic liquids with carbon bridge were designed. (Figure **2.7**)

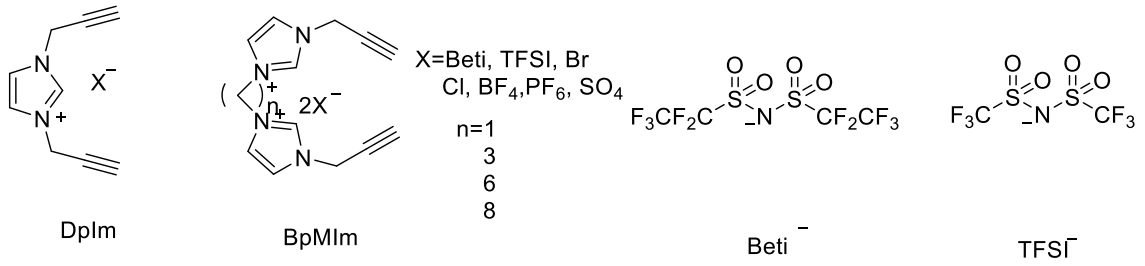

Figure 2.7 Propargylic ionic liquids.

So, surface properties will be investigated by changing the length of the carbon bridge. In addition, the effect of anions and calcine temperatures on surface properties will be discussed.

The surface area and CO_2 capacity will be tested, and they are the ultimate criterions to measure the carbon materials.

Project 7- linear crystalline porous organic polymer

In this project, I attempted to synthesize soluble linear polymer (Polymers of intrinsic porosity) *via* the imine condensation for membrane separations.

Polymers of intrinsic porosity (PIMs) have drawn much attention from scientists; their applications can be extended to membrane separations, heterogeneous catalysis, and hydrogen storage. Many types of condensation reactions were applied to the synthesis of PIMs. (Scheme 2.14)

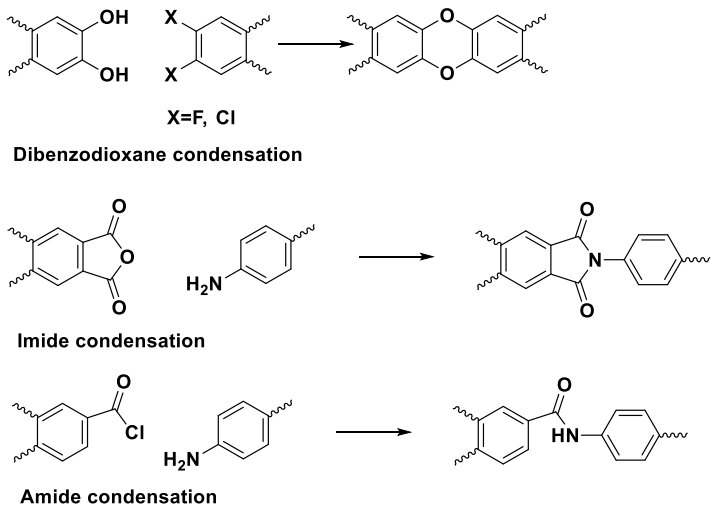

Scheme 2.14 Three common condensation methods in making PIMs.

However, there is no report associated with the imine condensation reaction in the synthesis of PIMs, which is the most common reaction in the synthesis of covalent organic frameworks (COFs). Imine groups have strong interactions with CO_2, so PIMs with imine groups might have a higher capacity for CO_2. (Scheme **2.15**)

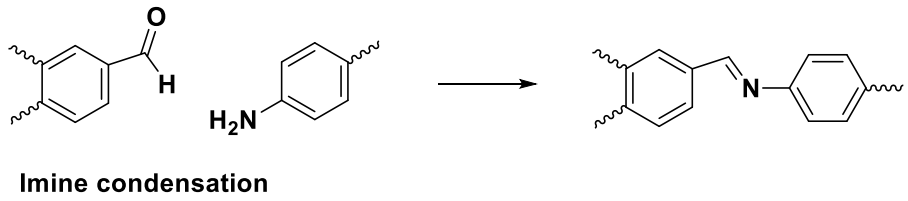

Scheme 2.15 imine condensation.

The 4,4'-(9-Fluorenylidene) dianiline and the terephthalaldehyde were selected as building blocks. (Scheme **2.16**)

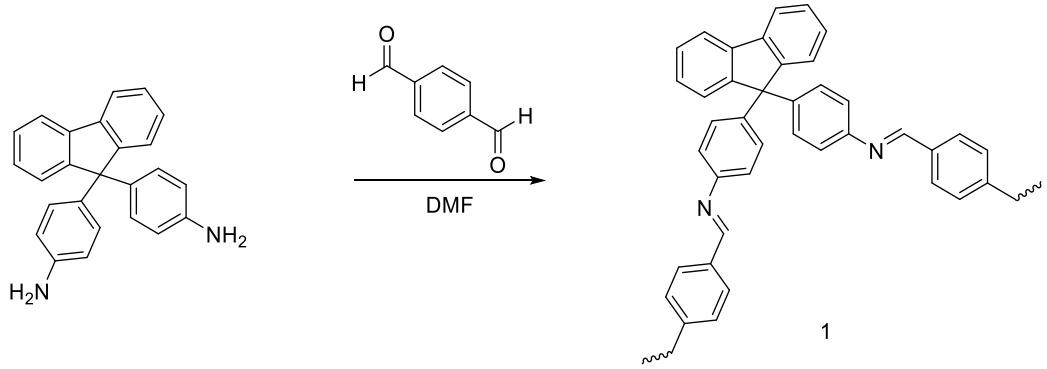

Scheme 2.16 The synthetic route for the polymer.

Molecular weight greatly impacts the surface area of polymers. In this work, effects that reaction conditions will bring to the product will be investigated.

Surface area will be tested as the ultimate criterion to measure this material.

References

73. B. E. Gurkan, J. C. de la Fuente, E. M. Mindrup, L. E. Ficke, B. F. Goodrich, E. A. Price, W. F. Schneider and J. F. Brennecke, *Journal of the American Chemical Society*, 2010, **132**, 2116-2117.
74. W. Wu, B. Han, H. Gao, Z. Liu, T. Jiang and J. Huang, *Angewandte Chemie International Edition*, 2004, **43**, 2415-2417.
75. D. J. Tao, F. F. Chen, Z. Q. Tian, K. Huang, S. M. Mahurin, D. e. Jiang and S. Dai, *Angewandte Chemie*, 2017, **129**, 6947-6951.
76. D. J. Tempel, P. B. Henderson, J. R. Brzozowski, R. M. Pearlstein and H. Cheng, *Journal of the American Chemical Society*, 2008, **130**, 400-401.

Chapter 3 α-Oximehydrazone Functionalized Ionic Liquid

Abstract

In this chapter, a highly active α-oximehydrazone zwitterion-type ionic liquid was designed, synthesized and applied to the capture of CO_2. A robust CO_2 capture up to equimolar amounts was achieved. The synthesis of intermediate α-oximeketone chloride was achieved in one step with a high yield 93% without the use of toxic sodium nitrite and dangerous nitrosyl chloride. The absorption of CO_2 was tracked by NMR, revealing a clear mechanism for the capture of CO_2. However, this ionic liquid was found being unable to release CO_2 and decomposed at 80℃.

Introduction

A great environmental problem has been caused by the vast amount of CO_2 which was produced by human activities. Capture, storage, and conversion of CO_2 have become an urgent social problem. Amine scrubbing method has been used as the most practical way to absorb CO_2, with alkanolamines as the effective ingredient.[77] This method performed high efficiency toward acidic gases such as CO_2, H_2S, and SO_2. However, the disadvantages included such as the loss of solvent, corrosion to facilities, and the high energy cost for recycling free amines from final solution, which significantly limited its application in the industry.

CO_2 was found to have the highest solubility among ethylene, ethane, methane, argon, oxygen, carbon monoxide in ionic liquids.[59] However, the solubility was still too low. The task-specific ionic liquid bearing amine group was developed to capture CO_2 specifically.[37] In this

method, half equivalent CO_2 was captured by consuming a mole of an ionic liquid. (Scheme **3.1**)

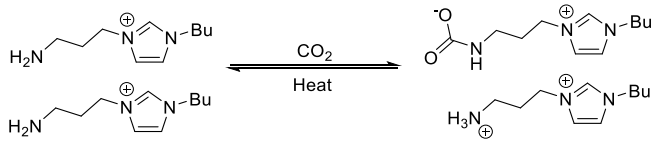

Scheme 3.1 Task-specific ionic liquid in capturing CO_2.

Later, Zhang's group has developed a series of amino acid derived ionic liquids, which can capture 0.5 moles of CO_2 by one mole of ionic liquid[78] (Scheme **3.2**).

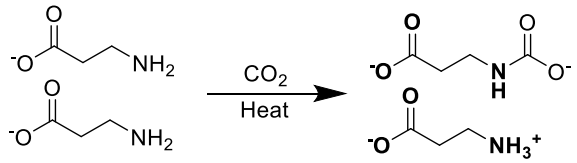

Scheme 3.2 Amino acid derived ionic liquids in capturing CO_2.

Dai's group developed a method by mixing ionic liquids with basic organic compounds, such as tetramethylguanidine, 1,8-diazabicyclo [5.4.0]undec-7-ene (DBU) and 1,3,4,6,7,8- hexahydro-1-methyl-2H-pyrimido[1,2-a]pyrimidine (MTBD). With the assistance of non-nucleophilic super-bases, imidazolium-based ionic liquids acting as acids, their conjugated bases can chemically bond into CO_2.[79] (Scheme **3.3**) However, super-base as additives will also suffer from evaporating from the system.

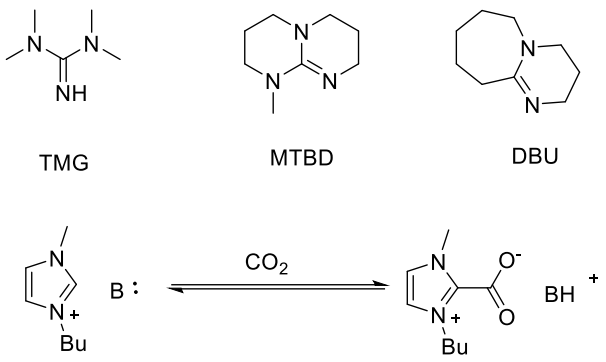

Scheme 3.3 Chemical structures of super-bases used in this work and the mechanism of capture CO_2.

An optimized method was then discovered for tuning the basicity of ionic liquids for equimolar CO_2 capture by Dai et. al.[80](Scheme **3.4**) Based on the above examples, a verdict can be concluded that the capture of CO_2 goes through either a basic functional group with proton acceptor or strongly basic functional group that can directly bond to CO_2.

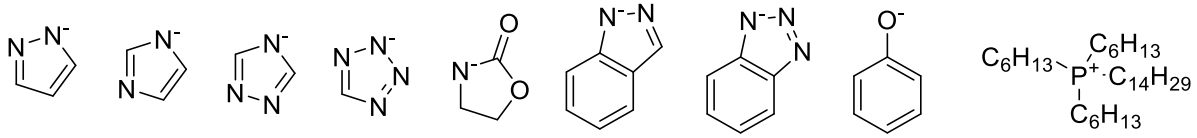

Scheme 3.4 Structure of anions and cations in tunable basic ILs for CO_2 capture.

Herein a zwitterion-type ionic liquid with the α-oximinohydrazone moiety was designed, which had both a basic group and a proton acceptor in one molecule. The p*K*a value of α-oximinhydrazone is approximately 9, which indicates its conjugated base has moderate basicity.

In the most cases, α-Oximinhydrazone is synthesized from α-Oximinketone (Scheme **3.5**).[81]

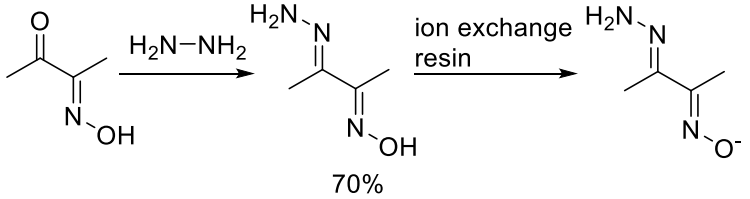

Scheme 3.5 Synthetic route of the α-oximinhydrazone anion.

The preparation of α-oximinoketone starts from ketone is with the use of $NaNO_2$,[82] or amyl nitrite.[83] An alternative method starts from butanedione by reacting with hydroxylamine.[84] (Scheme **3.6**)

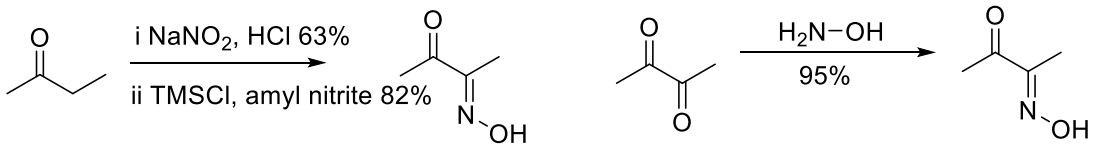

Scheme 3.6 Synthetic route for α-oximinoketone starts from butanedione or 2-butanone

However, an unexpected reaction occurred when methyl vinyl ketone was employed, and the α-oximinoketone chloride was produced. All details will be discussed.

Results and discussion

Oximehydrazone functionalized ionic liquid

α-Oximehydrazone zwitterion was designed as shown in Figure **3.1**. The target compound was achieved in 4 steps of synthesis, which can capture CO_2 up to the equimolar amount.

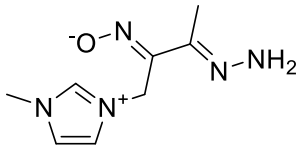

Figure 3.1 Oximehydrazone functionalized ionic liquid.

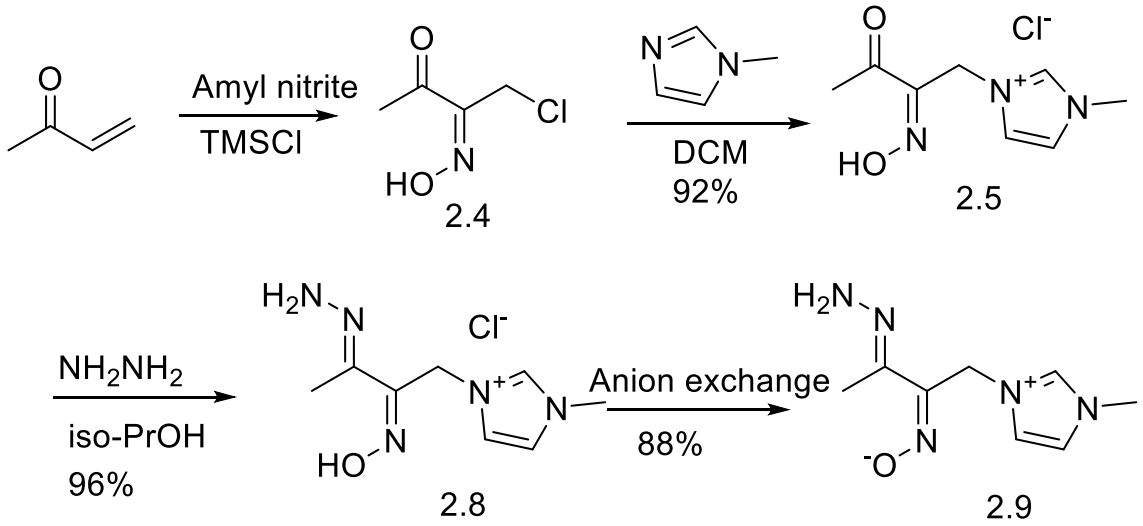

Scheme 3.7 Synthetic route for Oximinohydrazone functionalized ionic liquid.

This ionic liquid was synthesized from methyl vinyl ketone as shown in Scheme **3.7**. Corresponding compounds and the tracking of CO_2 capture were analyzed by NMR (Figure **3.2** and Figure **3.3**). The absolute configuration of oxime and hydrazine were unable to be determined. The hydroxyl proton was not observed in the spectrum of α -oximinoketone. However, α -oximinohydrazone showed both hydroxyl and hydrazone protons. After processing with the anion resin, a shift for all protons was observed. The hydroxyl proton signal disappeared, which indicates the deprotonation of the oxime.

After a CO_2 uptake test, the hydroxyl proton signal appeared again, which is a proof that instead of the oxime, CO_2 was selectively bonding to the hydrazine moiety (Scheme **3.8**).

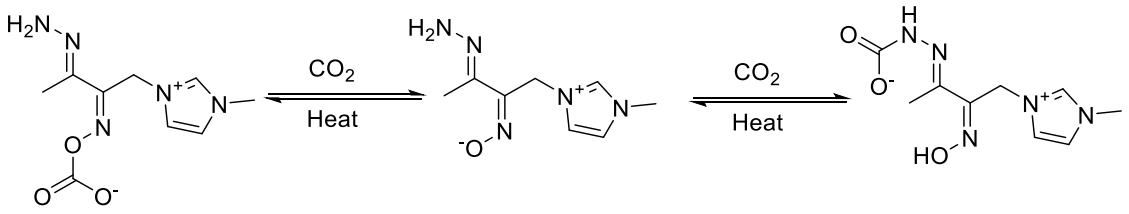

Scheme 3.8 Two sites for α -Oximinohydrazone absorbs CO_2.

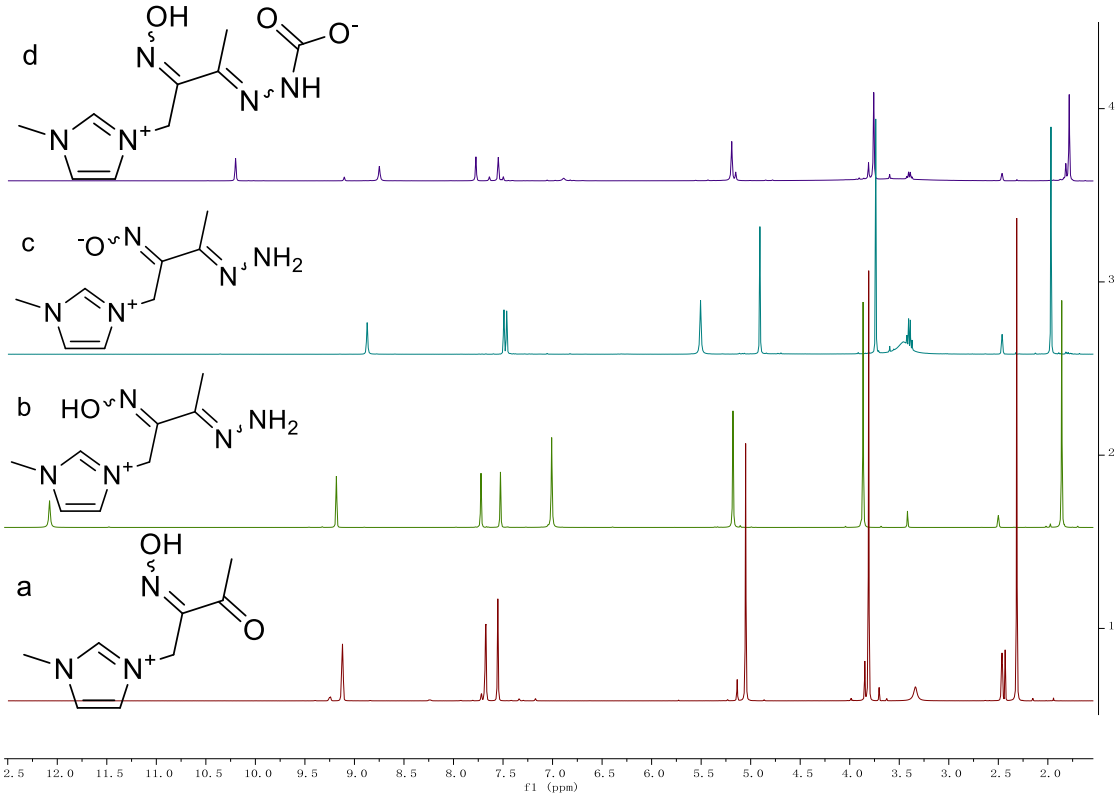

Figure 3.2 H^1-NMR of ILs and ILs-CO_2 abduct
a) α -oximinoketone. b) α -oximinohydrazone.

c) α -oximinohydrazone zwitterion d) α -oximinohydrazone zwitterion-CO_2 adduct

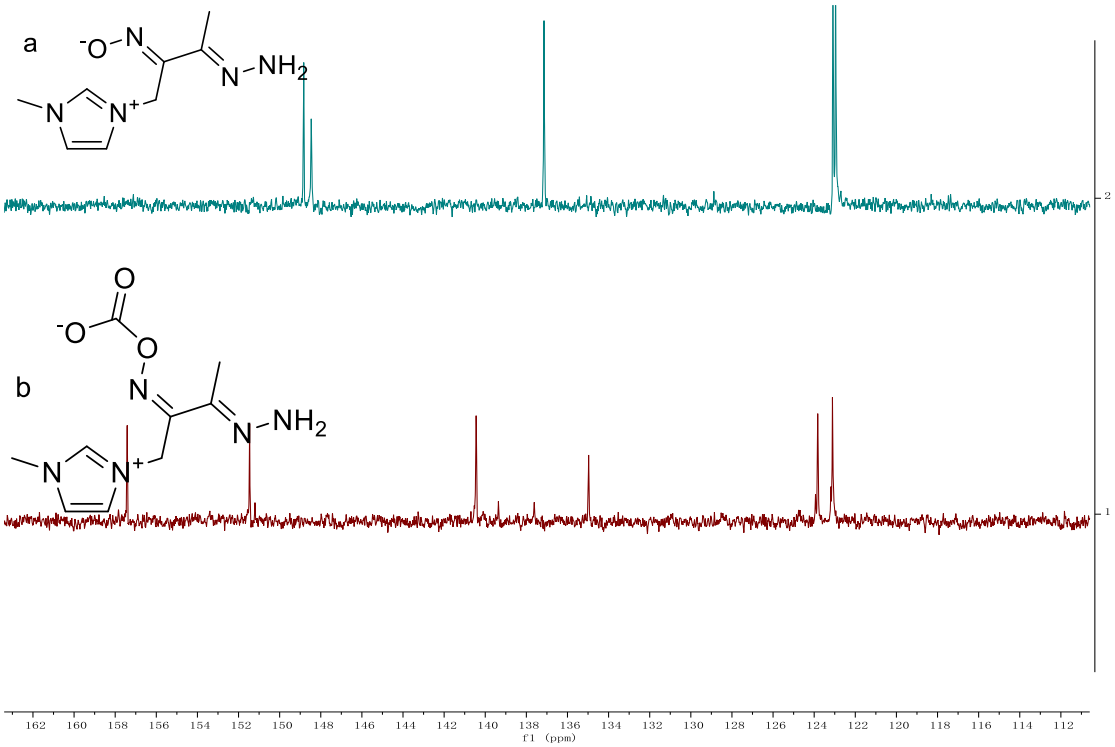

Figure 3.3 C^{13}-NMR of ILs and ILs-CO_2 abduct

a) α -oximinohydrazone zwitterion

b) α -oximinohydrazone zwitterion-CO_2 abduct

In C^{13}-NMR, an extra carbon peak appeared, which was a substantial proof that CO_2 bonded to ILs. However, two-dimensional nuclear magnetic resonance spectroscopy technique is needed to assign the carbon peak. A CO_2 desorption test was performed at 80℃, by bubbling dry N_2 into NMR tube. However, the NMR result showed that α-oximinohydrazone was decomposed. There are several possible reasons can explain this abnormality. The first is the conjugation effect caused by the α -oxime group. Alternatively, the second, the hydrazone-CO_2 abduct induced decompose.

Oxime functionalized ionic liquid **3.3** (Scheme **3.9**) was intentionally designed to test the response of the oxime anion group to CO_2.

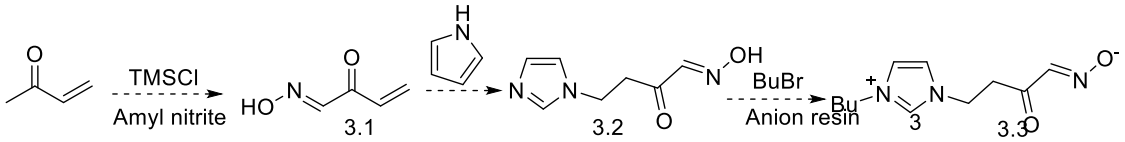

Scheme 3.9 Origin route in synthesizing oxime functionalized ionic liquid.

Methyl vinyl ketone was used as starting material. However, instead of compound **3.1**, compound **3.4** was obtained by applying chlorotrimethylsilane and amyl nitrite. Based on the report,[83] NOCl was generated *in situ* by mixing chlorotrimethylsilane and amyl nitrite. NOCl then added to the double bond. The reaction exclusively gave birth to product **3.4** instantly (Scheme **3.10**).

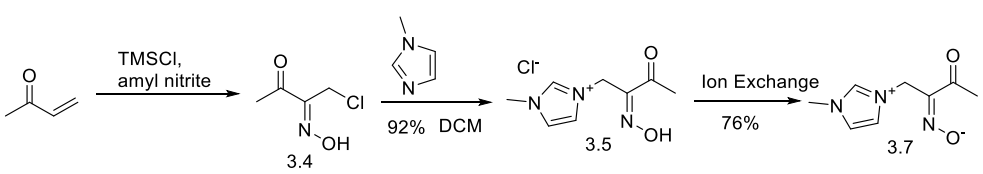

Scheme 3.10 The synthetic route of α -oximinoketone ionic liquid.

The compound **3.4** then reacted with 1-methylimidazole to produce the ionic liquid **3.5**, the reaction was instantaneous due to the high activity of the chloride. The solid ionic compound was precipitated out within 5 mins. After anion exchange with Lithium TFSI, the compound **3.6** was obtained with moderate viscosity. A CO_2 uptake study was conducted, and only the physical absorption was detected. The p*K*a value of α - oximinoketone is approximately 9.42,[85] which is about the same acidity as HCN (9.40) and NH_4^+ (9.25) and much higher than acetic acid(4.76). It means that the moderate basicity of its conjugated base enables the reversible reaction with CO_2 (Scheme **3.11**). There are two active sites that can bond with CO_2 (Scheme **3.11**). Deprotonation of oxime was performed with anion exchange resin. Orange color crystal zwitterion **3.7** was obtained.

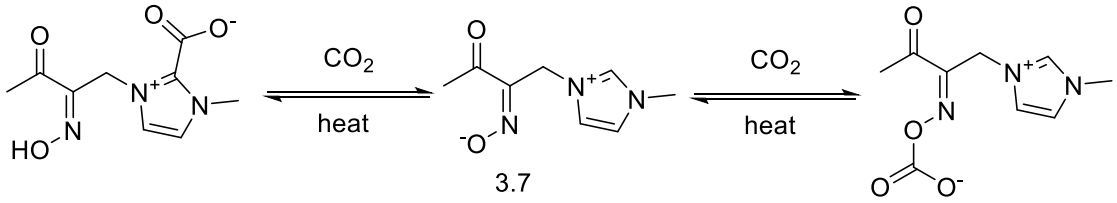

Scheme 3.11 Two possible sites for the capture of CO_2.

The zwitterion was dried in a vacuum while not to exceed 50℃, or it will lead to decomposition. Zwitterion was dissolved in [BMIM][TFSI] medium before the CO_2 uptake experiment. After bubbling in CO_2, the color of the ionic liquid turned to light orange. However, no significant changes occurred in weight and NMR, which indicated the CO_2 was not absorbed. According to hard-soft acid-base theory, CO_2 is a hard molecule; a hard molecule can react with it successfully. The

delocalization of the negative charge makes α -oximinoketone a soft base, which resulted in the Coulombic interaction between negative oxygen and CO_2 is not stronger (Scheme **3.12**).

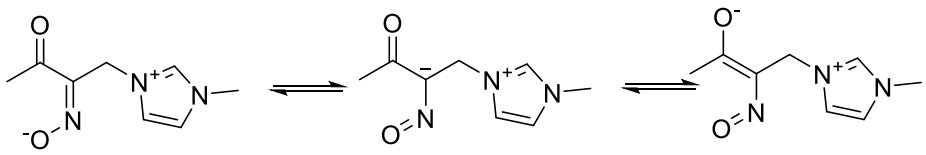

Scheme 3.12 Delocalization of negative charge.

Based on previous failures and successful examples from other groups, I realized the basicity of oximeketone anion is not strong enough to deprotonate hydrogen in position 2 of the imidazolium and not hard enough to react with carbon dioxide directly, therefore, a hard atom is needed in this ionic liquid. As I mentioned before, only a reaction with ultra-high conversion can be good for ionic liquid at this stage; thus, I decided to add a hydrazone group to it. The hydrazine was applied to react with α -oximinoketone to give the α -oximinohydrazone zwitterion.

Experimental

Chemicals and materials

Methyl Vinyl Ketone (Stabilized 95%, ACROS Organics), Amyl nitrite (TCI, 95.0%), Chlorotrimethylsilane (98%, ACROS Organics), 1-Methylimidazole (99%, ACROS Organics), Hydrazine hydrate (100%, ACROS Organics), Anion Exchange Resin (Thermo Scientific POROS 50 HQ), all chemicals above were use directly without further

purification. All organic solvents were purchased from Fisher scientific and without any further purification.

*3-(2-(hydroxyimino)-3-oxobutyl)-1-methylimidazolium (**3.7**)*

To a 50mL three neck round flask bottle, 7g (0.1 mol) of methyl vinyl ketone was added in 30mL DCM. The reactor was stirred in an -20℃ bath. 11.7g (0.1mol) of amyl nitrite was added slowly in one portion. The color of mixture turned light blue. 10.8g (0.1mol) Chlorotrimethylsilane was then added dropwise. The temperature was then raised to room temperature and keep stirring for additional 10 minutes.

6.8g of 1-methylimidazole was dissolved in 10mL DCM before mixing with **3.4** solution. An exothermic reaction occurred quickly within 5 minutes ending with the white precipitate. The precipitate was filtrated and washed with isopropanol:DCM 1:3 three times. (19.32g, 92%). δH (ppm) (DMSO-d_6): 9.13 (1H, s, N-*CH*-N), 7.68,7.55 (2H, s, N-*CH*-*CH*-N), 5.08 (2H, s, N-CH_2-CN), 3.88 (3H, s, N-CH_3), 2.30 (3H, s, CO-CH_3) δC (ppm) (DMSO-d_6): 190.28 (s, C-*CO*-C), 152.05 (s, C-*CN*-*O*), 138.43 (s, -N-CH -N), 127.25,126.38 (s, -N-*CH*-*CH*-N), 50.04 (s, N-CH_2), 33.90 (s, N-CH_3), 10.59 (s, CN-CH_3), m/z (ESI+):182; m/z (ESI-): 380, $[Beti]^-$

2g of 5 was dissolved in 5mL of methanol contains 10g of anion exchange resin. The solution was stirred for another 30mins. The orange color solution was filtrated and transferred to a vacuum oven. Red solid was obtained. (1.56g, 94%). δH (ppm) (DMSO-d_6): 8.95 (1H, s, N-*CH*-N), 7.52,7.65 (2H, s, N-*CH*-*CH*-N), 4.98 (2H, s, N-CH_2-CN), 3.86 (3H, s, N-CH_3), 1.95 (3H, s, CO-CH_3) δC (ppm) (DMSO-d_6): 189.28 (s, C-*CO*-C), 142.85 (s, C-*CN*-*O*), 141.43 (s, -N-CH -N),

126.33,126.15 (s, -N-*CH*-*CH*-N), 55.02 (s, N-*CH_2*), 34.12 (s, N-*CH_3*), 10.25 (s, CN-*CH_3*).

*3-hydrazineylidene-2-(hydroxyimino)butyl)-1-methylimidazolium Chloride (**3.8**), and 3-hydrazineylidene-2-(hydroxyimino)butyl)-1-methylimidazolium (**3.9**) zwitterion*

2.17g(1mmol) of **3.5** was dissolved in 10mL of ethanol in a 20mL vial equipped with a stirring bar, 0.10g (2mmol) hydrazine hydrate was then added. The mixture was allowed to stir for an addition 12 hour. Three-fourths of solvent was removed under reduced pressure. White powder precipitated out and collected by filtration. (2.21g, 96%). δH (ppm) (DMSO-d_6): 12.05 (1H, s, N-*OH*), 9.20 (1H, s, N-*CH*-N), 7.76,7.48 (2H, s, N-*CH*-*CH*-N), 7.01(2H, s, N-*NH_2*), 5.12 (2H, s, N-*CH_2*-CN), 3.88 (3H, s, N-CH_3), 1.89 (3H, s, CO-C*H_3*) δC (ppm) (DMSO-d_6): 193.28 (s, C-*CO*-C), 148.34 (s, C-*CN*-*O*), 122.58 (s, -N-CH -N), 128.25,128.18 (s, -N-*CH*-*CH*-N), 49.34 (s, N-*CH_2*), 24.12 (s, N-*CH_3*), 8.89 (s, CN-*CH_3*), m/z (ESI+):196.1

2g of 8 was dissolved in 5mL of methanol contains 10g of anion exchange resin. The solution was stirred for another 30mins. The yellow color solution was filtrated and transferred to a vacuum oven. Red solid was obtained. (1.49g, 88%). δH (ppm) (DMSO-d_6): 8.92 (1H, s, N-*CH*-N), 7.50,7.48 (2H, s, N-*CH*-*CH*-N), 5.48(2H, s, N-*NH_2*), 4.96 (2H, s, N-*CH_2*-CN), 3.88 (3H, s, N-CH_3), 2.01 (3H, s, CO-C*H_3*) δC (ppm) (DMSO-d_6): 148.4 (s, C-*CN*-CH_3), 148.15 (s, C-*CN*-CH_2), 137.23 (s, -N-CH -N), 122.14,123.15 (s, -N-*CH*-*CH*-N), 48.56 (s, N-*CH_2*), 23.98 (s, N-*CH_3*), 9.23 (s, CN-*CH_3*).

Summary

In this chapter, an α-oximehydrazone zwitterion-type of ionic liquid was synthesized. This ionic liquid was able to capture equimolar CO_2. In addition, α-oximeketone zwitterion was also synthesized and tested and had no activity towards CO_2, which can be ascribed to the delocalization of the charge. This α-oximehydrazone zwitterion decomposed above 80℃, which can be attributed to the effect that is caused by a conjugated electron-withdrawing group.

Abbreviates

BMIM 1-Butyl-3-methylimidazolium

DCM Dichloromethane

DMF Dimethylformamide

DMSO Dimethyl sulfoxide

NMR Nuclear magnetic resonance

THF Tetrahydrofuran

References

77. S. Choi, J. H. Drese and C. W. Jones, *ChemSusChem*, 2009, **2**, 796-854.
78. J. L. Anthony, E. J. Maginn and J. F. Brennecke, *The Journal of Physical Chemistry B*, 2002, **106**, 7315-7320.
79. E. D. Bates, R. D. Mayton, I. Ntai and J. H. Davis, *Journal of the American Chemical Society*, 2002, **124**, 926-927.
80. J. Zhang, S. Zhang, K. Dong, Y. Zhang, Y. Shen and X. Lv, *Chemistry – A European Journal*, 2006, **12**, 4021-4026.
81. C. Wang, H. Luo, X. Luo, H. Li and S. Dai, *Green Chemistry*, 2010, **12**, 2019-2023.
82. C. Wang, X. Luo, H. Luo, D.-e. Jiang, H. Li and S. Dai, *Angewandte Chemie International Edition*, 2011, **50**, 4918-4922.
83. P. Chakrabarti, V. G. Puranik, J. P. Naskar, S. Hati and D. Datta, 2000.
84. W. Semon and V. Damerell, *Organic Syntheses*, 1930, 22-22.
85. A. H. Mohammed and G. Nagendrappa, *Tetrahedron Letters*, 2003, **44**, 2753-2755.

Chapter 4 Guanidine Tethered Ionic Liquids

Abstract

In this chapter, guanidine functionalized ionic liquids were designed for CO_2 capture purpose. The synthetic strategies of these ionic liquids were explored through multiple ways. A convergent strategy was proven as an effective way of synthesizing guanidine functionalized ionic liquids. The non-substituted ionic liquid was synthesized in 5 steps; the tetramethyl substituted ionic liquid was synthesized in 4 steps. An analogue with zwitterion structure was designed and synthesized to verify the target molecular structure by single crystal X-ray diffraction. Not as we expected, target compounds showed no activity towards CO_2.

Introduction

Guanidines can be classified as nitrogenous analogues of carbonic acid, in which the carbonyl group in carbonic acid is replaced by an imine group, and oxygen is replaced by nitrogen. They have stronger basicity than amines.

A method was developed by Dai's group by mixing an ionic liquid with a basic organic compound such as tetramethylguanidine, 1,8-diazabicyclo [5.4.0] undec-7-ene (DBU) and 1,3,4,6,7,8- hexahydro-1-methyl-2H-pyrimido[1,2-a] pyrimidine (MTBD). With the help of non-nucleophilic super-base, imidazolium cation showed acidity, and its conjugate base will be bonding to CO_2.[79] (Scheme **3.3**) However, super-base as an additive suffered from evaporating from the system.

Results and Discussions

A series of ionic liquids was designed (Figure 4.1) to test the effect of substitution of guanidine on the viscosity.

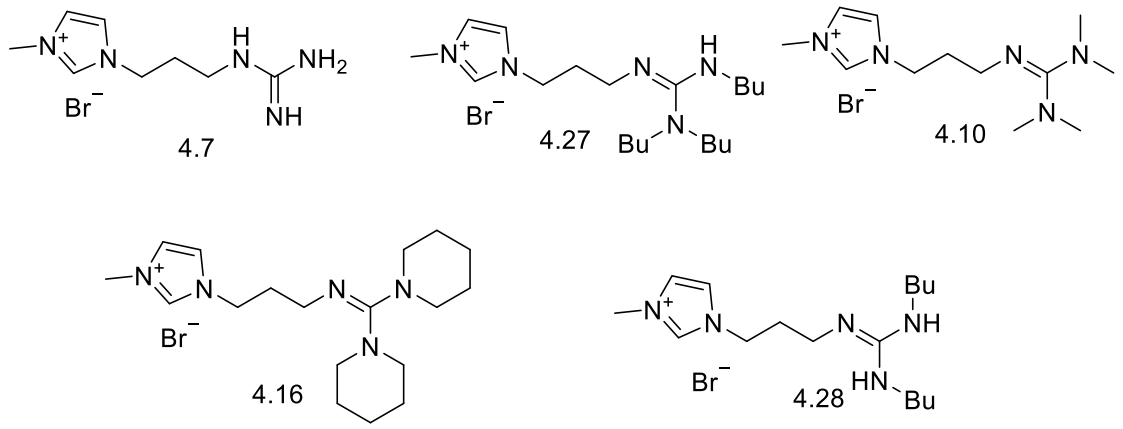

Figure 4.1 Target guanidine functionalized ionic liquids.

Only **4.7** and **4.10** were synthesized as shown in Scheme **4.1**.

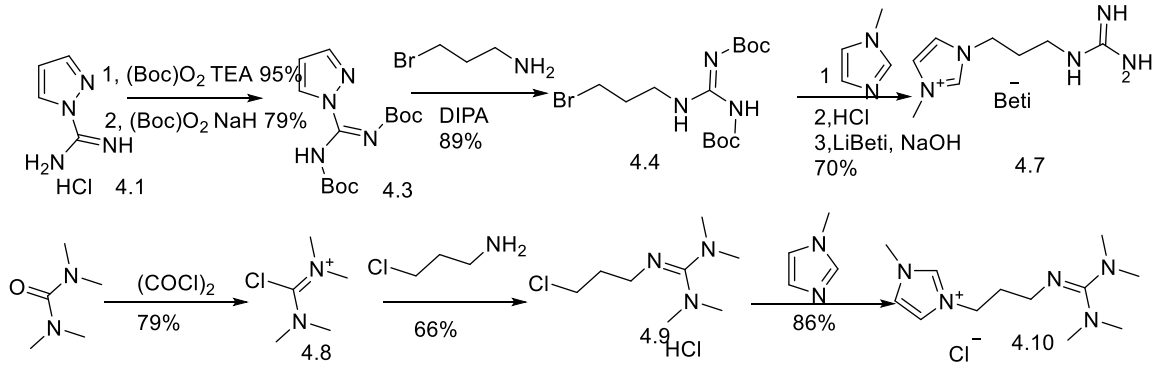

Scheme 4.1 Synthetic route for guanidine-ILs **4.7** and **4.10**.

The CO_2 uptake experiment was tested. However, this material exhibited no capacity towards CO_2.

To prove if the structure of the ionic liquid is right, I synthesized the ionic liquid **4.13**. (Scheme **4.2**)

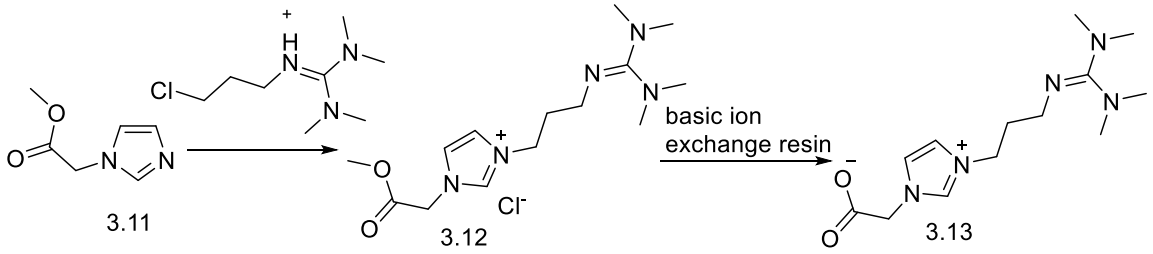

Scheme 4.2 Synthetic route for tetramethylguanidine zwitterion.

The zwitterion is more likely to crystallize because of the higher lattice energy,[86] which enables the crystallization of the ionic liquid and solving the structure of this ionic liquid. A single crystal was grown in DCM with the protection of nitrogen gas. However, a molecule of water is involved in crystal formation (Figure **4.2**).

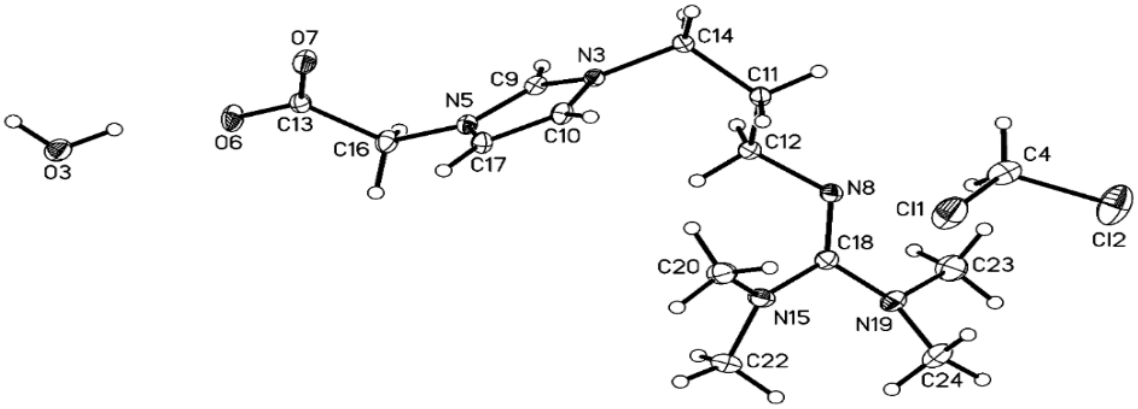

Figure 4.2 Single crystal structure of guanidine zwitterion.

Synthesis of compounds **4.15**, **4.17** and **4.23** was attempted in a linear synthetic route (Scheme **4.3**).

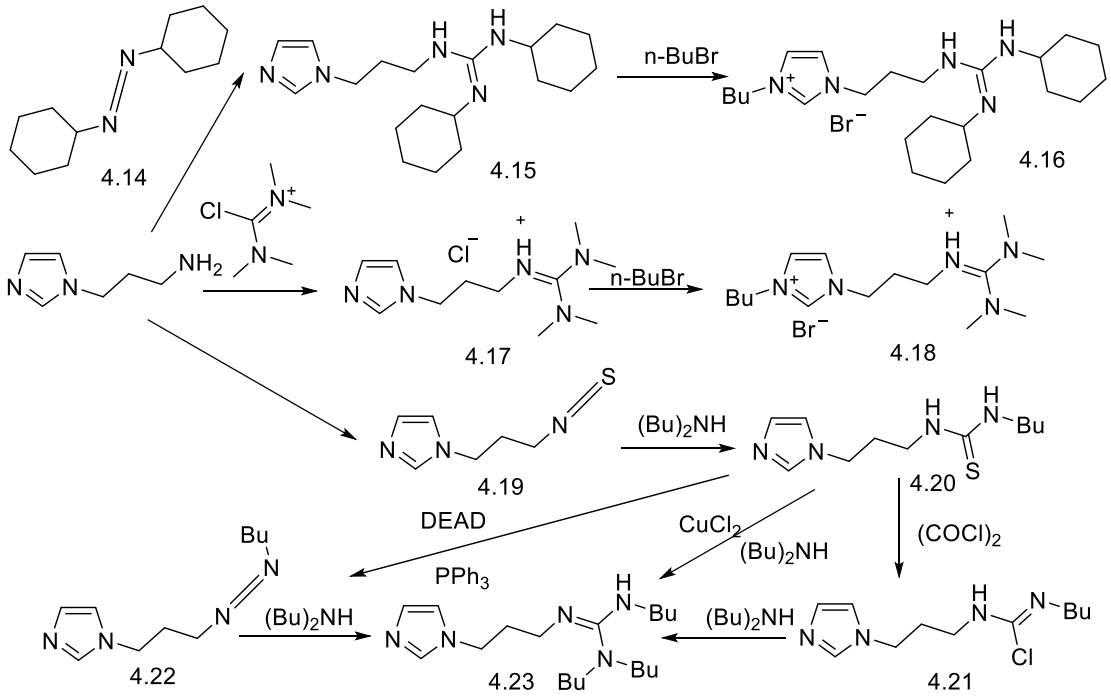

Scheme 4.3 Linear synthetic route for guanidine-ILs.

A linear strategy was proved not a good option for guanidine functionalized ionic liquids, imidazole moiety with another strong polar group made the compound difficult to be purified by normal phase column chromatography. Ionic liquids have properties such as high polarity, non-crystallizable, and negligible vapor pressure makes it hard to be purified through conventional methods. All materials need to be extensively purified before the final formation of quaternary nitrogen. Because of the high polarities, compound **4.15**,**4.17** and **4.23** were unable to be purified by column chromatography. Compound

4.21 was synthesized and applied to next step without a column purification. Compound **4.23** was even detected by mass spectrum in the mixture. Compound **4.22** has strong activity and will be captured by the silica gel. For carbodiimide compounds, distillation was the most common purification method. The Kugelrohr distillation (Figure **4.3**) was applied; however, only triphenylphosphine oxide was condensed.

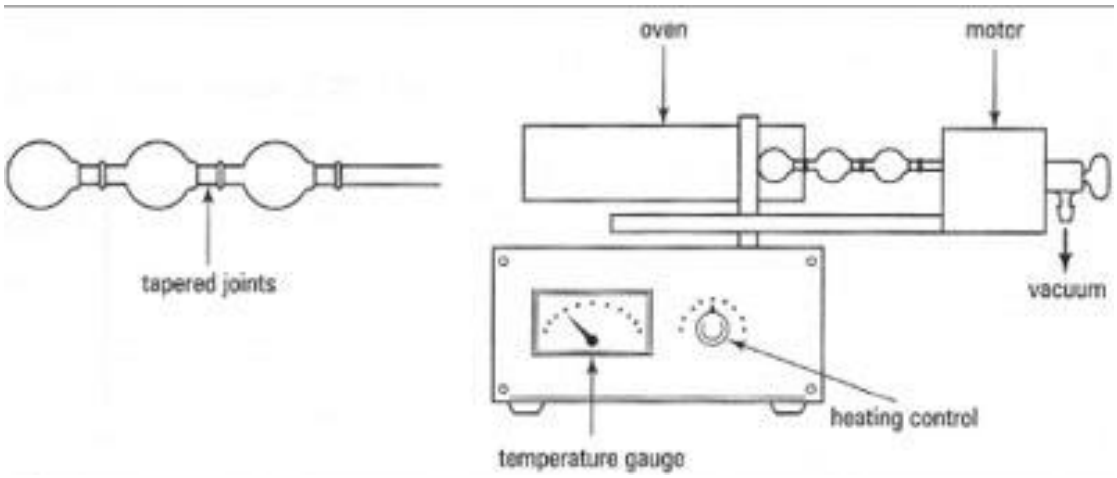

Figure 4.3 Kugelrohr distillation.

Instead of the linear route, I designed a convergent strategy (Scheme **4.4**).

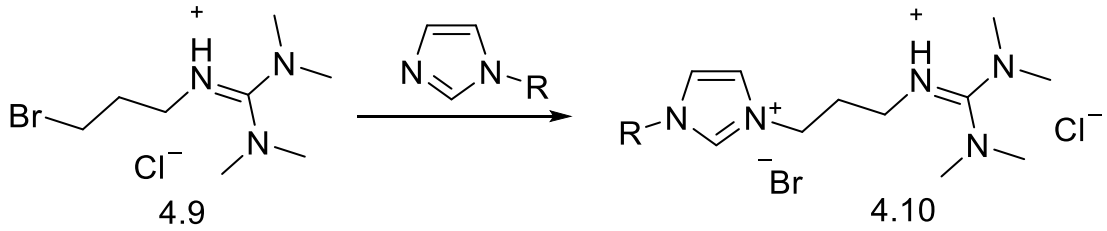

4.9 4.10

Scheme 4.4 Convergent strategy in synthesizing guanidine-ILs.

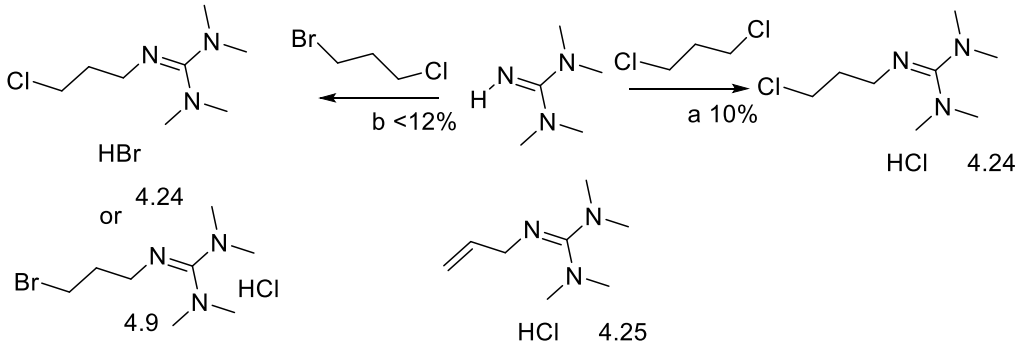

Scheme 4.5 1,3-Dichloropropane and 1-bromo-3-chloropropane as starting materials.

As sketched in Scheme 4.5, I tried to synthesize **4.9** and **4.24** instead of **4.17.** I started from path a, and tetramethylguanidine was applied to react with 1,3-dichloropropane. A highly diluted reaction condition and large excess (5 equivalents) of 1,3-dichloropropane was employed to eliminate the coupling byproducts. However, E2 elimination reaction occurred due to the strong basicity of guanidine, and **4.25** was the unexpected primary product. Another side product, hydrogen chloride, quenched guanidines, which terminated the reaction. The yield was less than 10%. 1,3-Dichloropropane was replaced with 1-bromo-3-chloropropane, at room temperature conditions. However, this still resulted in a mixture of bromide, chloride and a large amount of **4.25.** A compared method using dihalopropane, the Vilsmeier's reagent (Scheme **4.6**) has achieved a much higher conversion.[87]

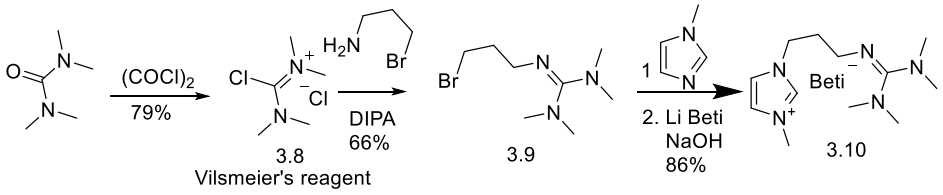

Scheme 4.6 Vilsmeier's reagent

Experimental

Chemicals and materials

1-H-Pyrazole-1-carboxamidine HCl (98%, AK Scitific Inc.), Sodium hydride (60% dispersion in mineral oil, ACROS Organics), Di-*tert*-butyl dicarbonate (99%, Sigma Aldrich), Triethylamine (99%, Fisher Chemical), 3-Chloropropylamine hydrochloride (98%, ACROS Organics), 1-Methylimidazole (99%, ACROS Organics), Bis(trifluoromethane)sulfonimide lithium salt (98%, 3M), Tetramethylurea (99%, Alfa Aesar), Oxalyl chloride (98%, ACROS Organics), Diisopropylamine (Certified, Fisher Chemical), all chemicals above were use directly without further purification. All organic solvents were purchased from Fisher scientific and without any further purification.

Synthetic protocols of non-substituted guanidine-IL (Scheme 4.7)

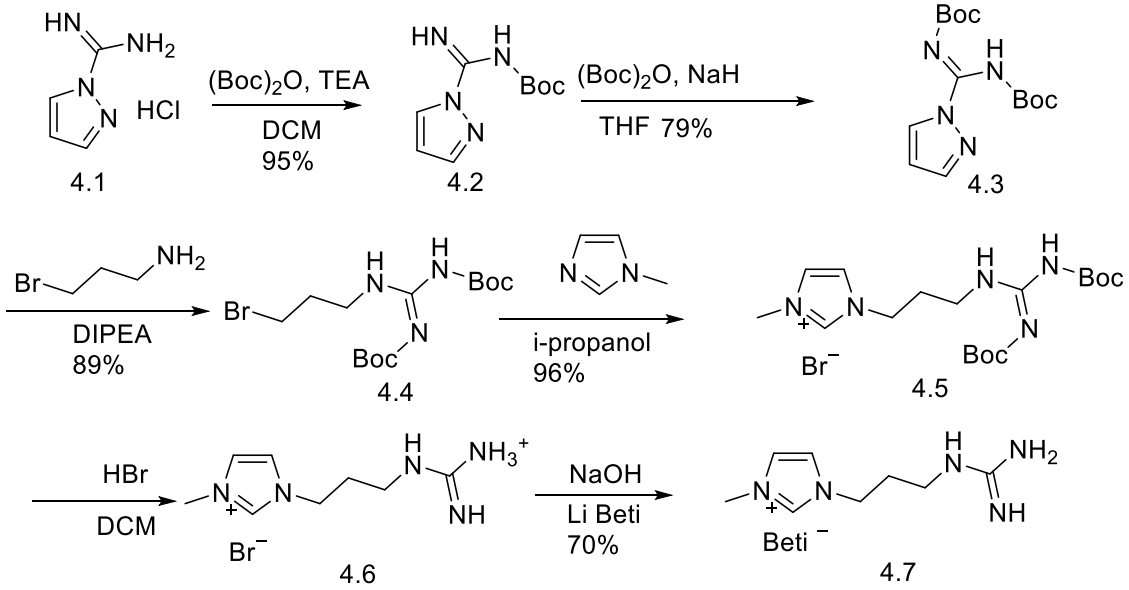

Scheme 4.7 Synthetic route for non-substituted guanidine-IL.

As illustrated in Scheme 4.7, starting with 1-H-pyrazole-1-carboxamidine. The purpose of the first two steps was to protect the active amine group. In the first step, for the protection of amine, a slight excess of $(Boc)_2O$ was used, the excessive $(Boc)_2O$ will not have an impact on the next step. In the second step, NaH was applied to deprotonate the imine to react with an additional one mole of $(Boc)_2O$.[88] This reaction needed to be conducted at a lower temperature. After it was done, the diluted citric acid solution (1M) was applied to decompose excess $(Boc)_2O$. In the third reaction, 3-bromopropylamine hydrobromide was used, and the order of adding reagents was essential in this step. The compound **4.3** was mixed with 3-bromopropylamine hydrobromide firstly, and then diisopropylethylamine was added dropwise. Column chromatography was applied to purify compound **4.4**. In the synthesis of compound **4.5**, a slight excessive **4.4** was used, because 1-methylimidazole was more readily dissolved in water, and **4.4** is insoluble in water. Since the product was more likely to be collected from the aqueous phase, excessive **4.4** can be easily extracted and removed by applying an organic solvent.

N-alkylimidazole was used to produce compound **4.5**. Cleavage of the protection group can be achieved by applying strong acids such as hydrochloride acid or trifluoroacetic acid. In this case, hydrochloride acid was used. In the last step, the ionic liquid was deprotonated by using sodium hydroxide and ion exchange with bis(perfluoroethylsulfonyl)imide (Beti) anion.

*PmImTmG(**4.10**)*

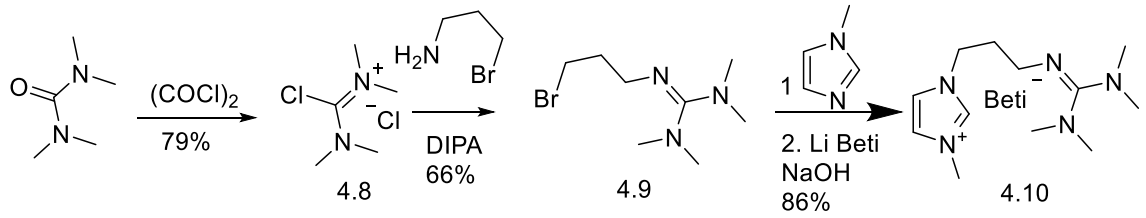

Scheme 4.8 Synthetic protocols for Tetramethylguanidine-ILs.

As sketched in Scheme 4.8, compound **4.8**, an active electrophile agent, was synthesized from tetramethylurea, Compound **4.8** is extremely hydrophilic and easily hydrolyzed to starting material, which requires quickly using up. In the synthesis of compound **4.9** diisopropylethylamine was used as the base, because the bulky size disabled it as a nucleophilic agent. The order of adding agents in this step was critical. The reaction needs to be run in acidic conditions to keep the guanidine group protonated. So, the adding of base needed to be slow and stirred well. The hydrochloride in compound **4.9** will be retained in the last step. Alkylimidazole was applied to react with **4.9** to give **4.10** following by the deprotonation process.

*Synthesis of N-tert-Butoxycarbonyl-1-amidinopyrazole (**4.2**)*

To a 250mL three neck round flask bottle, a 14.5g (0.1 mol) of **4.1** was added in 100mL methylene chloride. Place reactor in an ice bath. Di-tert-butyl dicarbonate (26.16g, 0.12mol) was added in one portion. Triethylamine (15g) was added dropwise within half an hour. Then reaction can react overnights at room temperature. The solvent was then removed carefully not exceed 55℃. Residues were dissolved in water, and extract with 10mL ethyl acetate three times. The organic layer was collected and washed with 10mL saturated sodium chloride solution three times. The organic layer was then dried over anhydrous

sodium sulfate before removing the solvent by reduced pressure. Yield white solid. (21.29g. 95%). δH (ppm) ($CDCl_3$-d_1) 9.17 (1H, br. s, NH), 8.42 (1H, s, N-CH-CH-*CH*-N), 7.68 (2H, m, N-CH-C*H*-CH-N), 6.40 (1H, d, J 1.5 Hz, N-C*H*-CH-CH-N), 1.52 (9H, s, t-Bu), δC (ppm) ($CDCl_3$-d_1) 163.0 (s, N-*CO*-O), 155.2(s, N-*C*N-NH), 142.9(s, N-*C*H-CH-CH-N), 129.1 (s, N-CH-CH-*CH*-N), 109.1 (s, N-CH-C*H*-CH-N), 80.0(s, O-*C*-CH_3), 28.2(s, O-C-*C*H_3). m/z (DART+):210.1

*N-N'-Di-(tert-butoxycarbonyl) guanidine (**4.3**)*

To a 50mL three neck round flask bottle, a 2.1g (0.01 mol) of **4.2** was added in 20mL Tetrahydrofuran. Place reactor in an ice bath. 0.44g of sodium hydride (0.011mol) was then added. Keep stirring for 2 hours. Di-tert-butyl dicarbonate (2.6g, 0.012mol) was added in five portions. Then reaction can react overnights at room temperature. The mixture was first quenched by few drops of methanol, then remove the solvent at a reduced pressure carefully not exceed 55℃. Residues were dissolved in critic acid solution(1M), and extract with 10mL ethyl acetate three times, and the organic layer was collected and washed with 10mL saturated sodium chloride solution three times. The organic layer was then dried over anhydrous sodium sulfate before removing the solvent by reduced pressure. Yield white solid (2.56g, 79%). δH (ppm) ($CDCl_3$-d_1) 9.32 (1H, s, N*H*), 8.52 (1H, s, N-CH-CH-*CH*-N), 7.82 (2H, t, N-CH-C*H*-CH-N), 6.30 (1H, d, N-C*H*-CH-CH-N), 1.56 (18H, s, t-Bu), δC (ppm) ($CDCl_3$-d_1) 168.0 (s, N-*CO*-O), 162.4 (s, NH-*CO*-O), 152.4(s, N-*C*N-NH), 145.2(s, N-*C*H-CH-CH-N), 132.9 (s, N-CH-CH-*CH*-N), 110.2 (s, N-CH-C*H*-CH-N), 86.2(s, *C*-O-CO-NH), 80.0(s, *C*-O-CO-N), 28.2(s, O-C-*C*H_3). m/z (DART+):310.14

*1,2-bis (tert-butyl carbonate)-3-(3-chloropropyl) guanidine (**4.4**)*

To a 50mL three neck round flask bottle, a 3.0g (0.01 mol) of **3.3** was added in 25mL methylene chloride. Place reactor in an ice bath. 3-chloropropane-1-amine hydrochloride (1.56g, 0.12mol) was added. Triethylamine (2mL) was added 5 drops per mins dropwise. Then take off the ice bath, stirring overnights at room temperature. The solvent was then removed carefully not exceed 55℃. Residues were dissolved in water, and extract with 10mL ethyl acetate three times. The organic layer was collected and washed with 10mL saturated sodium chloride solution three times. The organic layer was then dried over anhydrous sodium sulfate before removing the solvent by reduced pressure. Yield oily liquid. (3.1g, 89%) δH (ppm) ($CDCl_3$-d_1) 3.68 (2H, t, Br-C*H*$_2$-), 3.45 (2H, t, Br-CH_2-CH_2-*CH*$_2$), 3.25 (1H, br, CH_2-N*H*-C), 2.12 (2H, m, N-CH-C*H*-CH-N), 1.46,1.52 (18H, s, t-Bu), δC (ppm) ($CDCl_3$-d_1) 162.08 (s, N-*CO*-O), 159.43 (s, NH-*CO*-O), 155.33(s, N-*C*N-NH), 145.2(s, N-*C*H-CH-CH-CH-N), 132.9 (s, N-CH-CH-*CH*-N), 110.2 (s, N-CH-C*H*-CH-N), 84.69(s, *C*-O-CO-NH), 81.2(s, *C*-O-CO-N), 39.45 (s, Br-CH_2-CH_2-C*H*$_2$), 36.43 (s, Br-CH_2-C*H*$_2$-CH_2), 32.38 (s, Br-C*H*$_2$-CH_2-CH_2), 28.2(s, O-C-*C*H_3). m/z (DART+):379.11

1-(3-((bis(tert-butyl carbonate amino)methylene)amino)propyl)-3-methyl-imidazolium Chloride (**4.5**)

To a 50mL three neck round flask bottle, a 3.7g (0.01 mol) of **4.4** was added in 25mL isopropanol. 1-methylimidazole (0.7g, 0.009mol) was added in one potion. Stirring for two hours at room temperature then refluxed overnight. The solvent was then removed under reduced pressure. Residues were dissolved in water, and extract with 10mL

ethyl acetate three times. The aqueous layer was collected. Water was removed by reduced pressure. Yield oily solid. (4.13g, 96%) δH (ppm) (DMSO-d_6) 9.24(1H, s, N-C*H*-N), 7.76, 7.48 (2H, s, N-C*H*-C*H*-N), 4.33(3H, s, N-CH_3), 4.35 (1H, br, CH_2-N*H*-C), 4.25 (2H, t, N-CH_2), 3.72 (2H, t, N-CH_2-CH_2-*C*H_2), 3.35 (2H, t, N-CH_2-CH_2-*C*H_2-NH), 1.48,1.51(18H, s, t-Bu), δC (ppm) (DMSO-d_6) 159.08 (s, N-*CO*-O), 158.43 (s, NH-*CO*-O), 145.48(s, N-*C*N-NH), 143.46(s, N-*C*H-N), 126.38 (s, N-CH2-CH2-N), 126.11 (s, N-CH-C*H*-N), 84.69(s, *C*-O-CO-NH), 83.52(s, *C*-O-CO-N), 38.43 (s, N-CH_2-CH_2-CH_2-NH), 34.43 (s, N-CH_2-CH_2-CH_2-NH), 33.45 (s, NH-CH_2-CH_2-CH_2), 28.4(s, O-C-*C*H_3). m/z (ESI+):382.24

*1-(3-guanidinopropyl)-3-methyl-imidazolium chloride (**4.6** and **4.7**)*

1g of **4.5** is dissolved in 10mL dichloromethane and 2mL of concentrated HCl was added. Keep stirring for 12 hours and remove solvent under reduced pressure. Not until viscose liquid was completely dried in a vacuum oven then dissolved in 10mL of deionized water and a 0.25g of sodium hydroxide was added. The mixture was stirred for 4 hours. 1 g of Lithium bis(perfluoroethylsulfonyl)imide was dissolved in 5mL deionized water and then mixed with the ionic liquid solution. Ion exchange was completed within 10 mins and extracted with 10mL of dichloromethane three times. Yield oil to wax liquid. (0.92g, 70%) δH (ppm) (DMSO-d_6) 8.98(6H, s, N-C*H*-N), 7.98, 7.80 (2H, s, N-C*H*-C*H*-N), 5.25 (4H, br, CH_2-NH_2), 4.45(3H, s, N-CH_3), 4.12 (2H, t, N-CH_2), 3.75 (2H, t, N-CH_2-CH_2-*C*H_2), 3.15 (2H, t, N-CH_2-CH_2-*C*H_2-NH), , δC (ppm) (DMSO-d_6) 149.46(s, N-*C*N-NH), 142.35(s, N-*C*H-N), 125.38 (s, N-CH-*CH*-N), 122.45 (s, N-C*H*-CH-N), 39.15 (s, N-

CH_2-CH_2-C*H_2*-NH), 33.24 (s, N-C*H_2*-CH_2-CH_2-NH), 33.42 (s, NH-CH_2-C*H_2*-CH_2), m/z (ESI+):182.13, (ESI-): 380.14.

*N-[Chloro(dimethylamino)methylene]-N-methylmethanaminium chloride (**4.8**)*

To a 50mL three neck round flask bottle, a 3.7g (0.01 mol) of tetramethylurea was added in 25mL DCM. Oxalyl chloride (10mL) was added dropwise. Stirring overnight in 40℃. The solvent was then removed under reduced pressure. Yield pale yellow solid. (1.35, 79%). δH (ppm) (DMSO-d_6) 3.34(12H, s, C*H_3*). δC (ppm) (DMSO-d_6) 157.9 (*C*=N), 42.4(*C*H_3).

*2-(3-bromopropyl)-1,1,3,3-tetramethylguanidine (**4.9**)*

To a 50mL three neck round flask bottle, a 3.4g (0.02 mol) of **4.8** was added in 25mL DCM with the protection of nitrogen. 3-bromopropane-1-amine hydrobromide (3.3g, 0.019mol) was added in one potion. Placed flask in an ice bath. A 5.16g (0.04mol) of Diisopropylethylamine was then added dropwise (5 drops per minute). The mixture could stir for 12 hours at room temperature. Followed by removing solvent under reduced pressure. Residues were dissolved in water, and extract with 10mL DCM three times, and the aqueous layer was collected. Column chromatography (DCM:MeOH=5:1) was applied. Yield oil to wax solid (3.41g, 63%). δH (ppm) (DMSO-d_6) 3.45(2H, t, Br-C*H_2*). 3.47(2H, s, Br-C*H_2*-CH_2-C*H_2*). 2.24(2H, s, Br-CH_2-C*H_2*-CH_2). δC (ppm) (DMSO-d_6) 159.9 (*C*=N), 54.98(N-*C*H_2-CH_2), 40.4(*C*H_3), 36.25(Br-*C*H_2-CH_2), 29.25(Br-CH_2-*C*H_2). (ESI+): 236.08.

*1-(3-((bis(dimethylamino)methylene)amino)propyl)-3-methylimidazolium Beti (**4.10**)*

To a 50mL three neck round flask bottle, a 3.2g (0.01mol) of **4.9** was added in 25mL isopropanol. 1-methylimidazole (0.95g, 0.011mol) was added in one potion. Stirring for two hours at room temperature then keep 55℃ overnight. The solvent was then removed under reduced pressure. Residues were dissolved in water, and extract with 10mL DCM three times; the aqueous layer was collected. Then a 10 mL solution contains 0.5g of NaOH 5g of LiBeti in 5mL was added in one portion. Extract with 10mL DCM three times, and the organic layer was collected. Remove solvent under reduced pressure. Yield oil liquid (6.1g 86%). δH (ppm) (DMSO-d_6) 8.98(1H, s, N-C*H*-N), 7.54, 7.48 (2H, s, N-C*H*-C*H*-N), 4.29(3H, s, N-CH_3),3.56(2H, t, N-CH_2). 3.12(2H, s, NH-CH_2-CH_2-CH_2), 3.04 (6H, s, CH_3), 2.35(2H, s, N-CH_2-CH_2-CH_2-NH). δC (ppm) (DMSO-d_6) 154.46(N-*C*N-NH), 141.32(N-*C*H-N), 125.09 (N-CH-*CH*-N), 124.25 (s, N-C*H*-CH-N), 42.15 (s, N-CH_2-CH_2-CH_2-NH), 32.84 (s, N-CH_2-CH_2-CH_2-NH) (ESI+): 223.18.

*3-(3-((bis(dimethylamino)methylene)amino)propyl)-1-(2-methoxy-2-oxoethyl)-1H-imidazol-3-ium (**4.12**) and (**4.13**)*

To a 50mL three neck round flask bottle, a 3.2g (0.01mol) of **4.9** was added in 25mL isopropanol. Methyl2-(1-Imidazolyl)acetate (1.54g, 0.011mol) was added in one potion. Stirring for two hours at room temperature then keep 55℃ overnight. The solvent was then removed under reduced pressure. Residues were dissolved in 100mL deionized water, and extract with 10mL DCM three times, and the aqueous layer was collected. 10mL concentrated HCl was then added to aqueous solution and reflux overnight. Water was removed under reduced pressure. Residues were then passed through the anion exchange

resin column. The product was carefully crystalized in DCM. δH (ppm) (DMSO-d_6) 9.02(1H, s, N-C*H*-N), 7.66, 7.54 (2H, s, N-C*H*-C*H*-N), 4.89(3H, s, N-CH_2-CO),3.25(2H, t, N-CH_2). 3.21(2H, s, NH-CH_2-CH_2-CH_2), 3.10 (6H, s, CH_3), 2.38(2H, s, N-CH_2-CH_2-CH_2-NH). δC (ppm) (DMSO-d_6) 174(*C*OO), 155.86(N-*C*N-NH), 142.29(N-*C*H-N), 124.08 (N-CH-*CH*-N), 123.22 (s, N-C*H*-CH-N), 54.3(CH_2-CO), 42.31 (s, N-CH_2-CH_2-CH_2-NH), 32.70 (s, N-CH_2-CH_2-CH_2-NH)

Summary

In this chapter, two guanidine functionalized ionic liquids were synthesized. The synthetic strategy is the vital factor in the synthesis of guanidine type ionic liquids. As same as imidazole moiety, guanidine groups are strong polar groups, which have strong interactions with silica gel. This made the separation unable to be achieved. A modified method was developed by utilizing a convergent strategy. The final product was achieved in an overall yield of 43%. The uptake of CO_2 was tested, and no absorption was observed.

Abbreviates

DCM Dichloromethane

DMSO Dimethyl sulfoxide

THF Tetrahydrofuran

DMF Dimethylformamide

Beti Bis(pentafluoroethanesulfonyl)imide

$(Boc)_2O$ Di-tert-butyl dicarbonate

TEA Triethylamine

References

86. M. Yoshizawa, M. Hirao, K. Ito-Akita and H. Ohno, *Journal of Materials Chemistry*, 2001, **11**, 1057-1062.
87. W. Kantlehner and U. Greiner, *Synthesis*, 1979, **1979**, 339-342.
88. J. A. Castillo-Meléndez and B. T. Golding, *Synthesis*, 2004, **2004**, 1655-1663.

Chapter 5 Amidine Functionalized Ionic Liquids

Abstract

In this chapter, an amidine functionalized ionic liquid was designed for the capture of carbon dioxide, and this ionic liquid was synthesized through a basic strategy. This strategy enabled the synthesis of cyclic amidine in one step by employing sodium methoxide as a base. The reaction was achieved at a higher temperature (100℃). Pure product was obtained without any further purification. However, this amidine functionalized ionic liquid was tested to have no activity toward CO_2. The acidic strategy was also tried by the modified Pinner reaction with *tert*-butanol instead of methanol as a reagent, which exclusively gave birth to an imidic ester, with conversion up to 99%. However, because of the bulky size of *t*-butyl groups, this imidic *t*-butyl ester was unable to be converted to amidine.

Introduction

Many procedures[89] (Scheme **5.1**) have been applied to synthesizing amidine compounds such as those using thioamides,[90] imidic esters,[91] amination of nitriles,[92] or ammonium chloride precursors.[93]

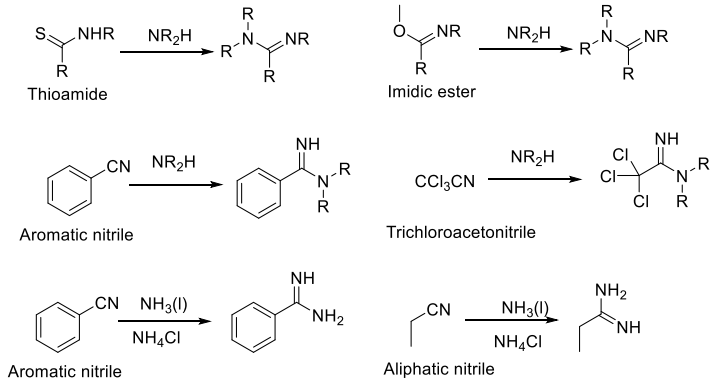

Scheme 5.1 Common synthetic routes to achieve amidine.

The synthesis of amidines through the imidic ester *via* the Pinner reaction is the most common method.[94] In most cases, the Pinner reaction is conducted in an acidic condition, and low temperature is required, usually below 5℃. Hydrochloride acid was found as the only acid that can induce the opening of nitriles. The mechanism is believed a cyclic intermediate state (Scheme **5.2**). [95]

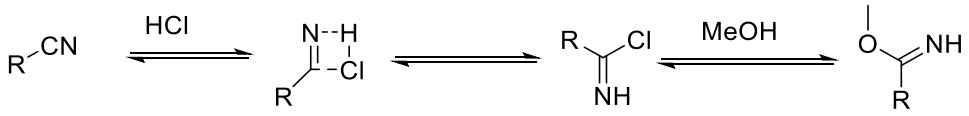

Scheme 5.2 Opening of nitrile induced by Hydrochloride acid.

The unexpected side reactions will occur at high temperature, or in the existence of water (Scheme **5.3**).

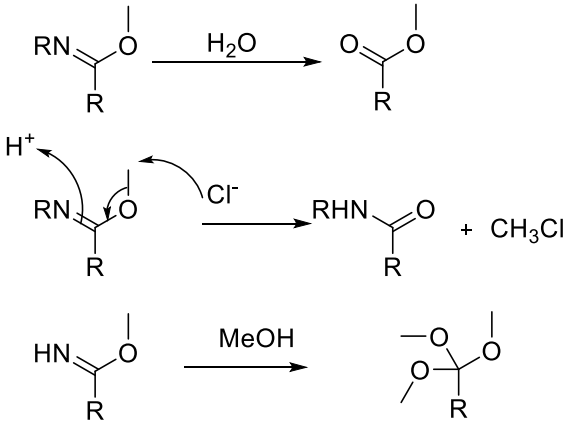

Scheme 5.3 Side reactions.

The basic strategy was also studied,[96] which was firstly investigated by Nef in 1895.[97] In his work, sodium methoxide was used as a base. However, conversions were low (1%) for aliphatic nitriles, and high for aromatic nitriles (100%) or nitriles with electron-withdrawing groups (Scheme **5.4**).

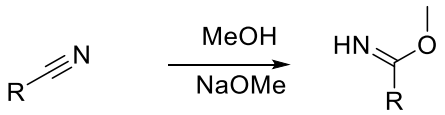

Scheme 5.4 Base assisted method in synthesizing imidic ester.

There are two strategies can introduce a functional group to ionic liquids. One is the synthesis with the using of building blocks that contain functional groups. In this case, amidine is a basic functional group, which requires a protection group to prevent it from reacting with itself (Scheme **5.5**).

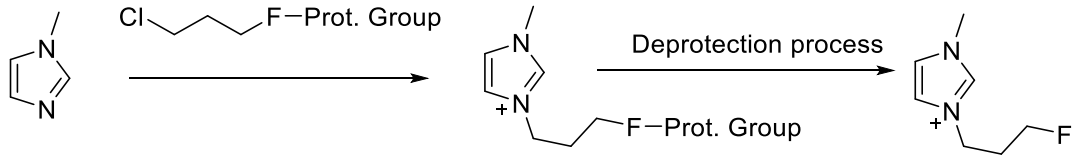

Scheme 5.5 Protective strategy in synthesizing basic group tethered ILs.

Another strategy is to convert one functional group into the desired functional group in the last step, a so-called linear strategy (Scheme **5.6**), which is more restricted in the yield and the post-purification. Because ionic liquids are almost unable to be purified in the last step by classic purification methods such as recrystallization, chromatography, and distillation. Only reactions with a nearly 100% yield can be employed.

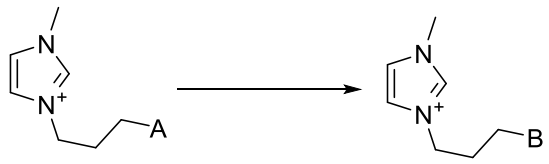

Scheme 5.6 Linear strategy in synthesizing functional ILs.

There is no case that has been studied to introduce an amidine group into the ionic liquid in a straightforward way. The ammonolysis reaction from nitriles to amidines is narrowly limited in the use of metal amides,

acidic conditions with liquid ammonia,[93] or a two-step reaction from an imidic ester.

A sequence of base or acid catalyzed Pinner reaction, and ammonolysis reaction was studied here. (Scheme **5.7**)

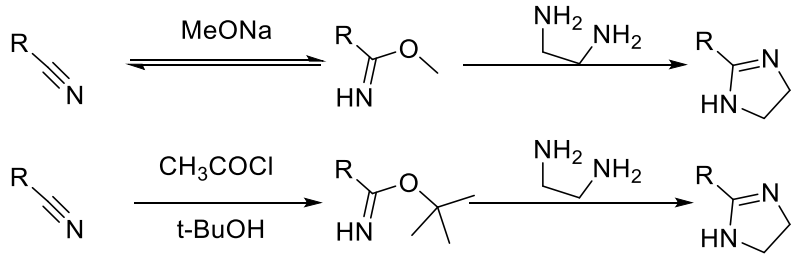

Scheme 5.7 Base/Acid-catalyzed Pinner reaction and ammonolysis reaction.

Results and discussion

Acidic strategy

The acidic condition was first to be considered by applying the classic Pinner reaction. (Scheme **5.8**)

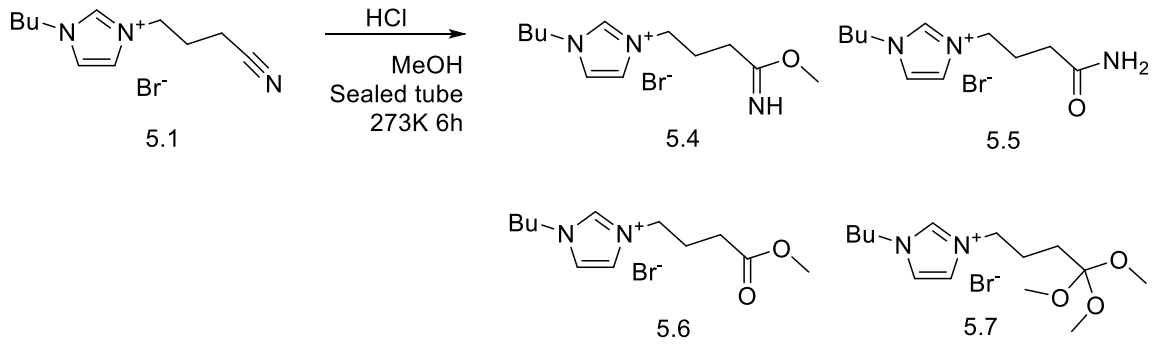

Scheme 5.8 Reaction of nitriles with alcohols in acidic conditions. **5.5**, **5.6** and **5.7** are side-products.

However, unexpected side products occurred irreversibly. To diminish side reactions, the amount of alcohol, temperature, and reaction time needed to be controlled precisely. A higher temperature will result in

the byproducts **5.5** and **5**.**6.** The excess alcohol will give **5.7**. For the conventional compounds, products can be separated and purified by extraction, column chromatography, or distillation. However, none of these techniques were effective for ionic liquids. In this reaction, gaseous HCl was recommended. However, the handle of gaseous HCl is not convenient. In a study, acetyl chloride was used to generate hydrochloride in situ by reacting with methanol[98](Scheme **5.9**).

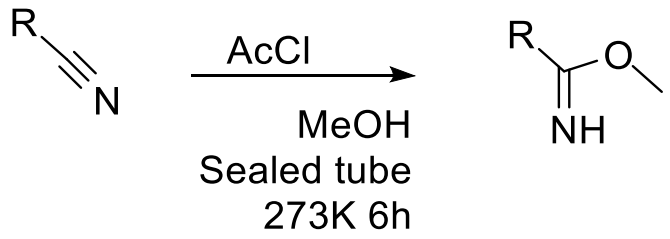

Scheme 5.9 HCl is generated in situ.

Methanol was first to be tried, even with the careful control of temperature, byproducts were still observed. To avoid side reactions, we use a bulky *tert*-butanol in another trial. Because *tert*-butanol is bulkier than other alcohols, this eliminated the possibility of the occurrence of the poly-substituted reaction, and the E2 elimination reaction was also ceased. The reaction was firstly conducted at 0℃. However, no reaction occurred since no product was found within first 60 hours. Then the reaction temperature was adjusted to 100℃ and kept for 24 hours (in a sealed tube). 20% of product (Figure **5.1**) was found by NMR characterization.

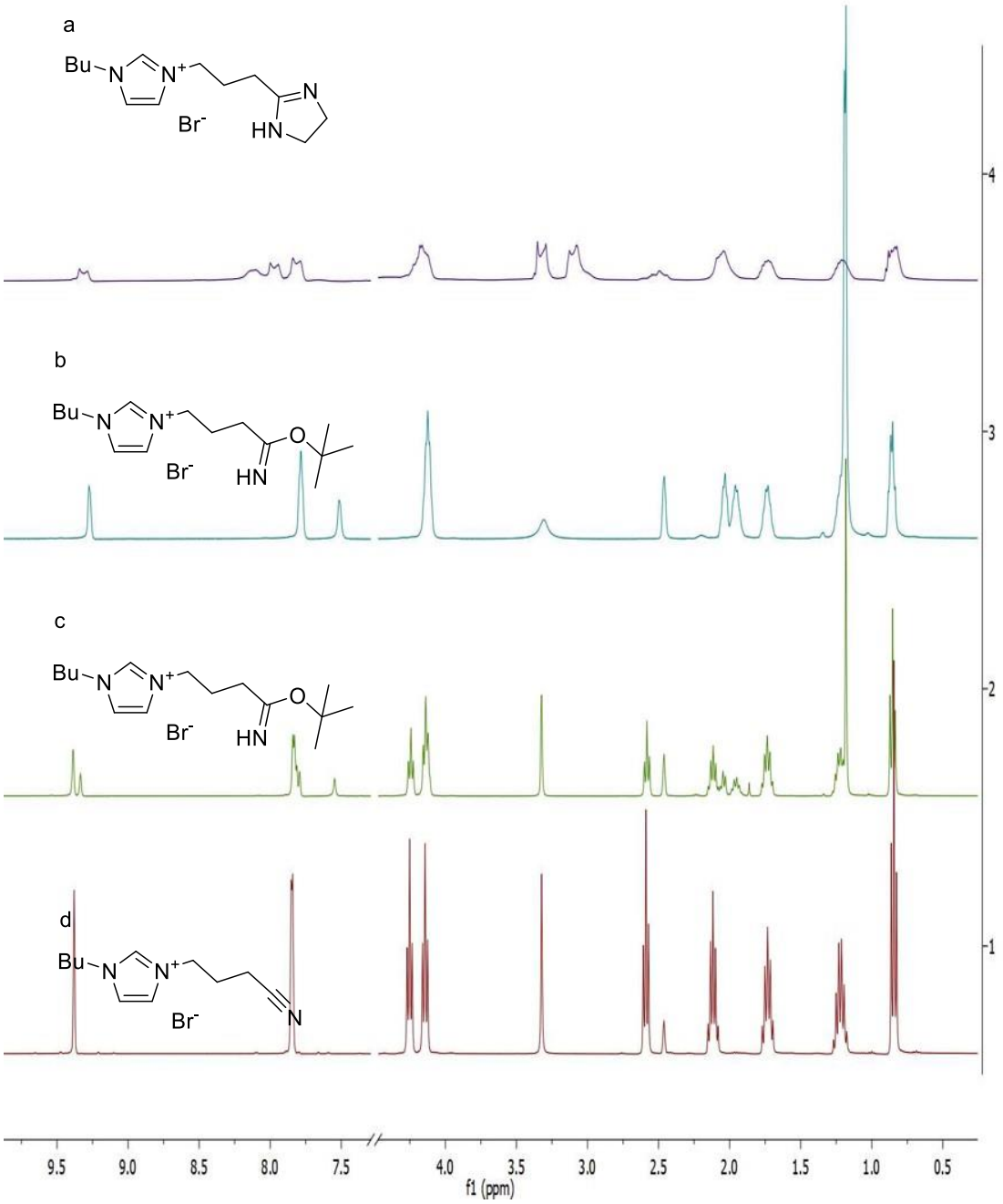

Figure 5.1 a), NMR spectrum of **3** without any purification. b), the reaction of **2** after 60 hours. c), the reaction of **2** after 24 hours. d), starting material **1**

A triple peak at 2.6ppm was shifted to 2.1 ppm with the extension of reaction time (Figure **5.1**. d, c, b). Moreover, the amidine proton had appeared at 7.5ppm. The *t*-Butyl protons had a position at 1.25ppm, which was overlapped with methylene protons. The reaction could be reacted for additional 48 hours, no peak at 2.6 ppm indicated the disappearance of the starting materials. (Figure **5.1**. d) The merging of two peaks at 4.35ppm and 4.2ppm was observed. These two peaks corresponded to the protons in methylene that is adjacent to imidazolium nitrogen.

Under the acidic condition, the imidic ester was synthesized in almost 100% yield, and gaseous ammonia was applied to the following amidine formation reaction (Scheme **5.10**).

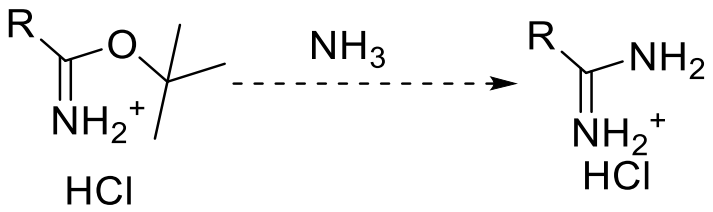

Scheme 5.10 Amidine formation reaction.

The reaction was conducted in a sealed tube at 100℃. However, after 24 hours, starting materials were not consumed at all. The reason can be that ammonia is not as good as other primary amines in term of nucleophilicity. So, ethylenediamine was employed because it has a trend to form a five-member ring, which is both thermodynamically and kinetically favored. However, even after 60 hours, no products were found.

Basic strategy

Sodium methoxide was used as a catalyst; gaseous ammonia was employed as designed (Scheme **5.11**). Gaseous ammonia was bubbled to ice-cold methanol for 5 mins. The reaction then allowed to react for 60 hours at 100℃ in a sealed tube. No any new peak appeared in NMR spectrum indicated no reaction occurred. Alternatively, ethylenediamine was used.

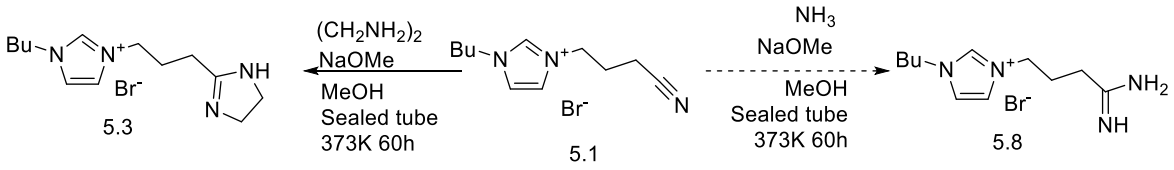

Scheme 5.11 Ammonia or ethylene diamine as nucleophiles.

The reaction was completed within 48 hours with a good yield by NMR analysis (Figure **5.1** a).

Experimental

Experiment chemicals and materials

1-butylimidazole (TCI, 98%), 4-Bromobutyronitrile (Sigma-Aldrich, 97%), Ethylenediamine (ACROS Organics, 99%), Acetyl chloride (ACROS Organics,99%), Sodium methoxide (ACROS Organics,97%). All chemicals above were used directly without further purification. All organic solvents were purchased from Fisher scientific and without any further purification. Compound **5.2** and **5.3** were synthesized from **5.1**

(1-butyl-3-(3-cyanopropyl)imidazolium Bromide) (Scheme **5.12**)

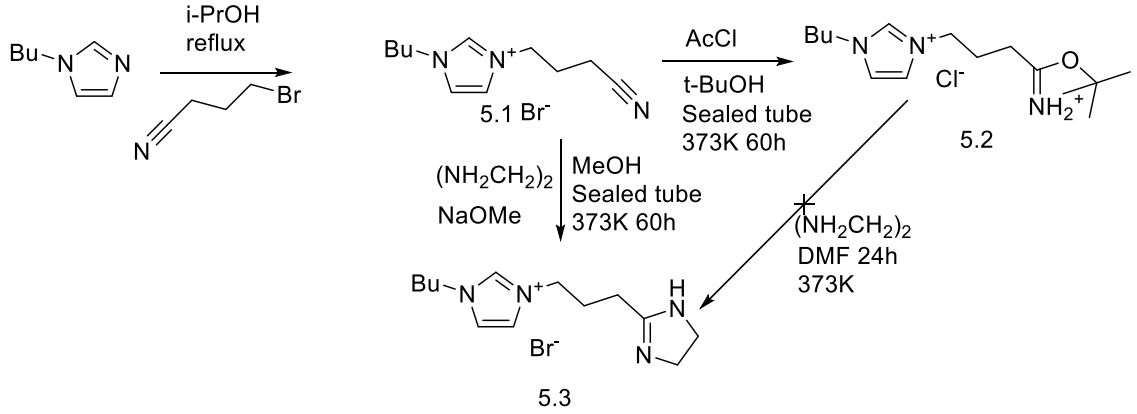

Scheme 5.12 synthetic route for cyclic amidine-ILs.

*1-butyl-3-(3-cyanopropyl)imidazolium Bromide (**5.1**)*

To a 50mL three neck round flask bottle, a 12.4g (0.1 mol) of 1-butylimidazole was added in 30mL *iso*-Propanol. The reactor was stirred in an ice bath. A 16.6g (0.11mol) of 4-bromobutylnitrile was added slowly in one portion. The temperature was then raised to flux overnights at room temperature. The solvent was then removed carefully not exceed 55℃. Oily honey colored residues were dissolved in deionized water, and extract with 10mL of ethyl acetate three times, and the aqueous layer was collected, the solvent was removed by reduced pressure. Honey colored oil product was obtained. (22.65g, 98%). δH (ppm) (DMSO-d_6) 9.33(1H, s, N-C*H*-N), 7.98 (2H, s, N-C*H*-C*H*-N), 4.25(2H, t, N-C$H_2$$CH_2CH_2CH_3$), 4.12 (2H, t, N-C$H_2$-$CH_2CH_2CH_2$), 2.65 (2H, t, C$H_2$-CN), 2.10 (2H, tt, N-$CH_2$-C$H_2$-$CH_2$), 1.74 (2H, dd, N-$CH_2$-$CH_2$-$CH_2$-$CH_3$), 1.23(2H, dt, N-$CH_2$-$CH_2$-C$H_2$-$CH_3$), 0.79(3H, t, CH_2-CH_3). δC (ppm) (DMSO-d_6) 143.46(N-*C*H-N), 126.38 (N-*C*H-CH-N), 126.11 (N-CH-*CH*-N), 122.8(-*C*N), 53.6(N-CH_2-CH_2-

CH_2-CH_3), 52.43 (N-*CH_2*-CH_2-*CH_2*-CN), 34.43 (N-CH_2-*CH_2*-CH_2-CN), 30.25 (N-CH_2-C*H_2*-CH_2-CH_3), 20.4(*CH_2*-CH_3), 14.4(*CH_2*-CN),. m/z (ESI+):192.18

*3-(4-(tert-butoxy)-4-iminobutyl)-1-butylimidazolium chloride (**5.2**)*

To a 50mL thick wall tube equipped with Teflon cap, 1g of **5.1** was added in 20mL *t*-Butanol. The tube was cooled down to -20℃ and 2.2g of acetyl chloride were added dropwise. Then put the reactor into an oil bath and stirring for 60 hours under 100℃. To monitor the extent of reaction, we tested the sample by NMR. Then, the solvent was removed by blowing in dry nitrogen under 100℃ for 5 hours. Yield clear liquid. (1.5g, 97%) δH (ppm) (DMSO-d_6) 9.37(1H, s, N-C*H*-N), 7.92(1H, br, N*H*), 7.87 (2H, s, N-C*H*-C*H*-N), 4.22(2H, t, N-C*H_2*$CH_2CH_2CH_3$), 4.21 (2H, t, N-C*H_2*-$CH_2CH_2CH_2$), 2.10 (2H, tt, N-CH_2-C*H_2*-*C*H_2), 2.05 (2H, t, C*H_2*-C=N), 1.74 (2H, tt, N-CH_2-*CH_2*-CH_2-CH_3), 1.23(2H, qt, N-CH_2-CH_2-C*H_2*-CH_3),1.21(9H, s, t-Bu) 0.79(3H, t, CH_2-C*H_3*). δC (ppm) (DMSO-d_6) 143.46(N-*C*H-N), 126.38 (N-*C*H-CH-N), 126.11 (N-CH-*CH*-N), 53.6(N-*CH_2*-CH_2-CH_2-CH_3), 52.43 (N-*CH_2*-CH_2-*CH_2*-C=N), 34.43 (N-CH_2-*CH_2*-CH_2-CN), 30.25 (N-CH_2-C*H_2*-CH_2-CH_3), 20.4(*CH_2*-CH_3), 14.4(*CH_2*-CN),. m/z (ESI+):133.61

*1-butyl-3-(3-(4,5-dihydro-1H-imidazole-2-yl)propyl)imidazolium bromide(**5.3**)*

To a 50mL three neck round bottle, equipped with a condenser. 1g (0.0036mol) of **4.1** was added in 20mL dimethylformamide. Followed by 0.04g (0.72mmol) of Sodium Methoxide. 2g of Ethylene diamine was added in one portion. Then the reactor was placed to 100℃ oil bath and stirring for 60 hours. To monitor the extent of reaction, I tested

the sample by NMR. Then, the solvent was removed by blowing in dry nitrogen under 100 ℃ for 5 hours. Yield syrup colored liquid. (0.93g, 95%). δH (ppm) (DMSO-d_6) 9.39(1H, s, N-C*H*-N), 7.89 (2H, s, N-C*H*-C*H*-N), 4.22(2H, t, N-C*H*$_2$CH$_2$CH$_2$CH$_3$), 4.21 (2H, t, N-C*H*$_2$-CH$_2$CH$_2$CH$_2$), 3.32 (4H, t, NH-*CH*$_2$-*CH*$_2$-NH), 2.10 (2H, tt, N-CH$_2$-C*H*$_2$-*C*H$_2$), 2.09 (2H, t, C*H*$_2$-C=N), 1.73 (2H, tt, N-CH$_2$-*CH*$_2$-CH$_2$-CH$_3$), 1.22(2H, qt, N-CH$_2$-CH$_2$-C*H*$_2$-CH$_3$), 0.79(3H, t, CH$_2$-C*H*$_3$). δC (ppm) (DMSO-d_6) 159.3(*C*=N), 143.40(N-*C*H-N), 126.26 (N-*C*H-CH-N), 126.15 (N-CH-*CH*-N), 53.6(N-*CH*$_2$-CH$_2$-CH$_2$-CH$_3$), 52.43 (N-*CH*$_2$-CH$_2$-CH$_2$-C=N), 34.43 (N-CH$_2$-*C*H$_2$-C*H*$_2$-C=N), 30.25 (N-CH$_2$-C*H*$_2$-CH$_2$-CH$_3$), 22.8(*CH*$_2$-CH$_2$-C=N), 20.34(*CH*$_2$-CH$_3$), 14.5(*CH*$_2$-CN),. m/z (ESI+): 235.19

Summary

In this work, amidine functionalized ionic liquid was synthesized through the basic strategy. The final product of high purity was obtained. A CO_2 uptake test was conducted by a bubbling method, but no chemical absorption was found during CO_2 uptake process. A modified Pinner reaction was investigated and proved that the *tert*-butanol cannot function well as primary alcohols. In addition, the activity of ethylene diamine and ammonia was compared, and it turned out that ammonia was too weak to react with the imidic ester.

Abbreviates

DCM Dichloromethane

DMSO Dimethyl sulfoxide

NMR Nuclear magnetic resonance

References

90. D. J. Heldebrant, P. K. Koech, M. T. C. Ang, C. Liang, J. E. Rainbolt, C. R. Yonker and P. G. Jessop, *Green Chemistry*, 2010, **12**, 713-721.
91. R. L. Shriner and F. W. Neumann, *Chemical Reviews*, 1944, **35**, 351-425.
92. G. BESPALOVA, V. SEDAVKINA and L. KULIKOVA, *KHIMIKO-FARMATSEVTICHESKII ZHURNAL*, 1989, **23**, 949-952.
93. D. D. Le, A. T. Cortesi, S. A. Myers, A. L. Burlingame and D. G. Fujimori, *Journal of the American Chemical Society*, 2013, **135**, 2879-2882.
94. H. Wang, Y. Wang, D. Liang, L. Liu, J. Zhang and Q. Zhu, *Angewandte Chemie International Edition*, 2011, **50**, 5678-5681.
95. E. F. Cornell, *Journal of the American Chemical Society*, 1928, **50**, 3311-3318.
96. Z. Wang, in *Comprehensive Organic Name Reactions and Reagents*, John Wiley & Sons, Inc., 2010, DOI: 10.1002/9780470638859.conrr504.
97. S. Peterson and J. M. Williams, *Journal of the American Chemical Society*, 1966, **88**, 2866-2866.
98. F. C. Schaefer and G. A. Peters, *The Journal of Organic Chemistry*, 1961, **26**, 412-418.
99. J. U. Nef, *Justus Liebigs Annalen der Chemie*, 1895, **287**, 265-359.
100. E. Kozma, G. Estrada Girona, G. Paci, E. A. Lemke and P. Kele, *Chemical Communications*, 2017, **53**, 6696-6699.

Chapter 6 Ultra-pure Ionic Liquid as An Electrolyte

This chapter is a revised version of an original publication by Junjun Peng, Nanqing Chen, Rui He, Zhiyong Wang, Sheng Dai, Xianbo Jin. I only provided the ultra-pure ionic liquid and did some basic electrochemical tests.

Peng, J.; Chen, N.; He, R.; Wang, Z.; Dai, S.; Jin, X., Electrochemically Driven Transformation of Amorphous Carbons to Crystalline Graphite Nanoflakes: A Facile and Mild Graphitization Method. *Angewandte Chemie* 129 (7), 1777-1781

Abstract

In this chapter, an ultra-pure ionic liquid (N-butyl-N-methylpyrrolidinium bis-trifluoromethanesulfonylimide) was synthesized as an electrolyte in characterizing battery materials. Electrode materials, porous petaloid graphite nanoflake, was synthesized by melting salt method electrochemically in molten $CaCl_2$ (1100K). It allows a fast and reversible insert and disinsert of ion, which makes it a promising material for use as an electrode in a battery. The performance of this graphite was tested in an ionic liquid electrolyte. A 116mAhg^{-1} capacity was achieved at a rate of 1800mAg^{-1} when charged to 5.25V, and capacity stayed stable during multiple cycling. Only a decrease of about 8% was noticed when the charge and discharge rate was adjusted to 10000mAg^{-1} .

Introduction

Graphite is a thermodynamically stable allotrope of carbon. It is hard to convert amorphous carbon into graphite. The transformation of amorphous carbon to graphite is highly demanded in the industry.[99] The conditions for this process usually require higher temperatures and pressures.[100] However, only limited amorphous carbon can be converted to graphite under the high temperature and the high-pressure method,[101] all others are believed to be non-convertible to graphite. Graphitization of amorphous carbon in relatively lower temperature is in high demand. Some transition metals were utilized in the transformation of amorphous carbon at 1300K, but this method has the main drawback that a large amount of catalyst was unable to be removed.[102, 103]

This method provides a compatible way to convert those believed “non-convertible” carbon to graphite. In mild conditions (1300K), molten calcium chloride was employed as media, and petaloid like graphite was synthesized. Carbon black (CB, XC-72) was used to illustrate the transformation.

Results and discussion

The ultra-pure ionic liquid $Pyr_{14}TFSI$: (N-butyl-N-methylpyrrolidinium bis-trifluoromethanesulfonyl-imide) was synthesized (Scheme 6.1).

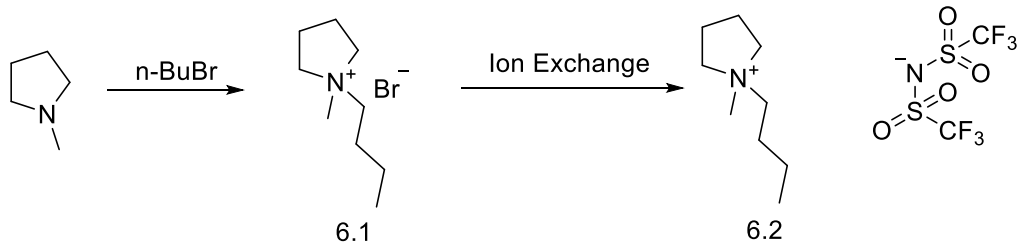

Scheme 6.1 Synthetic route for $Pyr_{14}TFSI$.

The synthesis of ultra-pure ionic liquids is critical for the following test. Conventional methods in purifying ionic liquid by washing with organic solvent, cannot meet this requirement. The potential window of ionic liquid $Pyr_{14}TFSI$ is about 5.7 V (Figure **6.1**). This enables the insertion and desertion of TFSI ion in graphite.

After the electrochemical graphitization of carbon black, a significant change in morphology was proven by the scanning electron microscopy (Figure **6.2**).

The size of nanoparticles in carbon black was 30-100 nm in diameter, which dramatically dropped to 1nm and 10-20nm in thickness, while the shape changed from amorphous to petaloid-like flakes.

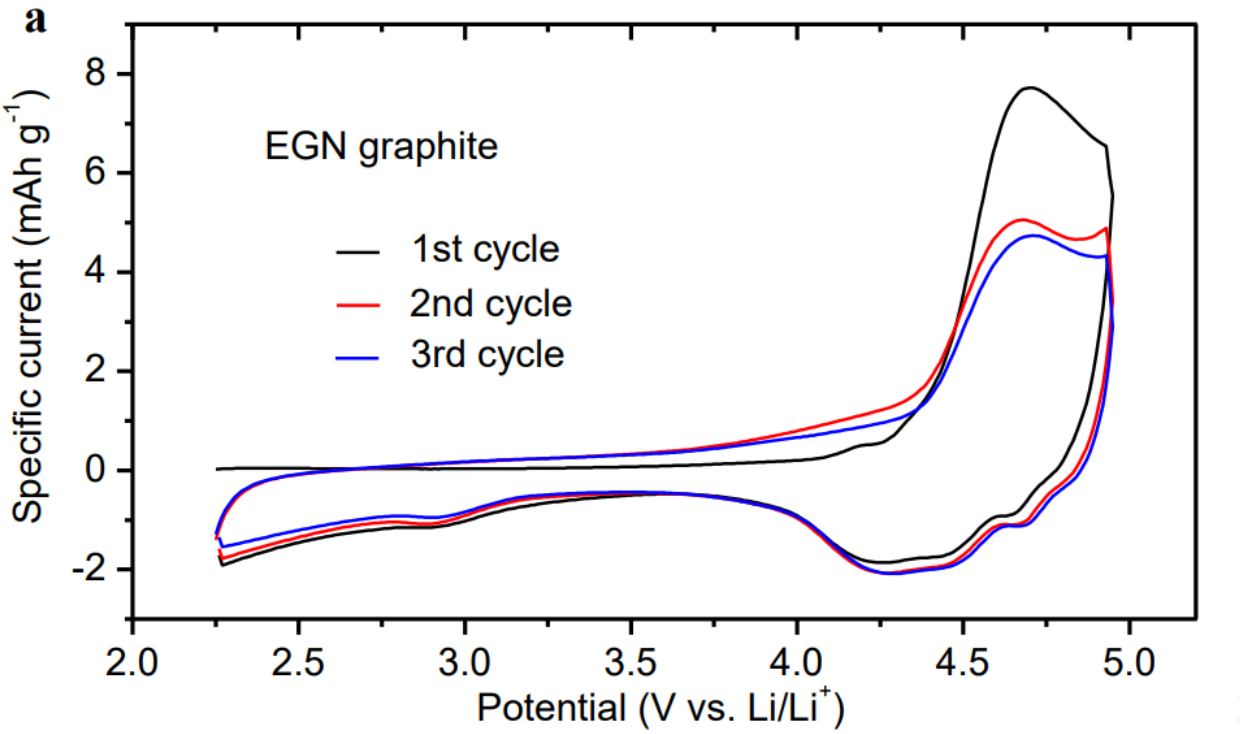

Figure 6.1 Cycle voltammograms (CVs) at a scan rate of 10 mVs^{-1}

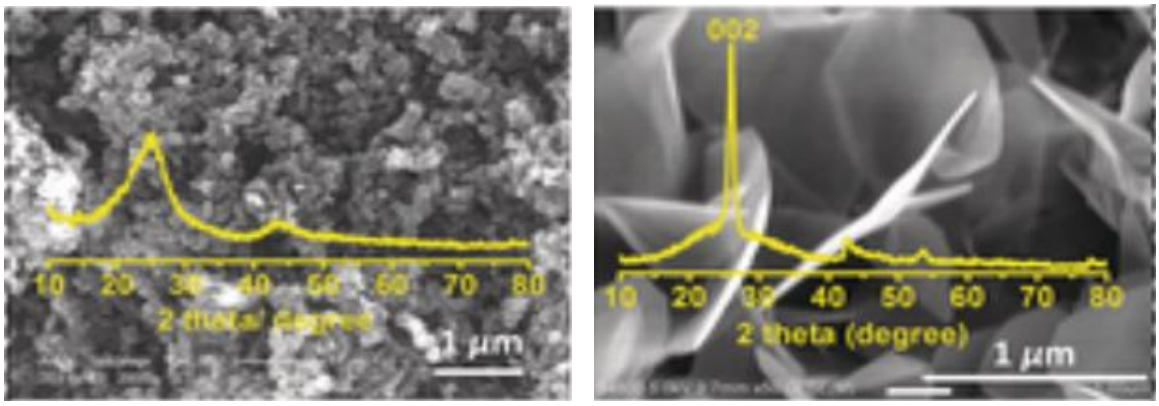

Figure 6.2 Left amorphous carbon, Right graphite.

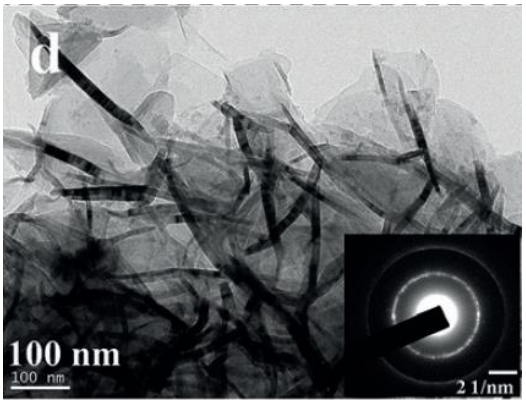

Figure 6.3 TEM of flake like graphite.

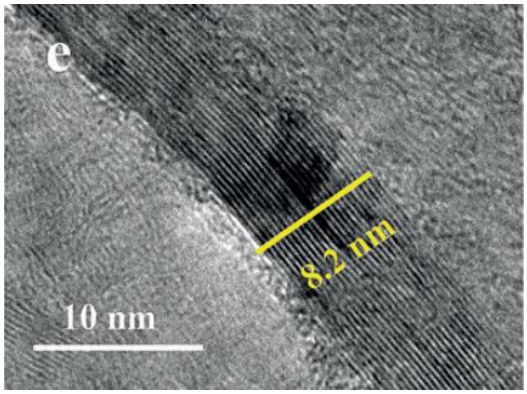

Figure 6.4 Thickness of graphite

Figure 6.3 is a TEM image of these flakes. Figure 6.4 shows that the thickness of a single flake is about 8.2 nm. A 24–25 layer of graphitic planes suggested a lamellar spacing of 0.33–0.34 nm, which greatly matches the structure of graphite. A possible mechanism is the existence of a long distance rearrangement during the electrochemical process, which is different from another graphitization process such as transition metal induced high-temperature graphitization, during which an onion-like carbon is produced[104]. A significant disadvantage in traditional graphitization process, which utilized transition metals as catalysts is the existence of largely excessive transition metal residues. However, as depicted by TGA (Figure **6.5**) and XPS (Figure **6.6**), no $CaCl_2$ was found. Figure **6.7** and Figure **6.8** provide the solid evidence of the existence of long-distance rearrangement during the graphitization process. After a polarization process in cathode at 2.4 V and 1100 K for 2 h, the petaloid-like flakes formed (Figure **6.7**). There are no significant changes before and after graphitization.

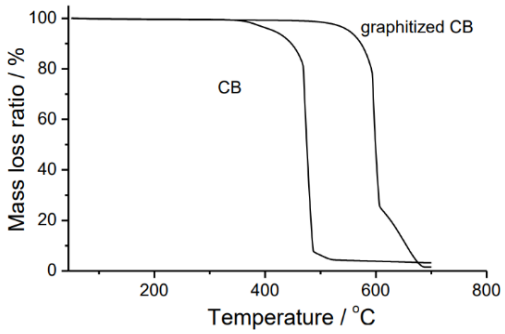

Figure 6.5 TGA curves of Carbon Black (CB), and graphitized carbon black.

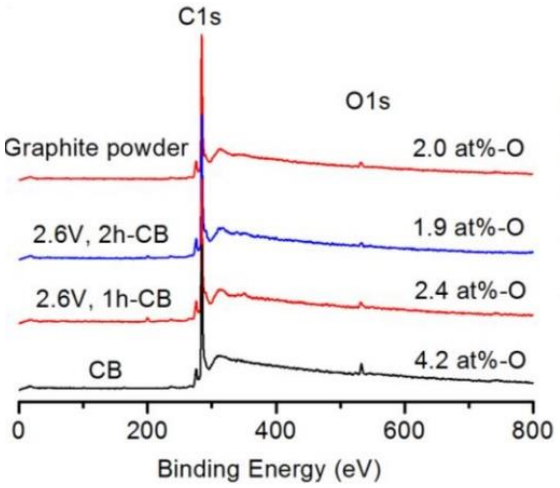

Figure 6.6 XPS patterns of CB before and after a constant voltage at 2.6 V for 1 h and 2h. Reveal a deoxygenation process.

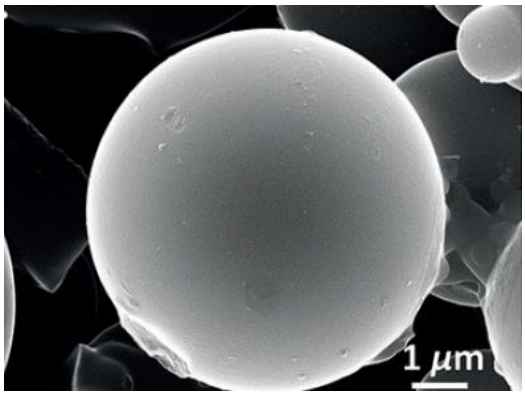

Figure 6.7 SEM of Carbon Black (CB).

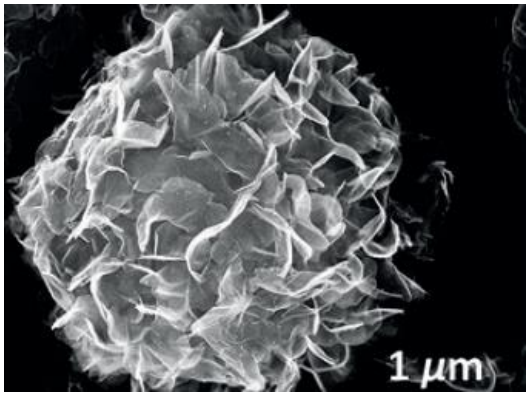

Figure 6.8 SEM of graphitized carbon black.

It is also evidence that this electric process occurs from the surface of particles, which enables the formation of graphite particle with the same size. Followed by the diffusion of less stable carbon black particles to graphite, this eventually forms a 25-layer graphite. These discoveries reveal mobility of carbon atom in melting calcium chloride media.

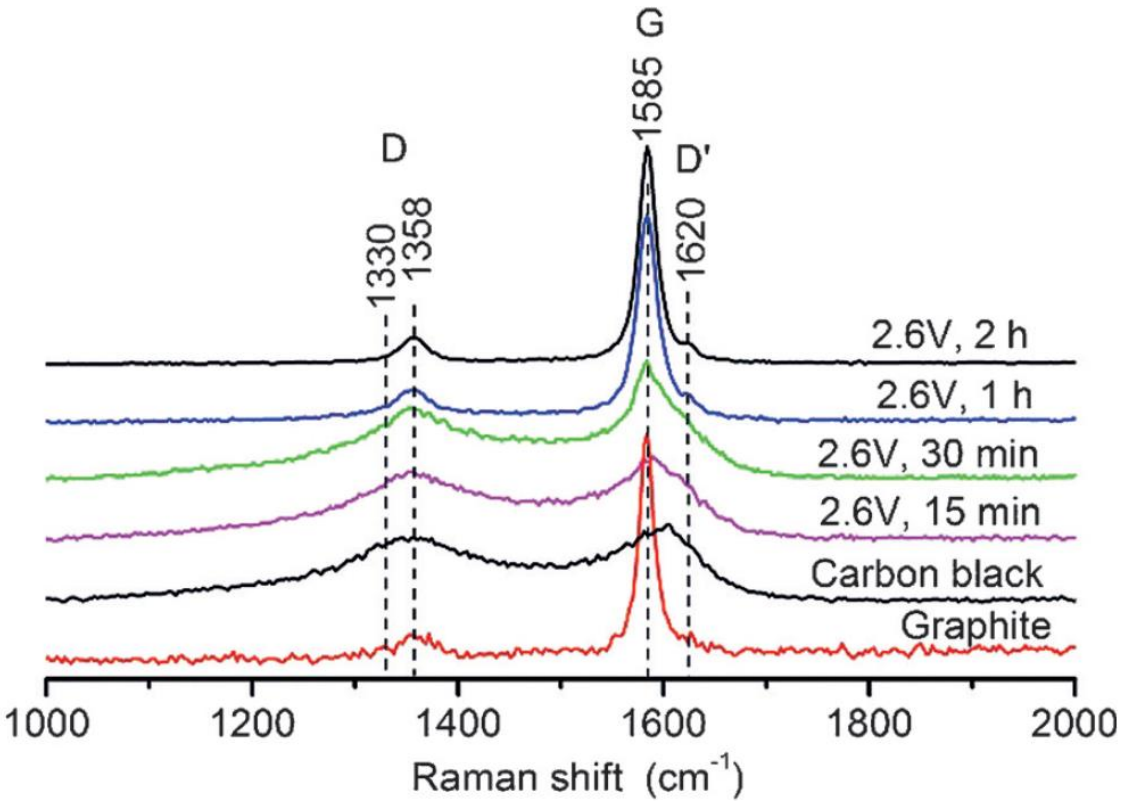

Figure 6.9 Raman- spectrum of graphitization process.

A Raman Spectrum (Figure **6.9**) was utilized to monitor the extent of graphitization. The graphite has a strong peak at 1580cm^{-1}, which represents the sp^2 hybridization of the graphite. A peak at 1360cm^{-1} corresponds to the disordered carbon, and a peak at 1330cm^{-1} represents the sp^3 hybridization of carbon atoms.

The effect of the cathodic potential in the graphitization process has been studied by employing a molybdenum cavity electrode to measure the cyclic voltammogram (CV).

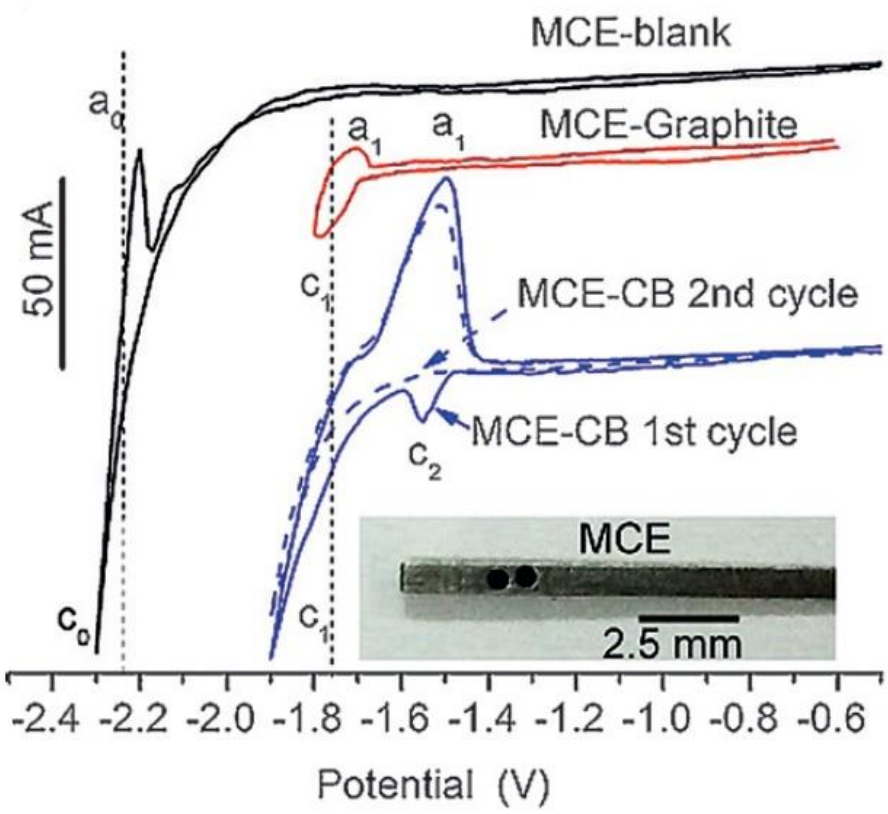

Figure 6.10 CVs of the molybdenum cavity electrode, and MCEs loaded with carbon black (CB) and graphite powder in $CaCl_2$ at 1093 K (20 mVs@1).

A redox couple (C_0/A_0) at around 2.23V is attributed to the deposition and redissolution of calcium (Figure **6.10**). After loading with graphite powder, a redox couple (C_1/A_1) occurred at around 1.77 V, which represents the oxidation and re-oxidation of CaC_2. Corresponding to the higher surface area, C_1/A_1 is greater when compared with graphite.

Before C_1, a reduction peak C_2 appeared at potentials ranging from 1.48 V to 1.6 V, which can be attributed to the oxygen atoms bonded to the surface. It matches the result why this phenomenon always occurs in the first scan. It also corresponds to the Fusion Oxygen Analysis result (4.8 wt% in carbon black).

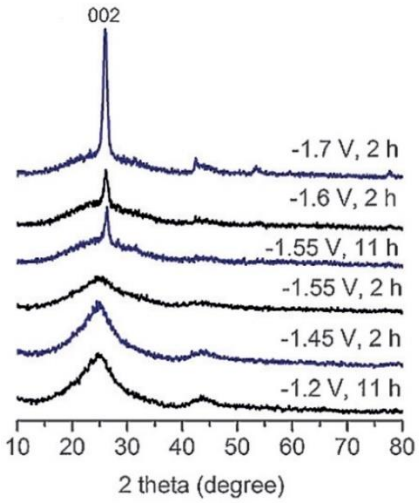

Figure 6.11 XRD patterns of CB after cathodic polarization at different potentials for the times indicated.

C_2 could be the signal that removes oxygen atoms in the carbon black $O@C+2e^-=C+O_2$. The removal of oxygen from metal oxides in molten salt media electro-chemically, such as TiO_2 is much easy.[105]It was found with fewer oxygen atoms on the surface; a better graphitization can be achieved. Simply by starting with a more negative potential than C_2(1.6) (Figure **6.11**). It also indicates to achieve a faster graphitization rate; a larger polarization potential is needed. Meanwhile, the formation of CaC_2 needs to be reduced by a higher polarization potential than -

1.77V. The formation of CaC_2 will cause a significant loss of carbon (Table 6.1).

Table 6.1 The carbon recovery after electrolysis carbon black in $CaCl_2$ at 1093 K.

Electrode potential	Time	Carbon Recovery
Open potential	10	93.2%
-1.45V	2	94%
-1.55V	2	86.7%
-1.55V	11	80.4%
-1.6V	2	80%
-1.7V	2	50.9%
-1.8V	2	13.7%
-1.9V	1	5.2%

A quick graphitization with 80% yield can be achieved by the potential at around 1.6 V. The loss of mass could be partially attributed to the removal of oxygen. When the carbon was recovered by washing the sample, the loss of carbon particles was observed, which can be reduced by optimizing electrode designs or operations. The effect of both temperature and time on the graphitization process was also studied and revealed critical roles played by these two factors in the structural transformation. Furthermore, the cathodic polarization of carbon black was carried out in a mixture of molten salts of NaCl and $CaCl_2$. The melting point for the pure NaCl is 820℃. The graphitization process was conducted in the mixture of $CaCl_2$ and NaCl because

NaCl was unable to accommodate O^{2-} ions, which makes it difficult to remove oxygen from the carbon black surface.

For a long time, the anode in lithium-ion batteries was made from graphite, because the reversible intercalation and deintercalation of lithium ions are allowed in graphite. The intercalation and deintercalation of some other ions are also allowed in graphite, which makes graphite a low-cost, high-safety cathode material. However, inherent poor rate performance and low specific capacity greatly limited the performance[106-108].

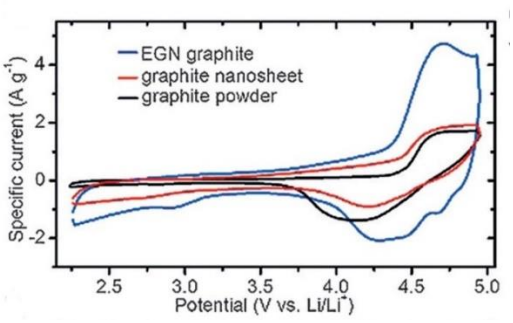

Figure 6.12 The 2nd CVs (10 mVs^{-1}).

Benefited from the nanoflake structure of graphite, generated electrochemically, the diffusion of ions and an effective volume buffer against the expansion of the nanoflakes on intercalation of some large anions. The examination of graphite in Ionic Liquid Pyr14TFSI (N-butyl-N-methylpyrrolidinium bis-trifluoromethanesulfonylimide) in membrane electrodes (ca. 2 mg cm^{-2}) shows the potential as a good cathode material. As shown in Figure 6.12, the second CVs of EGN graphite, commercial graphite nanosheet, and graphite powder are between 2.25 and 4.95 V vs. Li/Li+ in Pyr_{14}TFSI at room temperature.

An oxidation peak and reduction peak were found at 4.7V and 4.2V for all three samples. A more reversible with significantly higher capacity in charge and discharge of electrochemically generated nano-graphite (denoted as EGN). A discharge current was found both in EGN graphite and commercial graphite at around 2.7V indicated the intercalated TFSI ion is difficult to remove. With the cycling, the 2.7V discharge capacity decreased gradually; the 4.2V discharge capacity is increased for all samples (Figure **6**.**13**-**15**).

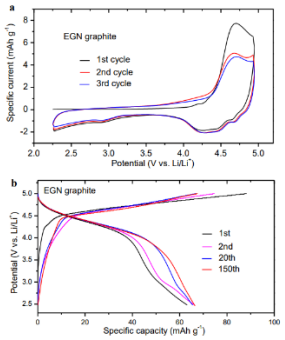

Figure 6.13 Electrochemical performance of the commercial graphite in Pyr14TFSI.

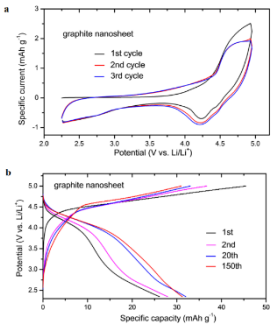

Figure 6.14 Electrochemical performance of the EGN in Pyr14TFSI.

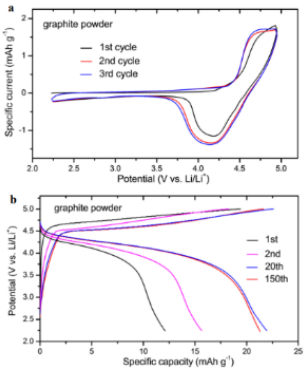

Figure 6.15 Electrochemical performance of the graphite powder in Pyr14TFSI.

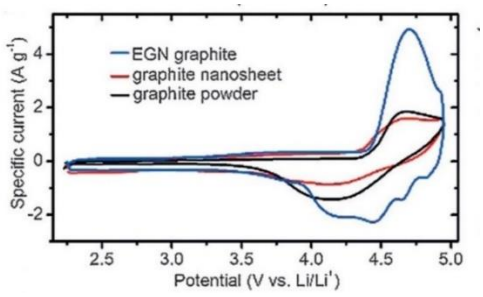

Figure 6.16 The 150th CVs in Pyr14TFSI.

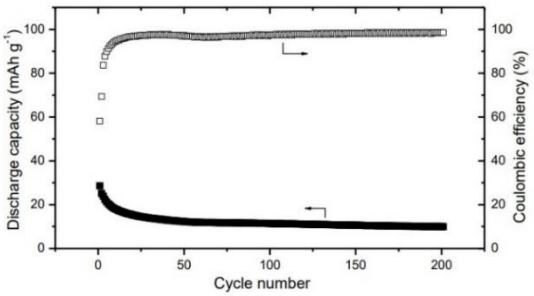

Figure 6.17 Specific discharge capacity and coulombic efficiency during the long-term cycling.

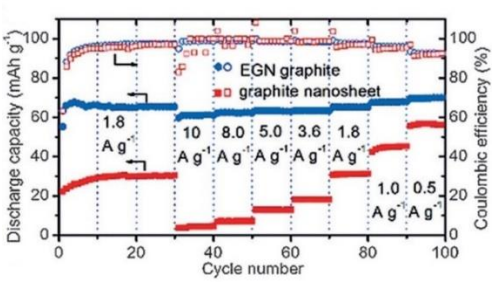

Figure 6.18 Rate performances.

The cycles of charge and discharge CVs after 150 are shown in Figure **6.17**, and the cycles of charge and discharge CVs of EGN graphite shows a more reversible and fast intercalation/deintercalation of TFSI@ ions. A charge and discharge cycling under current density of 1800 mA g^{-1} between 2.25V and 5.0V depicted high stability of the three samples. In addition, EGN graphite has a specific capacity of 65 $mAhg^{-1}$, and 99% coulombic efficiency. Apparently, the specific capacity of EGN graphite is competitive when compared with commercial graphite nanosheet (ca. 31 mAh g^{-1}) and graphite powder (ca. 21 mAh g^{-1}). However, the original carbon black shows a capacitor behavior with a reversible specific capacity of only about 10 $mAhg^{-1}$ (Figure **6.16**). Figure **6.18** compares the rate performance of EGN graphite with commercial graphite nanosheet.

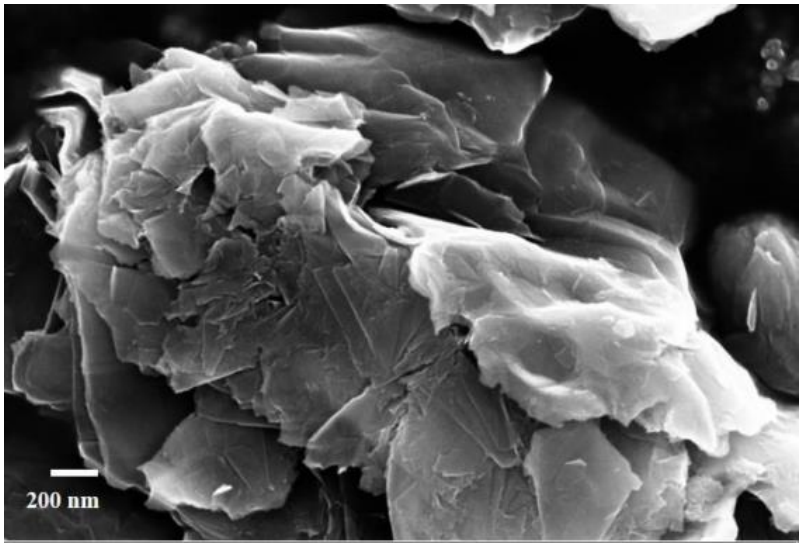

Figure 6.19 SEM image of the commercial graphite nanosheet.

The commercial graphite nanosheet has a poor rate capability, as it has a capacity of 56 $mAhg^{-1}$ at a current density of 0.5 Ag^{-1}, and dramatically decreased to 4 $mAhg^{-1}$ at a current density of 1 Ag^{-1}. The low specific capacity could be largely attributed to the aggregative graphite nanosheets in a commercial sample (Figure **6.19**). By comparison, EGN exhibits an excellent high rate capability, with a specific capacity of 70 $mAhg^{-1}$ at 0.5 Ag^{-1} and a drop less than 10 $mAhg^{-1}$ at 1 Ag^{-1}, which is significant progress than all other reports with similar mass loading.[107, 108] Only for a thin-layer electrode in which porous copper act as a carrier for graphite with a mass loading 10 mg cm^{-2}.[109] The EGN electrode with a lower mass load only about 2 $mgcm^{-2}$, which is competitive to lithium-ion batteries that with the similar mass load.

Furthermore, with an increase in the upper limit charging potential to 5.25V, the specific capacity of EGN graphite dramatically increased to

116 $mAhg^{-1}$ (Figure 6.20) with a current density of $1.8Ag^{-1}$. As illustrated in Figure 6.20, a second charging plateau at 5.1 V and a discharging plateau at about 4.7 V attributed to the capacity increment (Figure 6.21).

The ionic liquid will undergo anodic oxidation, which causes a slight lower Coulombic efficiency (Figure 6.22) Under similar conditions, the specific capacity of graphite nanosheet and graphite powder are only 47 and 40 $mAhg^{-1}$, respectively.

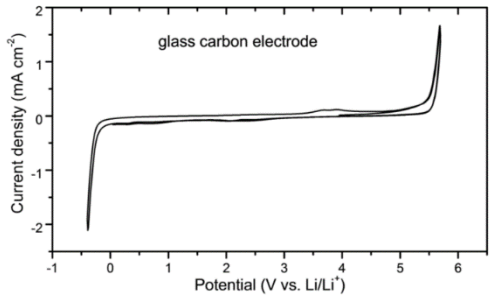

Figure 6.20 Electrochemical window of the $Pyr_{14}TFSI$ ionic liquid

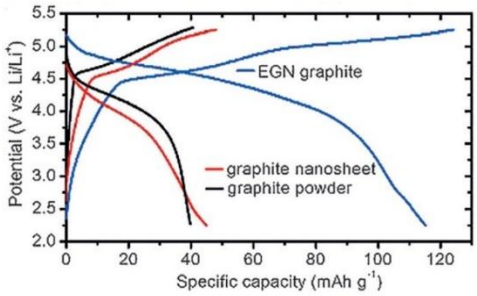

Figure 6.21 The charge/discharge curves for between 2.25V and 5.25 V

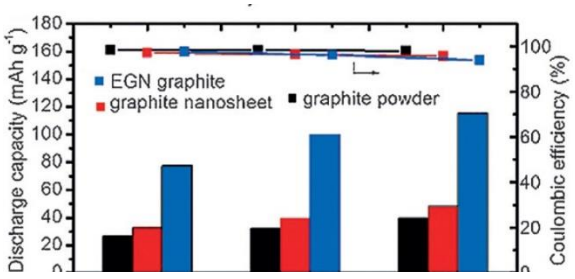

Figure 6.22 Specific discharge capacities and coulombic efficiencies at 1800 mA while the upper limit charging potential is increased to 5.25 V after the rate performance tests.

Experimental

A cathode was composed of 0.2-2 g of carbon black that was compressed into a small pellet before packed between two nickel foam. Then paired with graphite anode in melting anhydrous calcium chloride (750g) and a mixture melting calcium chloride and sodium. The experiment was conducted in a graphite crucible (diameter 9.5cm, height 23.5cm). Place crucible in a furnace which was equipped with sealable retort with the protection of inert atmosphere (Argon). The temperature was raised to 673K gradually and stay for 12 hours, then to 1100K. A pre-electrolysis was conducted at 2.6V for 12 hours by graphite anode and nickel anode to remove electrical sensitive impurities. Cyclic voltammograms were measured by a molybdenum cavity electrode, loaded with pulverous material that under investigation. A silver electrode was used as reference electrode which was sealed in a tube made with ceramic. Charged for 2 hours at a voltage 2.6V. Then cathode was cooling down to room temperature before washed with deionized water and dried in vacuum pump overnight. For a precise result, carbonaceous powder sample was pressed to pellet (15mm in diameter,10mm in thickness) in the pressure of 10Mpa before being applied to test. Pellet was then placed between nickel foam, with the molybdenum wire current collector. The cathode was washed with HCl (0.1M) several times and dried in vacuum oven at 80℃ before further characterization.

A Powder X-Ray Diffraction (PXRD) was tested under conditions Cu Kα1 radiation in λ = 0.15405 nm. Transmission Electron Microscopy with Selected Area Electron Diffraction, Field-Emission Scanning

Electron Microscopy and the chemical compositions of samples were analyzed. A Fusion Oxygen Analysis was tested as a supplement to the oxygen element. The Confocal Raman Micro-Spectroscopy result was obtained in an incident laser at 514.5nm.

Chemicals and materials

Carbon black (Cabot, Vulcan XC-72), graphite nanosheet (XG Sciences, xGnP-M-25), commercial graphite powder (Grade #38, Fisher Scientific. Coke carbon (WISCO), N-methylpyrrolidine (97%, Sigma Aldrich), 1-Bromobutane (99%, ACROS Organics), Lithium bis-trifluoromethanesulfonyl imide (98%, 3M), all chemicals above were used directly without further purification. All organic solvents were purchased from Fisher scientific and without any further purification.

*N-butyl-N-methylpyrrolidinium chloride(**6.1**)*

To a 250mL three neck round flask bottle, an 8.5g (0.1 mol) of N-methylpyrrolidine was added in 100mL acetonitrile. n-Butyl chloride (18.2g, 0.2mol) was added in one portion. Keep reaction reflux overnight. Before stop reaction, THF was added to the mixture under reflux condition dropwise until the first precipitate comes out. Then, the reaction was cooled down to room temperature gradually with stirring. The mixture was put into a nitrogen protected filter to prevent the contact of moisture. Washes with THF/Acetonitrile=5:1 three times. The white crystalline powder was then dried in vacuum oven. Yield white solid (11g, 63%).

*N-butyl-N-methylpyrrolidinium bis-trifluoromethanesulfonyl-imide(**6.2**)*

Dissolve 5g (0.028mol) of N-butyl-N-methylpyrrolidinium chloride in 10mL deionized water. In a new vial, 8.49g (0.03mol) of lithium bis-

trifluoromethanesulfonyl imide was dissolved in 10mL of deionized water. Then two solutions were mixed and stirred for 2hours. Ionic liquid was put into a centrifuge tube and separated at 8000rpm for 5 mins and damp water in the top layer. Add another 10mL deionized water in a centrifuge, shake well and repeated 6 times. In the last time, the bottom layer ionic liquid was put in a clean vial and bubbling with dried nitrogen gas in 100℃ for 5 hours.

δH (ppm) (DMSO-d_6): 3.42 (4H, m, *CH_2*-2,5), 3.28 (2H, t, N-*CH_2*-), 2.89 (3H, s, N-*CH_3*), 2.01 (4H, s, *CH_2*-3,4), 1.53 (2H, multi, N-CH_2-*CH_2*-), 1.30 (2H, sextet, N-CH_2-CH_2-*CH_2*-CH_3), 0.90 (3H, t, N-CH_2-CH_2-CH_2-*CH_3*). δC (ppm) (DMSO-d_6): 118.26 (q, $^1J_{13C-19F}$ = 318.3 Hz, (-SO_2*C*F_3), 62.35 (s, N-*CH_2*-), 61.50 (s, *CH_2*-3,4), 50.04 (s, N*C*H_3), 23.90 (s, N-*CH_2*-CH_2-CH_2-CH_3), 20.59 (s, N-CH_2-*CH_2*-CH_2-CH_3), 19.89 (s, N-CH_2-CH_2-*CH_2*-CH_3), 14.08 (s, N-CH_2-CH_2-CH_2-*CH_3*). m/z (ESI+): 564, $[Pyr14]^+$; m/z (ESI-): 280, $[TFSI]^-$

The graphite was tested as cathode membrane (2mg cm^{-2}) in this ionic liquid. The potential window of ionic liquid Pyr_{14}TFSI is about 5.7 V. Titanium mesh supported rolled membrane composed of 70% active component plus 20% acetylene black and 10% polytetrafluoroethylene. Titanium mesh is used because the good performance in working as current collector which remains good stability during the experiment.

An Ag wire reference electrode was employed as a reference to the working electrode and was calibrated by a Li/Li+ electrode in advance. To avoid contamination of the electrolyte, we applied a capacitive electrode as the counter electrode.

Summary

A new graphitization process for the preparation of high-energy nanostructured graphite materials is introduced in this chapter. It involves the removal of oxygen atoms from the surface of carbon and long-distance rearrangement of carbon atoms with cathodic polarization. For the carbon black precursor, Yield flake graphite up to 80% was obtained with an energy consumption of about 5.5 Wh per gram of graphite. The new electrochemical technique has proved to be versatile. Not only non-graphitizable carbon black was investigated, but the graphitization of activated carbons, carbon fibers, and graphitizable cokes has also been tested. In addition, petaloid flakes like graphite were obtained for all precursor, no matter what size, specific area, and oxygen. This finding is providing a promising method for converting various amorphous carbons that can be obtained in a large amount from renewable biomaterials to high-performance electrode materials.

Abbreviations

Pyr14 TFSI (N-butyl-N-methylpyrrolidinium bis-trifluoromethanesulf-onylimide)

CV Cycle voltammograms

CB Carbon black

MCE Molybdenum cavity electrode

EGN Electrochemical generated nano-graphite

PXRD Powder X-Ray diffraction

NMR Nuclear magnetic resonance

SEM Scanning electron microscopy

TEM Transmission electron microscopy

XPS X-ray photoelectron spectroscopy

TGA Thermal gravimetric analysis

References

101. H. O. Pierson, *Handbook of carbon, graphite, diamonds and fullerenes: processing, properties and applications*, William Andrew, 2012.
102. M. Inagaki, F. Kang, M. Toyoda and H. Konno, *Advanced materials science and engineering of carbon*, Butterworth-Heinemann, 2013.
103. *Proceedings of the Royal Society of London. Series A. Mathematical and Physical Sciences*, 1951, **209**, 196-218.
104. J. Qian, C. Pantea, J. Huang, T. Zerda and Y. Zhao, *Carbon*, 2004, **42**, 2691-2697.
105. F. Maldonado-Hódar, C. Moreno-Castilla, J. Rivera-Utrilla, Y. Hanzawa and Y. Yamada, *Langmuir*, 2000, **16**, 4367-4373.
106. M. Sevilla and A. B. Fuertes, *Carbon*, 2006, **44**, 468-474.
107. G. Z. Chen, D. J. Fray and T. W. Farthing, *Nature*, 2000, **407**, 361.
108. J. A. Read, A. V. Cresce, M. H. Ervin and K. Xu, *Energy & Environmental Science*, 2014, **7**, 617-620.
109. S. Rothermel, P. Meister, G. Schmuelling, O. Fromm, H.-W. Meyer, S. Nowak, M. Winter and T. Placke, *Energy & Environmental Science*, 2014, **7**, 3412-3423.
110. T. Ishihara, M. Koga, H. Matsumoto and M. Yoshio, *Electrochemical and solid-state letters*, 2007, **10**, A74-A76.
111. M.-C. Lin, M. Gong, B. Lu, Y. Wu, D.-Y. Wang, M. Guan, M. Angell, C. Chen, J. Yang, B.-J. Hwang and H. Dai, *Nature*, 2015, **520**, 324.

Chapter 7 Heterogenous Viologen Catalysts for Metal-free and Selective Oxidations.

Abstract

Metal-free oxidation, a green chemistry process，has drawn more attention from the catalysis community. However, most oxidation processes were performed with homogeneous metal-free catalysts, while heterogeneous metal-free materials have been developed with limited success. In this work, polymerized ionic networks (PINs) with N, N'-dialkyl-4,4'-bipyridinium units were as heterogeneous viologen type of catalysts exhibiting high efficiency in oxidizing aromatic sulfide/alcohol to sulfoxide/aldehyde, respectively (Conv.: >90%, Sel.: >95%). The catalytic performance of PINs originates from the electron-accepting ability of the viologen unit, which can reduce the H_2O_2 into active species. Especially, the synthesis of PIN catalysts was a simple one-step polymerization of benzyl bromide and bipyridine. The metal-free heterogeneous feature, the high selectivity, the mild conditions (60^{o}C, 1 h), and the facile preparation of catalyst made current selective oxidation attractive.

Introduction

The oxidation of sulfides and alcohols to corresponding sulfoxides and aldehydes is an important process in the petrochemical industry. A vast number of the sulfur compounds are present in crude oil such as mercaptans, sulfides, disulfides, and thiophenes, and the boiling point of crude oil is increased by those compounds.[110] Traditionally, strong oxidizing agents such as potassium permanganate,[111] periodic acid,[112] potassium dichromate,[113] nitrogen dioxide,[110] iodanes,[114] potassium hydrogen persulfate,[115] and other hypervalent metal salts, have been employed for those dehydrogenation reactions. However, excess

oxidants are required, which causes corrosion to facilities, higher costs to treat contaminations, suffers from toxic heavy metal ions, and result in over oxidation. In this research, hydrogen peroxide (H_2O_2) was employed as a green source of oxygen, and no poisonous byproducts were generated.

In general, catalysts that contain metal elements are used either by activating H_2O_2 or organic substances.[116, 117] The Fenton system goes through a mechanism with Fe^{2+}-induced H_2O_2 splitting into •OH radicals active species for the oxidative hydroxylation of benzene into phenol.[118-120] Another possible way is the formation of reactive •OOH radical with the decomposition of H_2O_2. On others, metal catalysts may have interaction with organic molecules.[121-123] For instance, in the oxidation of sulfides (R_2S), the single electron transfer occurs between R_2S and metal catalyst results from the reactive $R_2S\bullet^+$ species, which is ready to be oxidized by hydrogen peroxide.[124] Even though a comprehensive study of metal catalyst-H_2O_2 systems has been performed in the past decades, metal-free heterogeneous catalysts for selectively oxidizing sulfides to sulfoxide has rarely been studied.[125-128] In terms of green and sustainable chemistry, the design of metal-free catalysts in selective oxidation is highly desired with great difficulty.

A class of metal-free heterogeneous viologen catalysts is introduced in this work, which selectively oxidizes sulfides and alcohols to the corresponding sulfoxides and aldehydes with high performance and sustainable activity. Group of viologens (dialkyl viologens) have been well investigated in electrochemistry as electron acceptors, in the inherent redox reactions ($V^{2+} \leftrightarrow V^{+} \leftrightarrow V^{0}$).[129, 130] Those redox processes

can be induced reversibly by either chemical, photochemical or electrochemical, and no side reactions were observed.[131-135] The redox and reactive properties of viologens inspires us to study the catalytic activity in the oxidation reaction. In previous research, we observed a phenomenon that the color change of polymerized viologen was caused by protons. (viologen radical cations usually show the blue color), and their chemical structure showed us that PINs are highly cross-linked viologens with abundant 4,4'-bipyridinium fragments(Figure 7.2 and Scheme **7.1**).[136, 137]

A series of viologens were synthesized with 4,4'-bipyridinium moieties, and with different anions were prepared by ion exchange. The polymer was synthesized by an S_N2 nucleophilic substitution reaction of bromomethyl benzene and 4,4-bipyridine.[137] This reaction requires no inert atmosphere and is not moisture sensitive, compared with radical polymerization, so it is practical. Both ionization and polymerization of 4,4'-bipyridine were combined in one step. All viologen-based polymers are insoluble in any solvents, which indicates these PINs may serve as the safer viologen catalysts. In contrast, viologen molecules are highly toxic with good solubilities, such as paraquat (Figure **7.1**), which was one of the most widely used herbicides in the world.[138]

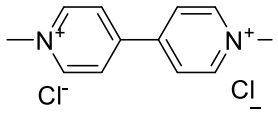

Figure 7.1 Paraquat

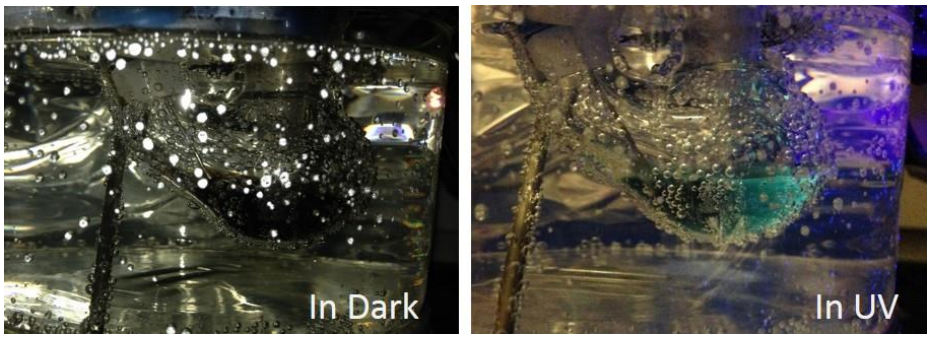

Figure 7.2 Pictures of PIN-1 in the dark or UV conditions.

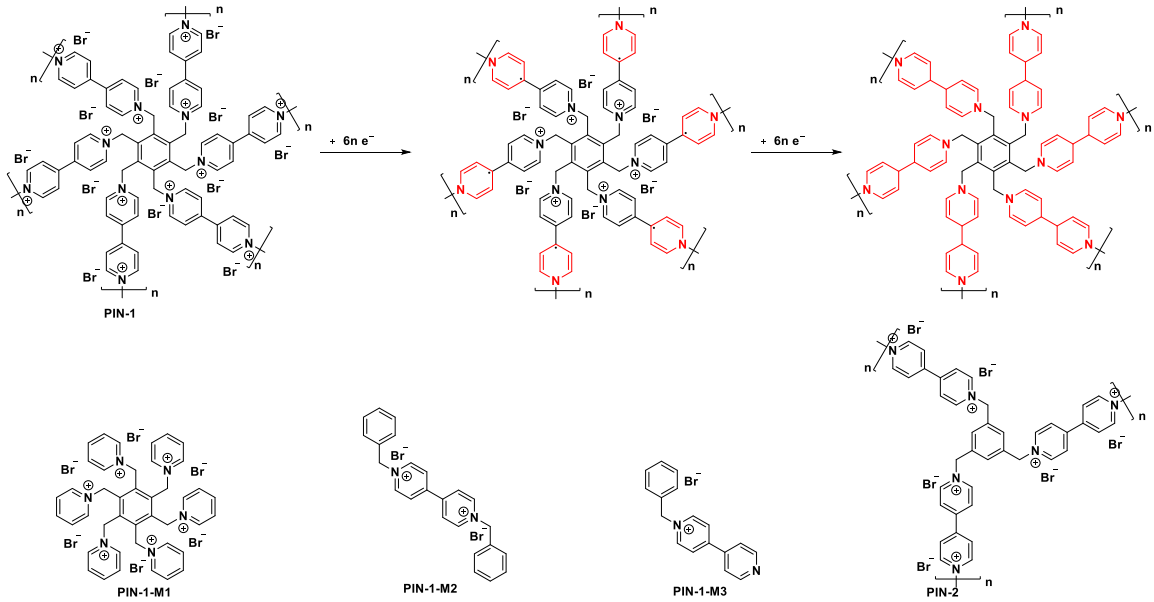

Scheme 7.1 Chemical structures of polymerized ionic networks and model molecules.

Results and Discussion

Oxidation of thioanisole to methyl phenyl sulfoxide was selected as a model reaction, with 30% of hydrogen peroxide in acetonitrile[139, 140]. In the blank run, no product was detected. (Table **7.1, Entry 1**). A good conversion is achieved (88%) by employing PIN-1 as a catalyst; sulfoxides were produced in a high selectivity (98%) (Table **7.1, Entry 2**). It is believed that viologen cation is the active group that is responsible for the catalytic activity. However, series model molecules were prepared to exclude the effect caused by another component. PIM-1-M1 was tested, a similar ionic molecule with six pyridinium cations. The result showed that this species had no catalytic activity for this oxidation reaction (Table **7.1, Entry 3**). Then, PIM-1-M2 was tested in same reaction condition, and a moderate conversion (27%) was achieved (Table **7.1, Entry 4**), indicating that the viologen motif was the actual component induced this reaction. In the polymerization of PIN polymer, due to the bulky steric effect, the undesired single substituted bipyridinium will be formed. To further exclude the possible effect caused by a single substituted viologen, single substituted 4,4'-bipyridinium bromide (PIM-1-M3) was synthesized. The result indicated it did not have catalytic activity in this oxidation reaction (Table **7.1, Entry 5**). We attributed the possible reason to the poor electron accepting of PIM-M3, which revealed the necessity of the doubly substituted 4,4'-bipyridinium structure for catalysis. Then, a lower charge density of viologen structure (PIN-2) was tested to evaluate the effect of ion density in catalytic activity.

Table 7.1 Selective oxidation of methyl phenyl sulfide by PINs-based catalysts.

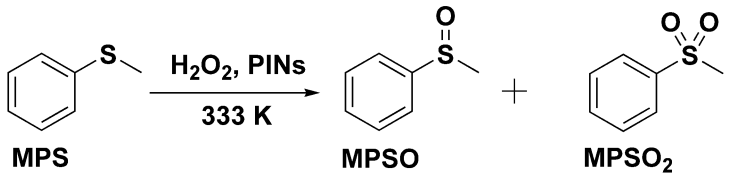

MPS MPSO $MPSO_2$

Entry	Catalyst	Conversion	Selectivity	
			MPSO	$MPSO_2$
1	—	2%	—	—
2	PIN-1	88%	98%	2%
3	PIN-1-M1	2%	—	—
4	PIN-1-M2	27%	97%	2%
5	PIN-1-M3	2%	—	—
6	PIN-2	16%	>99%	—
7 [b]	PIN-1	28%	97%	3%
8 [c]	PIN-1	—	—	—
9 [d]	PIN-1	48%	93%	7%

Reaction conditions: 1mmol thioanisole, 20mg catalyst, 4mL CH_3CN, 2mmol 30%H_2O_2, 60 °C, 1 h. b 10 mg PIN-1 was used in this run. c No H_2O_2 was added. d additional 0.5 mL ethanol added.

This resulted in a decrease in the conversion of thioanisole, which indicated the ion density was another factor in oxidation process (Table **7.1, Entry 6**).

Besides, the catalytic efficiency closely corresponded to the amount of PIN-1 employed in the oxidation. A decrease in conversion of MPS was up to 28%, with the half amount of PIN-1 cut. (Table **7.1, Entry 7**). Also, in a parallel experiment without hydrogen peroxide, no products were observed, which confirmed that the hydrogen peroxide was acting as an oxidant for the oxygen-addition into sulfide (Table **7.1, Entry 8**). When 0.5mL of ethanol was added as an •OH radical scavenger, the oxidation of thioanisole still occurred, however, with a decrease in conversion [141](Table **7.1, Entry 9**).

A cycling test of catalyst was tested, and the color of the catalyst turned to yellow, besides, the activity after one cycle was dramatically dropped and which might be caused by the distortion of the bipyridinium (i to iii). Because the polymer is highly condensed, and the collapse of the structure will cause the irreversible bending of bipyridinium (Scheme **7.2**).

No apparent difference was found by changing stirring speed from 300 to 1200 rpm. Thus, the mass transfer is not the rate-determining factor in this process. All catalytic reactions were performed at a stirring speed of 300 rpm. The evolution of the catalytic performance as a function of time and reaction temperature was studied over PIN-1 in detail (Figure **7.3**).

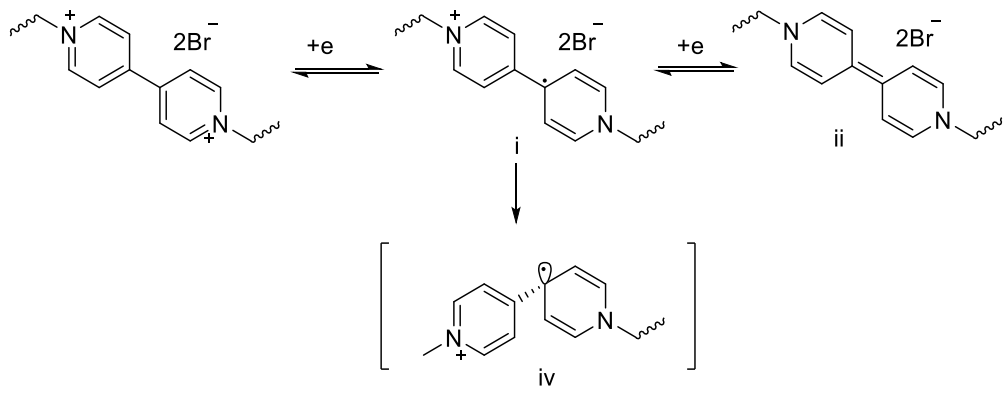

Scheme 7.2 Possible mechanism for the deactivation of PIN-1.

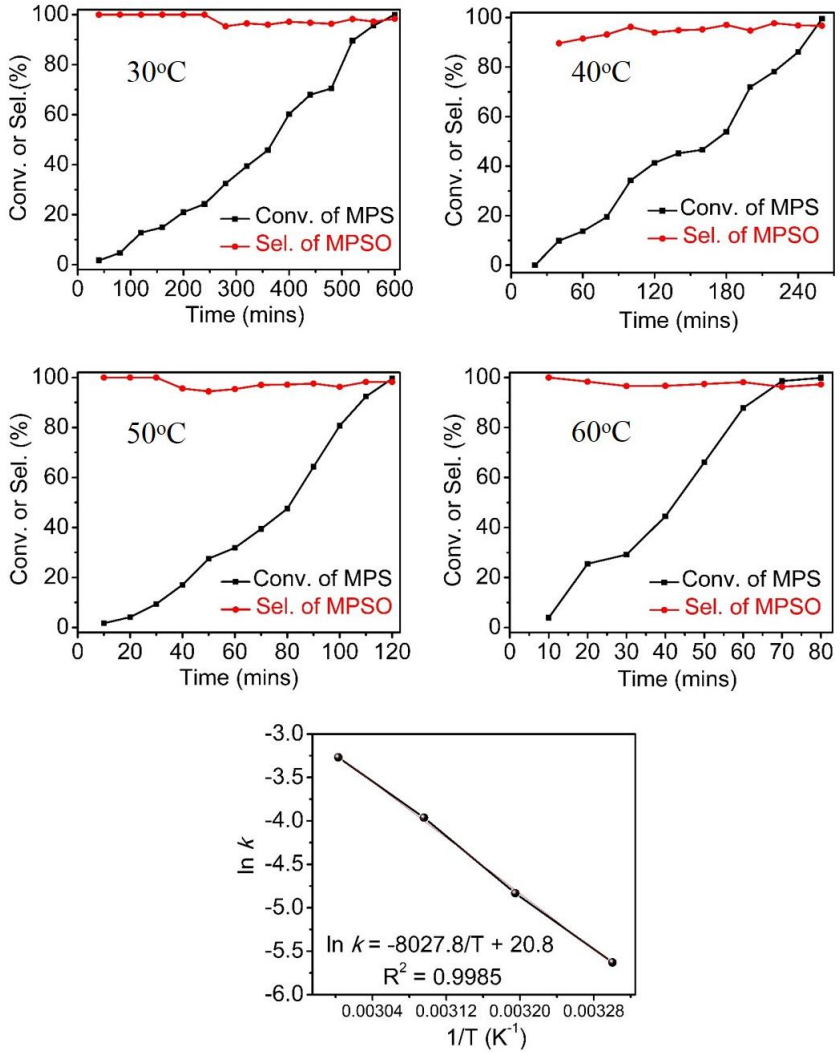

Figure 7.3 The conversion and selectivity vs. time plots for the oxidation by PIN-1/H_2O_2 at different temperatures. Reaction conditions: thioanisole 1 mmol, PIN-1 20 mg, 30%H_2O_2 2 mmol, 4mL CH_3CN, 30-60 ℃. Temperature dependence of the rate parameter in the Arrhenius coordinates for the PIN-1/H_2O_2 system.

As shown in the curves, reaction temperature plays a critical role in the oxidation. With an increasing temperature reaction rate was dramatically increased. The reaction time for complete conversion of thioanisole ranged from 70 mins to 600 mins when the reaction temperature decreased from 60 ℃ to 30 ℃. However, a lower temperature (30 ℃) in the industry is desired.

Another result is the conversion of thioanisole increased linearly with the reaction time. Initial reaction rates were calculated from the kinetic curves at low conversions. The rate constants of reaction (k) were 0.0036 h^{-1} (30℃), 0.0079 h^{-1} (40℃), 0.0190 h^{-1} (50℃), 0.0381 h^{-1} (60℃). This catalyst system roughly followed the Van't Hoff approximation rule of a 2 to 3 times increase in the rate constant with a 10K increase in reaction temperature. The activation energy was then calculated by Arrhenius plots.[142] When the reaction temperature fit the rate constant (ln *k*), a straight line with a correlation coefficient of 0.9985 was achieved. The activation energy (E_a) for thioanisole oxidation by H_2O_2 was 66.7 kJ mol^{-1}, and this appropriate value indicates that the oxidation can be conducted in mild conditions (Figure 7.3).

To explore the catalytic activities of PIN-1/H_2O_2, we investigated some other methyl phenyl sulfides under same conditions. Comparing with thioanisole, the oxidation of electron-withdrawing groups (-F, -Cl, -Br) substituted thioanisoles took a longer time. All reactions turned out to have a good conversion and selectivity. (Table **7.2**)

Table 7.2 Selective oxidation of various sulfides by the PIN-1/H_2O_2 system.

Entry	Substrate	Product	Time(h)	Conv. (%)	Sel. (%)
1	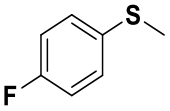	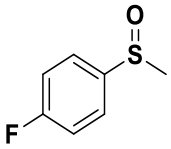	2.5	99%	95%
2	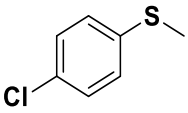	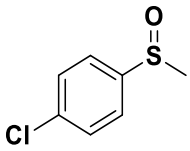	4	99%	>99%
3	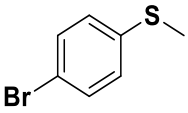	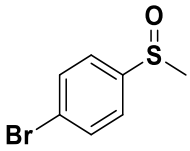	4	99%	>99%
4	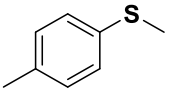	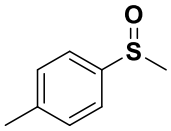	1.1	99%	>99%
5	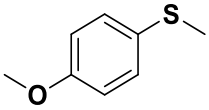	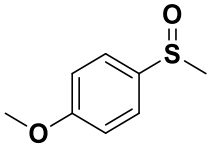	1	88%	>99%

The conversion and selectivity vs. time plots for the oxidation by PIN-1/H_2O_2 at different temperatures. Reaction conditions: sulfide 1 mmol, PIN-1 20 mg, 30%H_2O_2 2 mmol, 4mL CH_3CN, 30-60 °C, 1 h.

The catalyst had better activities towards molecule with electron-donating groups (-CH_3, -OCH_3). 4-methylthioanisole can even be completely oxidized (conversion >99%) to 4-(methyl phenyl) methyl sulfoxide (selectivity >99%) within 1.1 h. Hence, it is confirmative to say that PIN-1 is a good metal-free catalyst in dealing with oxidation reaction of sulfide.

Another important process in the industry is the catalytic dehydrogenation of benzyl alcohols to corresponding aldehydes. Inspired by the excellent performance of PIN-1 in oxidizing sulfides catalytically, we applied this method to the oxidation of benzyl alcohol. Compared with the oxidation of thioanisoles, much longer time was required when oxidizing benzyl alcohol to aldehyde (6 hours). A high conversion of benzyl alcohol to benzaldehyde was achieved in 7 h (conversion 94%, selectivity 99%), while in a parallel reaction with blank catalyst, a limited conversion of benzyl alcohol was detected (5%). A series benzyl alcohol with electron-withdrawing or electron-donating groups (Table **7.3**) were oxidized effectively with high selectivity and conversion. Therefore, it is convincing that the PIN-1 is a potential multi-functional catalyst for the selective oxidation of thioanisoles and benzyl alcohols.

Table 7.3 Selective oxidation of benzyl alcohols by PIN-1-Br/H_2O_2 system.

Entry	Substrate	Product	Conv.	Sel.
1	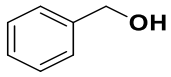	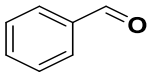	94% (5%)	>99%
2	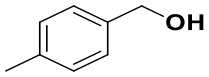	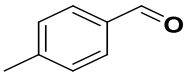	82%	>99%
3	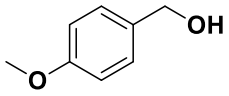	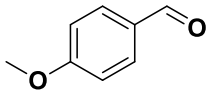	93%	>99%
4	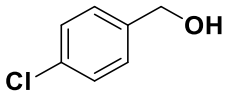	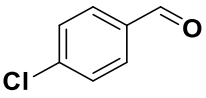	86%	>99%
5	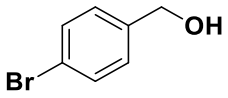	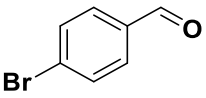	79%	>99%

Reaction Conditions: Benzyl alcohol 1 mmol, CH_3CN 3 mL, 30% H_2O_2 2 mmol, PIN-1-Br catalyst 20 mg.

Experiment

Chemicals and materials

4,4'-Bipyridine (98%, Alfa Aesar), Pyridine (99%, ACS reagent, ACROS Organics), Hydrogen Peroxide (30%, Fisher Chemical), Sodium Chloride (99%, Fisher Chemical), Sodium tetrafluoroborate (98%, ACROS Organics), Sodium hexafluorophosphate, (98.5%, ACROS Organics), Sodium Bromide (99%, Fisher Chemical), Benzyl Bromide (98%, ACROS Organics), hexakis(bromomethyl)benzene (98%, TCI), 1,3,5-Tris(bromomethyl)benzene (TCI 98%), Thioanisole (99%, ACROS Organics), Methyl p-tolyl sulfide (99%, Sigma Aldrich), 4-Fluorothioanisole (97%, Alfa Aesar), 4-Chlorothioanisole (98%, Alfa Aesar), 4-bromothioanisole (98%, Alfa Aesar), 4-methoxylthioanisole (98%, TCI), Benzyl Alcohol (Certified, Fisher Chemical), 4-Methoxyphenethyl alcohol (99%, Sigma-Aldrich), 4-Methylphenethyl alcohol (98%, TCI), 4-Bromophenethyl alcohol (97%, Alfa Aesar), 4-Chlorophenethyl alcohol (98%, Alfa Aesar), all chemicals above were use directly without further purification. All organic solvents were purchased from Fisher scientific and without any further purification.

As depicted in Scheme **7.3**, catalyst (PIN-1) was synthesized in one step by the reaction of hexakis(bromomethyl)benzene and 4,4-bipyridine. Followed be ion exchange to give the product various ions, which was designed to test the effect impacted by different counter ions.

A series PINs were synthesized as in Scheme **7.4**, PIN-1-M1 and PIN-1-M3 were designed to test whether pyridinium had the similar effect in the same condition.

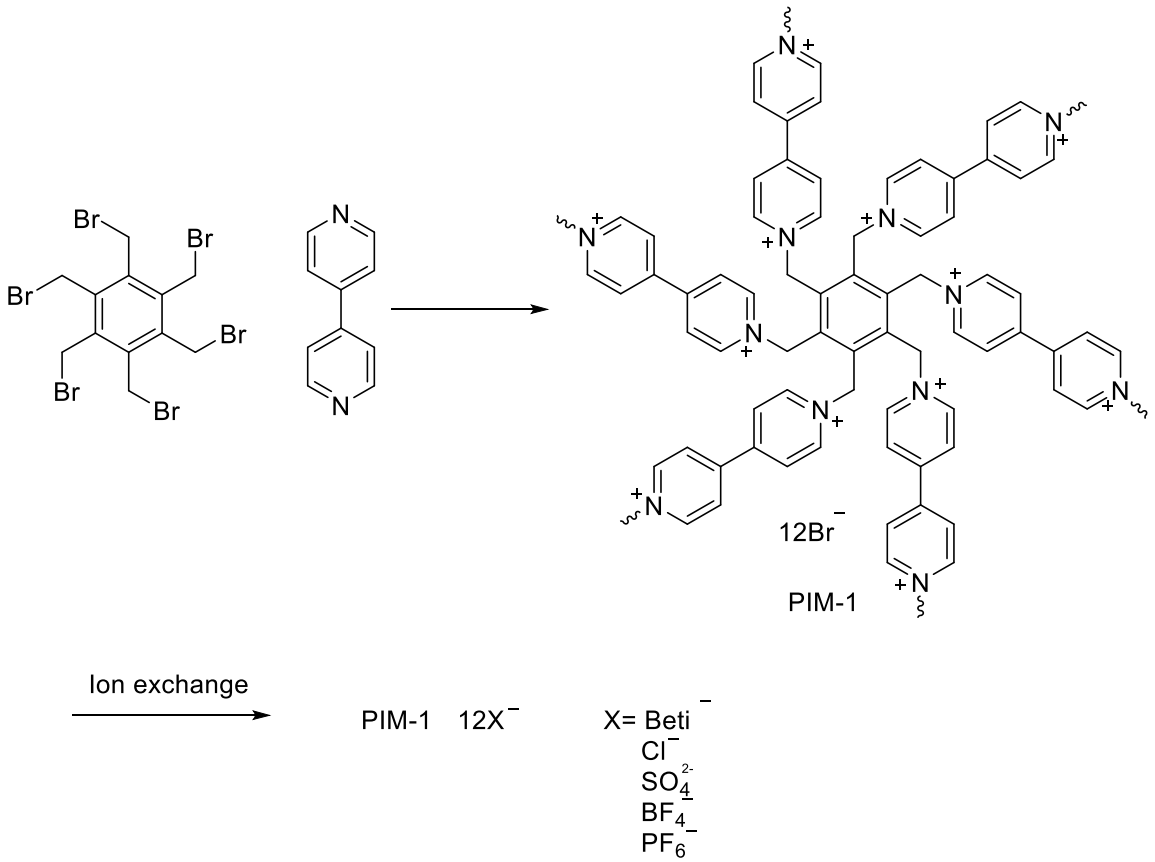

Scheme 7.3 Synthetic protocol of PIM-1.

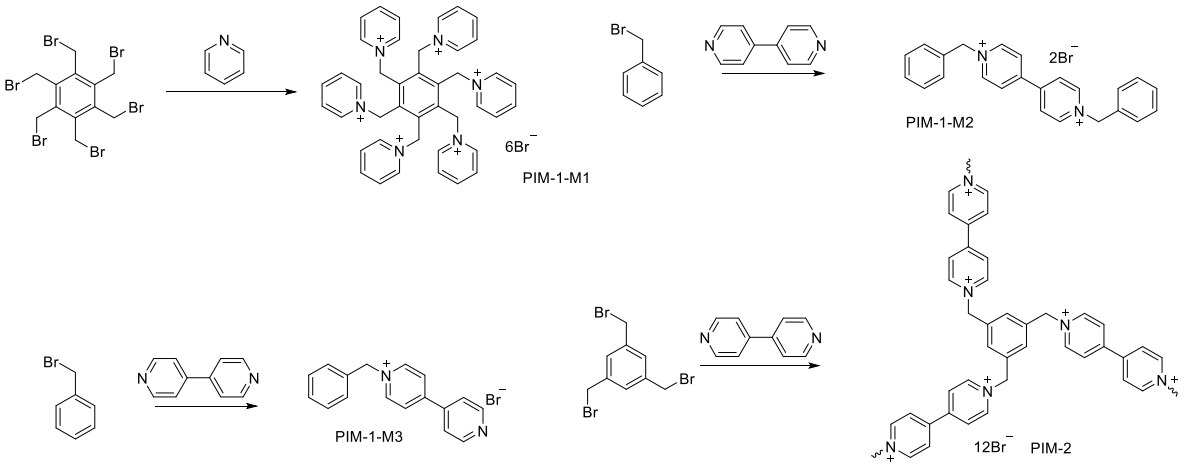

Scheme 7.4 Synthetic route for PIM-1-M1, PIM-2, PIM-1-M2, PIM-1-M3.

PIN-2 was designed to compare the differences in activity with different charge density. PIN-M2 is believed to be an effective part of this catalyst. In the synthesis of PIN-M3, a 1:1 ratio of benzyl bromide and bipyridine was required.

PIN-1

To a 250mL three neck round flask bottle, a 6.35 g (0.1 mol) of hexakis(bromomethyl)benzene and 4.68g (0.3mol) 4,4-bipyridine was added in 100mL Dimethylformamide. Place reactor in an oil bath. Then reaction can react overnights in 80℃. Black mixture was then poured into ethanol. After filtrate, residues were dried in the vacuum oven prior to use. Yield black solid. (10g, 90%)

PIN-2

To a 250mL three neck round flask bottle, a 3.56g (0.1 mol) of 1,3,5-Tris(bromomethyl)benzene and 2.34g (0.15mol) 4,4-bipyridine was added in 100mL Dimethylformamide. Place reactor in an oil bath. Then allow reaction keep warm overnights in 80℃. Black mixture was then poured into ethanol. After filtrate, residues were dried in the vacuum oven prior to use. Yield black solid. (5.6g, 95%)

PIN-1-M1[143]

To a 250mL three neck round flask bottle, a 6.35g (0.01 mol) of hexakis(bromomethyl)benzene dissolved in 100mL pyridine. Place reactor in an oil bath. Then allow reaction keep warm overnights in 80℃. Black mixture was then poured into ethanol. After filtrate, residues were dried in the vacuum oven prior to use. Yield black solid. (10.7g, 97%). δH (ppm) (DMSO-d_6): 8.98 (s, 12H), 8.63 (tt, 6H), 8.10 (t, 12H), 4.44 (br, 12H).

PIN-1-M2[143]

To a 250mL three neck round flask bottle, a 3.4g (0.3 mol) of benzyl bromide was dissolved in 100mL Acetone. 2.34g (0.15mol) of 4,4-bipyridine was then added. Place reactor in an oil bath. The reaction was refluxed overnights. After done, most of the solvent was removed under reduced pressure. Residues were put in fridge before filtrated. Clear crystal was then collected and washed with isopropanol twice. The product was put in the vacuum oven prior to use. Yield yellowish solid (5.1g, 89%). δH (ppm) (DMSO-d_6): 8.82 (2H, d), 8.46 (2H, d), 8.30 (2H, d), 7.72 (2H, d), 7.44 (5H, s), 5.73 (2H, s).

PIN-1-M3

To a 250mL three neck round flask bottle, a 1.7g (0.15 mol) of benzyl bromide was dissolved in 100mL isopropanol. Followed by adding 2.34g (0.15mol) 4,4-bipyridine Place reactor at room temperature for additional 48 hours. After done, remove most of the solvent under reduced pressure, residues were put in fridge before filtrated. Clear crystal was then collected and washed with isopropanol twice. The product was put in a vacuum oven before use. Yield white solid. (3.2g, 80%)

Summary

In summary, a simple and efficient catalyst that enables the selective oxidation of thioanisoles and aromatic alcohols with good to high activities has been introduced. In addition, these catalysts worked in a heterogeneous way and did not contain metal elements, which elegantly enriched the limited library of metal-free solid catalysts

available for selective oxidation. The essential point of PIN-1 lied in the abundant viologen units which were incorporated in the solid backbone. When compared with highly toxic soluble viologens, PIN-1 solid materials exhibited as a safer catalyst.

References

112. P. S. Tam, J. R. Kittrell and J. W. Eldridge, *Industrial & Engineering Chemistry Research*, 1990, **29**, 321-324.
113. A. Shaabani, P. Mirzaei, S. Naderi and D. G. Lee, *Tetrahedron*, 2004, **60**, 11415-11420.
114. L. Xu, J. Cheng and M. L. Trudell, *The Journal of organic chemistry*, 2003, **68**, 5388-5391.
115. C. Srinivasan, A. Chellamani and S. Rajagopal, *The Journal of Organic Chemistry*, 1985, **50**, 1201-1205.
116. M. Ochiai, A. Nakanishi and T. Ito, *The Journal of Organic Chemistry*, 1997, **62**, 4253-4259.
117. B. M. Trost and D. P. Curran, *Tetrahedron Letters*, 1981, **22**, 1287-1290.
118. A. Prieto, M. Palomino, U. Díaz and A. Corma, *Catalysis Today*, 2014, **227**, 87-95.
119. A. Mahammed and Z. Gross, *Journal of the American Chemical Society*, 2005, **127**, 2883-2887.
120. J.-H. Yang, G. Sun, Y. Gao, H. Zhao, P. Tang, J. Tan, A.-H. Lu and D. Ma, *Energy & Environmental Science*, 2013, **6**, 793-798.
121. P. Zhang, Y. Gong, H. Li, Z. Chen and Y. Wang, *RSC Advances*, 2013, **3**, 5121-5126.
122. E. Brillas, I. Sirés and M. A. Oturan, *Chemical reviews*, 2009, **109**, 6570-6631.
123. R. Ricoux, M. Allard, R. Dubuc, C. Dupont, J.-D. Maréchal and J.-P. Mahy, *Organic & biomolecular chemistry*, 2009, **7**, 3208-3211.
124. K. Kaczorowska, Z. Kolarska, K. Mitka and P. Kowalski, *Tetrahedron*, 2005, **61**, 8315-8327.
125. F. P. Ballistreri, C. G. Fortuna, A. Pappalardo, G. A. Tomaselli and R. M. Toscano, *Journal of Molecular Catalysis A: Chemical*, 2009, **308**, 56-60.
126. A. M. Khenkin, G. Leitus and R. Neumann, *Journal of the American Chemical Society*, 2010, **132**, 11446-11448.
127. Y. Wang, X. Wang and M. Antonietti, *Angewandte Chemie International Edition*, 2012, **51**, 68-89.
128. D. S. Su, S. Perathoner and G. Centi, *Chemical Reviews*, 2013, **113**, 5782-5816.
129. A. Rostami and J. Akradi, *Tetrahedron Letters*, 2010, **51**, 3501-3503.
130. K. Chen, P. Zhang, Y. Wang and H. Li, *Green Chemistry*, 2014, **16**, 2344-2374.
131. L. A. Vermeulen and M. E. Thompson, *Nature*, 1992, **358**, 656.
132. A. Slama-Schwok, M. Ottolenghi and D. Avnir, *Nature*, 1992, **355**, 240.
133. D. R. Wheeler, J. Nichols, D. Hansen, M. Andrus, S. Choi and G. D. Watt, *Journal of the Electrochemical Society*, 2009, **156**, B1201-B1207.
134. W. W. Porter, T. P. Vaid and A. L. Rheingold, *Journal of the American Chemical Society*, 2005, **127**, 16559-16566.

135. D. Meisel, W. A. Mulac and M. S. Matheson, *The Journal of Physical Chemistry*, 1981, **85**, 179-187.
136. D.-L. Jiang, C.-K. Choi, K. Honda, W.-S. Li, T. Yuzawa and T. Aida, *Journal of the American Chemical Society*, 2004, **126**, 12084-12089.
137. Y. Ikeda, M. Ikeda and F. Ito, *Solid State Ionics*, 2004, **169**, 35-40.
138. P. Zhang, Z.-A. Qiao, X. Jiang, G. M. Veith and S. Dai, *Nano Letters*, 2015, **15**, 823-828.
139. P. Zhang, M. Li, B. Yang, Y. Fang, X. Jiang, G. M. Veith, X.-G. Sun and S. Dai, *Advanced Materials*, 2015, **27**, 8088-8094.
140. H. J. Beckie, *Pest Management Science*, 2011, **67**, 1037-1048.
141. T. Iwahama, S. Sakaguchi and Y. Ishii, *Tetrahedron Letters*, 1998, **39**, 9059-9062.
142. P. Zhang, Y. Wang, H. Li and M. Antonietti, *Green Chemistry*, 2012, **14**, 1904-1908.
143. X.-H. Li, J.-S. Chen, X. Wang, J. Sun and M. Antonietti, *Journal of the American Chemical Society*, 2011, **133**, 8074-8077.
144. Y. Li, X. Xu, P. Zhang, Y. Gong, H. Li and Y. Wang, *RSC Advances*, 2013, **3**, 10973-10982.
145. M. Albrecht, M. Yulikov, T. Kohn, G. Jeschke, J. Adams and A. Schmidt, *Journal of Materials Chemistry*, 2010, **20**, 3025-3034.

Chapter 8 Mesoporous Carbon Derived from Propargylic Ionic Liquids

Abstract

CO_2 storage materials are drawing much attention from scientists, because of the over emission of CO_2 from human activities. Series of porous materials have been developed. The porous carbon material is considered a prospective material for storing carbon dioxide. In this work, porous carbon materials with high surface areas were studied, and high CO_2 capacity was obtained by pyrolyzing task-specific ionic liquids (TSILs) under an inert atmosphere (nitrogen). Meanwhile, the effects of ionic liquids, the type of counter ions and pyrolysis conditions were studied. BpMIm500-Beti even performed the highest CO_2 absorption up to 5.5mmol/g at 0℃. However, compared with other studies, the lower nitrogen content of this carbon material indicates that the porous morphology has played a more critical role than nitrogen content in the gas capture. This research greatly diversifies the method for the investigation of new carbon materials for CO_2 capture and storage.

Introduction

CO_2 has caused great environmental problems, the sequestration of CO_2 in large scale is in high demand. The most widely used method is known as amine scrubbing, in which alkanolamines act as the effective ingredient.[144,77] This method shows high performance toward absorbing CO_2 and other acidic gases with few costs, however, the drawbacks include solvent loss, corrosion, and high energy costs for the regeneration, which are the driven force behind the development of new methods.

Stabilities, adsorption/desorption kinetics, and maximum capacities have been considered for an effective sorbent. Many different types of materials with high surface areas and excellent thermal stabilities have been examined including porous frameworks (e.g., metal organic frameworks,[64] covalent organic frameworks, [65] zeolite-imidazolate frameworks.[66]) and amine modified silicas (e.g., molecular basket sorbents,[67] hyperbranched aminosilica.[68]) and carbonaceous materials (e.g., pyrolysis of ILs,[69] coals[70], and natural materials.[71,72])

As one of the most abundant elements, carbon, has played an important role in many fields such as oxygen reduction reaction in fuel cells,[145, 146] supercapacitors,[147] and highly selective gas separation membranes.[148] Advanced synthetic methods are drawing more interest in controlling pore architectures and surface functionalities. These are the two main factors that mediate CO_2 adsorption. So, the study of the effects of the formation of carbon with hierarchical pore structures and high specific surface areas is important. Various kinds of mesoporous carbon have been obtained from different methods. By pyrolyzing natural precursors (e.g., coconut shell,[72] prawn shell.[71]), materials with a broad pore size distribution, a low specific surface area, and a small number of mesopores were obtained. Others can be obtained by activating nonporous carbon, which gives higher surface areas.[149,150] Soft-template method has been developed for making porous carbon.[151] Incorporation of hetero-atoms such as nitrogen-containing groups into the carbon during the synthesis process has been explored because these groups are believed to have an enhanced CO_2 capacity. Nitrogen-rich carbon materials with surface areas up to 3300m^2 g^{-1}

have been prepared by polymerizing organic nitriles with catalyst $ZnCl_2$ under an inert atmosphere at 400℃.[152] Even though no template is involved in this method, well-sealed reactors are required to prevent the loss of gaseous monomers. Acid was employed in post-treatment to remove $ZnCl_2$. Activation process with ammonia[146] and sodium amide[153] has been studied to increasing nitrogen component.

Ionic liquids are defined as semi-organic salts that exist in the liquid state below 100℃. Due to the negligible vapor pressure, non-flammability, and good thermal stability[154] of ionic liquids, their potentials as solvents for organic reactions has been investigated.[155] As emerging materials, ionic liquids were used as the precursor in preparing porous carbon materials.[156,157,158] In the ionothermal process, functional groups in the ionic liquid undergo a cross-polymerization process. Hetero-element doped carbon materials were obtained by pyrolyzing ionic liquids that contain hetero-atoms such as nitrogen, boron,[159] sulfur,[160] phosphorus. These hetero-atoms can either present in the cation or anion, which provides various ways of designing heteroatom-doped carbon for specific uses. Recently, Dai's group[158,157,69] have successfully illustrated the facile preparation of nitrogen-enriched porous carbon *via* ionic liquids using an ionothermal synthetic method. In their work, nitrogen-enriched carbon derived from ionic liquids with cross-linkable cations were investigated under various conditions. Under a thermal treatment at 800℃ in an inert atmosphere, ILs with nitrile groups either in the anions or cations were able to go through the cross-linking and carbonizing processes. A reasonable mechanism was proposed that high temperature can

induce the trimerization of nitrile groups, which formed frameworks, and the porous structure was constructed. The uptake of CO_2 was 4.39 mmol g^{-1}, with the surface area up to 942 m^2 g^{-1}. The porosity was well controlled by the calcinating temperature.

Propargyl groups are like nitrile groups, and the report about the behavior and reactivity in high temperature without catalyst has rarely been seen. In the presence of catalysts, acetylene can be polymerized to benzene[161,162] or 1,3-dienes.[163] This enlightened us to investigate the behavior of the ionic liquid bearing triple-bond at high temperature. In this chapter, a series of bication-type ionic liquids with different length and different anions were studied, as shown in Scheme **8.1**.

A possible mechanism of the trimerization or dimerization at high temperature, which leads to the formation of a 3-dimensional extended framework.

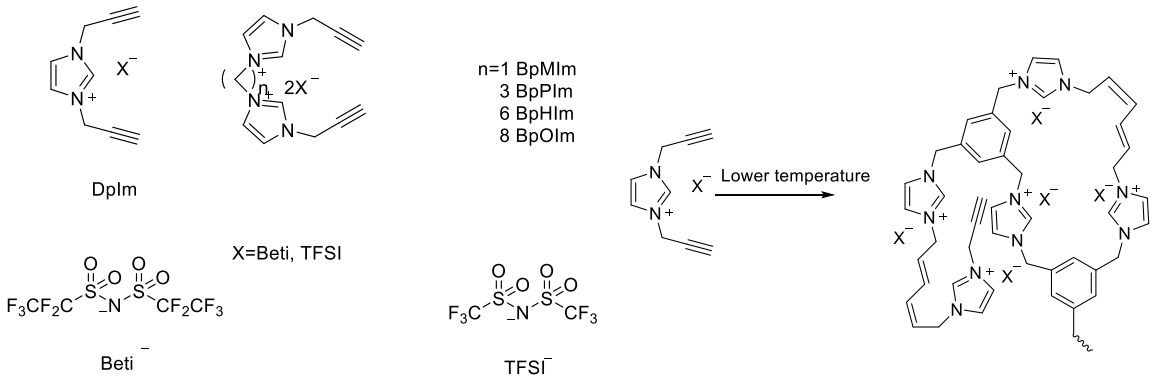

Scheme 8.1 Propargylic Ionic liquids, and proposed reaction mechanism for the trimerization of a propargyl containing

Results and discussion

Carbon yields of TSILs

Measured by TGA, as shown in Figure **8.1**, the carbonaceous yield of TSILs varied from 17-25%, which is much lower than the theoretical yield (30% as calculated from carbon). On the basis of the same cation, beti salts had a higher yield than TFSI salts. This matches our previous studies that in the ionothermal process, the final carbon yields result from the anions.[164,69]

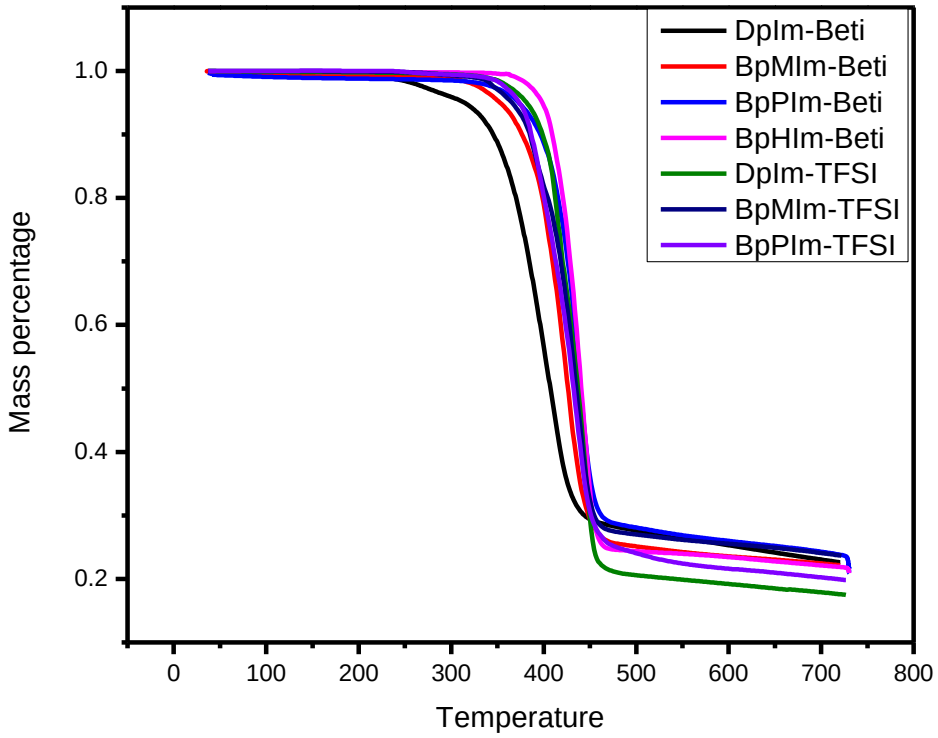

Figure 8.1 TGA of Ionic Liquids.

Based on TGA results, the ionic liquid starts decomposing at around 300-350℃ and stops at 450℃. To investigate the possible polymerization mechanisms, we use the IR technique to measure the change of ionic liquid before and after thermal treatment. Ionic liquid was heated up to 300℃ in an inert atmosphere (10℃ per mins), and black pitch-like solid was obtained. An IR spectrum of ionic liquid after thermal treatment showed the appearance of C=C stretch, and benzene stretch signal at 1600 cm^{-1}(Figure **8.2**), Which confirmed the proposed mechanisms.

To investigate the effect of the compound structure on the overall ILs compounds, we evaluated the fraction of mesopore by Brunauer–Emmett–Teller (BET) nitrogen sorption isotherms measured at 77 K (Figure **8.3**). This revealed propargyl-derived carbons showed type IV hysteresis loops for the BpPIm, BpMIm, and the BpHIm, indicating the presence of mesopores such as textural mesoporous. As shown in Figure **8.3**, an increasing fraction of mesopores was observed in isotherm plots, which revealed the relationship of the carbon bridge and mesopores. The length of carbon chain played a vital role in constructing mesopore structure. For DpIm Beti, which showed a type I hysteresis loop indicating a dominated micropore structure, only 28% of mesopores presented. With the increase in carbon number, BpOIm Beti has the highest mesopore fraction. However, the surface area dramatically dropped to 443 m^2 g^{-1}.

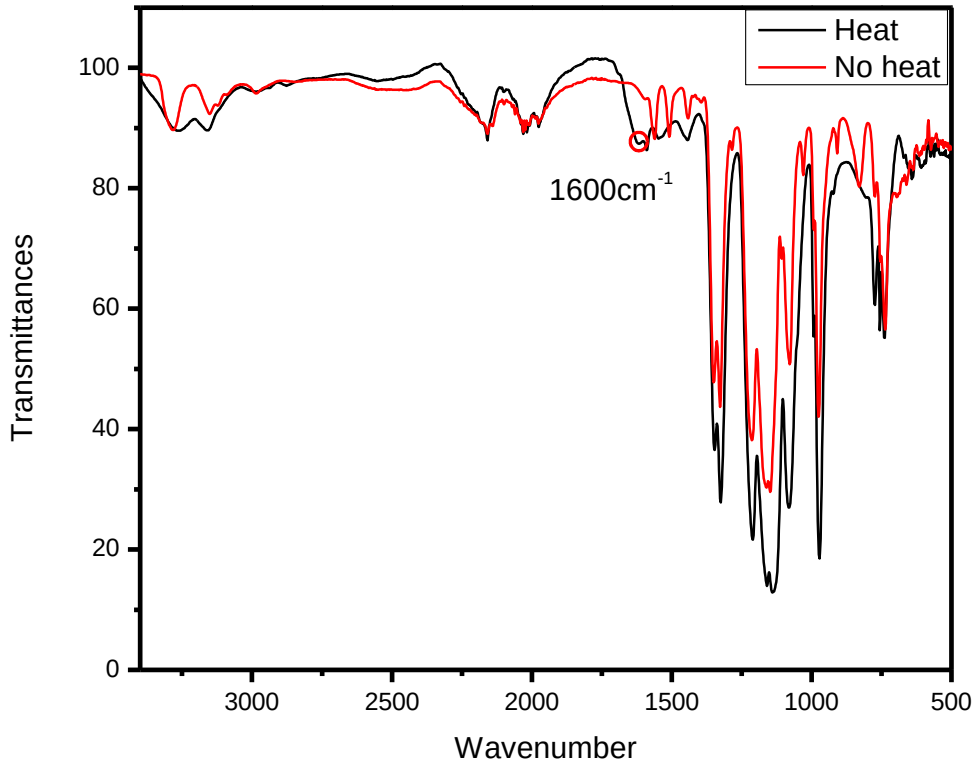

Figure 8.2 IR Spectrum of ionic liquid before and after the heat at 300℃.

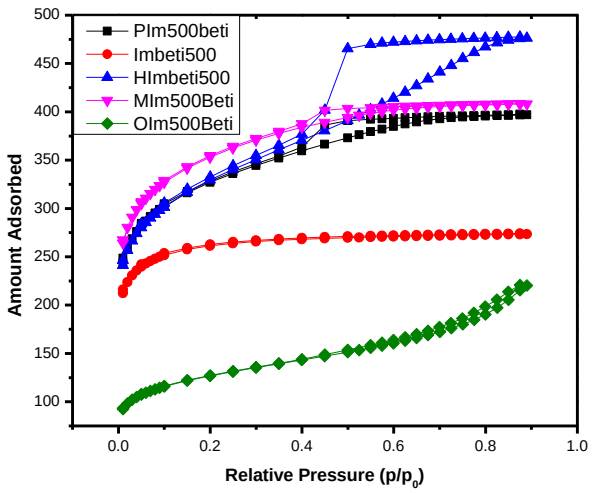

Figure 8.3 nitrogen sorption isotherms

Higher calcine temperature will have a greater impact on the surface area and CO_2 uptake. It was observed that the surface area decreased dramatically from 1150.75 m^2 g^{-1} to 978.50 m^2 g^{-1} as the temperature was increased from 500 ℃ to 800 ℃. A conclusion that carbon derived from Beti anion exhibit higher surface area than those from Tf_2N under same pyrolysis temperature. However, there are no significant correlations between anions and the fraction of micropores. Correspondingly, with an increase of one carbon, the fraction of micropore (S_{mic}/S_{BET}) decreased by one unit. High gas uptakes at a relatively high pressure indicate a large fraction of mesopores. As shown in Table **8.1**, the CO_2 uptake of BpMIm-Beti500 at 0℃ (5.0mmol g^{-1}) was significantly increased compared to it at 25℃ (3.8mmol g^{-1}), which has a higher performance in CO_2 capture than previously reported carbon dioxide adsorbents. The CO_2 uptake performance of propargylic-derived carbon is similar to that of nitrile-derived carbon, despite the lower nitrogen content. This indicates that the architecture structure of pore plays a significant role other than the content of nitrogen.

The CO_2 uptake capacity decreasing with the decreasing of micropore fraction was observed, which matches our previous research.

SEM images showed an amorphous carbon structure for all carbon materials (Figure **8.4**).

Table 8.1 Surface area and CO_2 uptake and fraction of micropore

Entry	$S_{BET}(m^2/g)$	CO_2(mmol/g)	S_{mic}/S_{BET}
DPIm-Beti500	1151	4.5	72%
DPIm-Beti800	979	4.3	71%
DPIm-Tf_2N500	866	4.4	69%
DPIm-Tf_2N800	609	3.6	81%
BpMIm-Beti500	1226	5.5	54%
BpPrIm-Beti500	1136	4.8	52%
DpHIm-Beti500	1149	4.0	47%
DpOIm-Beti500	443	2.5	45%

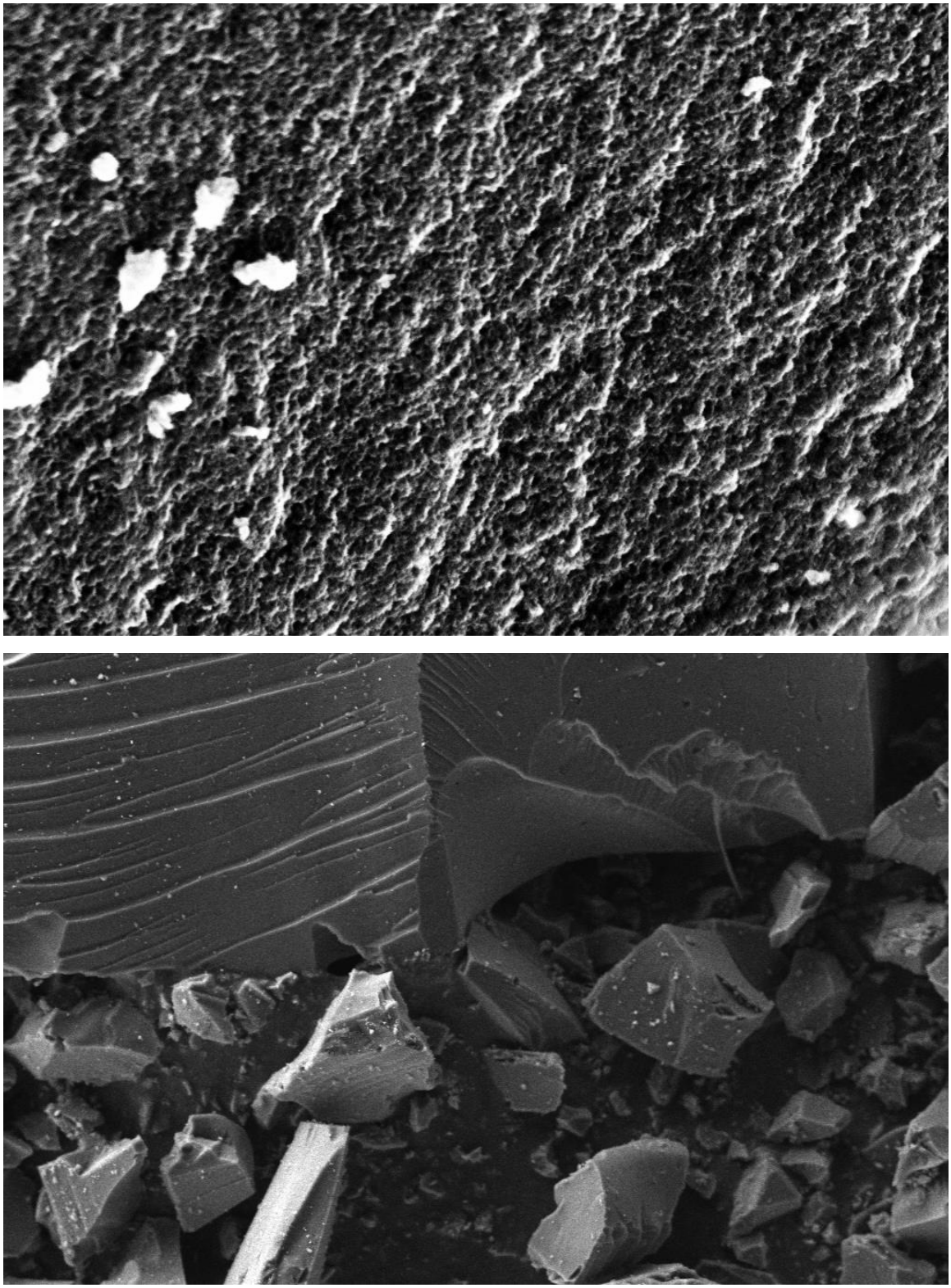

Figure 8.4 SEM image of carbon. Top), BpHIm- Beti500. Bottom), BpMIm-Beti500.

Experimental

Chemicals and materials

Imidazole (Aldrich 98%), Sodium hydride (T.C.I 60% dispersion in mineral oil), Propargyl Bromide (Sigma Aldrich 80 wt. % in toluene, contains 0.3% magnesium oxide as stabilizer), Bis(trifluoromethane)sulfonimide lithium (3M,98%), Bis(perfluoroethane)sulfonimide lithium (3M,98%).1,2-dibromoethane(Sigma Aldrich,98%), 1,3-dibromopropane (Sigma Aldrich,99%), 1,4-dibromobutane (Sigma Aldrich,98%), 1,5-dibromoheptane(Sigma Aldrich,97%), 1,6 -dibromohexane(Sigma Aldrich,96%), 1,8 -dibromooctane(Sigma Aldrich,98%), 1,10 -dibromohexane(Sigma Aldrich,97%). Deionized water were made from. All other solvents of A.C.S. grades were purchased from Fisher Scitific company without any further purification.

The ionic liquid precursor was synthesized in two steps (Scheme **8.2**)

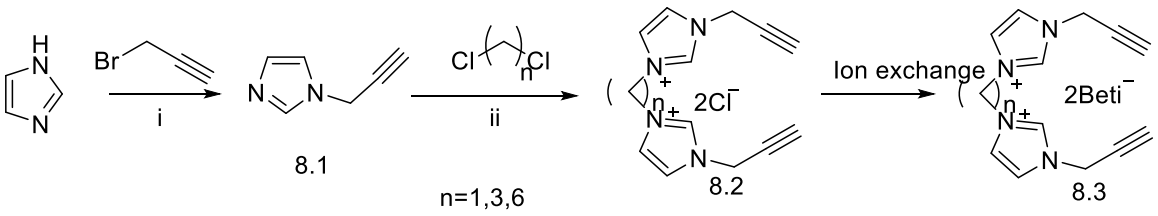

Scheme 8.8.1(i), THF, NaH, ice bath.(ii), i-propanol r.t. to reflux

*1-propargylimidazole (**8.1**)*[165]

To a 250mL three neck round flask bottle, an 8.0g (0.11 mol) of imidazole was added in 100mL anhydrous THF. Place reactor in an ice bath. 4.13g (0.12mol) of sodium hydride was added in five potions.

After done, the mixture was allowed for additional 2 hours. 14g of propargyl bromide was added *via* addition funnel, with speed not exceed 1 drop per second. After done, the ice bath was taking off, and keep stirring for additional 6 hours at room temperature. Few drops of methanol were then added to quench the reaction. Filtrate to get solvent. The solvent was washed with 10mL deionized water three times. The solvent was removed under reduced pressure. Oily Residue was stored in the dark and under the nitrogen atmosphere. (8.38g, 72%) δH (ppm) ($CDCl_3$-d_1) 7.53 (1H, s, N-C*H*-N), 6.92 (1H, s, N-C*H*-CH-N), 6.90(1H, s, N-CH-C*H*-N), 4.35 (2H, d, N-CH_2-CCH), 2.53 (1H, t, CC*H*). δC (ppm) ($CDCl_3$-d_1): 133.2 (N-*C*H-N), 132.85 (N-*C*H-CH-N), 121.43 (N-CH-*C*H-N), 79.35(CH_2-*C*C), 71.24 (s, CH_2-C*C*), 34.12 (*C*H_2).

The general procedure of bisimidazolium dibromide

1,1-bis(1-propargyl imidazolium)methane dibromide

To a 50mL three neck round flask bottle, a 1g (0.013 mol) of 1-propargyl imidazolium was added in 25mL isopropanol. 0.006mol of dihaloalkane was added in one potion. The mixture then refluxed for additional 10 hours. After finished, the solvent was removed carefully under reduced pressure. Dissolve mixture in 30mL deionized water and extract with 10mL methylene chloride three times to wash out excessive **8.1**. Water was removed under the reduced pressure, not exceed 60℃. The oily residue was yielded.

1,1-bis(1-propargyl imidazolium)methane dibromide

(2.2g, 96%) δH (ppm) (DMSO-d_6) 8.95 (2H, s, N-C*H*-N), 7.90 (2H, s, N-C*H*-CH-N), 7.83(2H, s, N-CH-C*H*-N), 7.31 (2H, s, N-CH_2-

N),4.14(4H, d, N-C*H*$_2$-CC), 3.04 (2H, t, CC*H*). δC (ppm) ($CDCl_3$-d_1): 144.2 (N-*C*H-N), 122.85 (N-*C*H-CH-N), 122.43 (N-CH-*C*H-N), 82.33(CH_2-*C*C), 74.92 (CH_2-C*C*), 60.35(N-*C*H_2-N)44.12 (N-*CH*$_2$).

1,6-bis(1-propargyl imidazolium)propane dibromide

(2.3g, 94%) δH (ppm) (DMSO-d_6) 8.89 (2H, s, N-C*H*-N), 7.93 (2H, s, N-C*H*-CH-N), 7.90(2H, s, N-CH-C*H*-N), 4.54 (4H, s, N-C*H*$_2$-CH_2-C*H*$_2$-N),4.26(4H, d, N-C*H*$_2$-CC), 3.09 (2H, t, CC*H*). 2.35 (4H, tt, N-CH_2-C*H*$_2$-CH_2-N). δC (ppm) ($CDCl_3$-d_1): 143.6 (N-*C*H-N), 123.25 (N-*C*H-CH-N), 123.56 (N-CH-*C*H-N), 81.33(CH_2-*C*C), 73.60 (CH_2-C*C*), 52.62(N-*C*H_2-CH_2-*C*H_2-N), 43.18 (N-*CH*$_2$), 30.84(N-CH_2-*C*H_2-CH_2-N).

1,3-bis(1-propargyl imidazolium)hexane dibromide

(2.4g, 90%) δH (ppm) (DMSO-d_6) 8.84 (2H, s, N-C*H*-N), 7.86 (2H, s, N-C*H*-CH-N(2.4g, 90%)), 7.81 (2H, s, N-CH-C*H*-N), 4.46 (4H, s, N-C*H*$_2$-$(CH_2)_4$-C*H*$_2$-N),4.30(4H, d, N-C*H*$_2$-CC), 3.01 (2H, t, CC*H*). 1.98 (4H, tt, N-CH_2-*CH*$_2$-CH_2-CH_2-*CH*$_2$-N), 1.18 (4H, tt, N-CH_2-CH_2-*CH*$_2$-CH_2-CH_2-N). δC (ppm) ($CDCl_3$-d_1): 143.3 (N-*C*H-N), 122.5 (N-*C*H-CH-N), 122.4 (N-CH-*C*H-N), 81.13(CH_2-*C*C), 73.92 (CH_2-C*C*), 48.35(N-C*H*$_2$-$(CH_2)_4$-C*H*$_2$-N), 41.27 (N-*CH*$_2$), 28.72(N-CH_2-*CH*$_2$-CH_2-CH_2-*CH*$_2$-CH_2-N), N-$(CH_2)_2$-(*CH*$_2$)-$(CH_2)_2$-N.

1,6-bis(1-propargyl imidazolium)octane dibromide

(2.4g, 82%) δH (ppm) (DMSO-d_6) 8.73 (2H, s, N-C*H*-N), 7.82 (2H, s, N-C*H*-CH-N), 7.76 (2H, s, N-CH-C*H*-N), 4.30(4H, d, N-C*H*$_2$-CC), 4.03 (4H, s, N-C*H*$_2$-$(CH_2)_6$-C*H*$_2$-N), 3.02 (1H, t, CC*H*), 1.93 (2H, tt, N-CH_2-*CH*$_2$-$(CH_2)_4$-CH_2-*CH*$_2$-N), 1.22 (8H, m, N-CH_2-CH_2-(*CH*$_2$)$_4$-CH_2-CH_2-N). δC (ppm) ($CDCl_3$-d_1): 142.8 (N-*C*H-N), 123.1 (N-*C*H-CH-N), 122.8 (N-CH-*C*H-N), 81.06(CH_2-*C*C), 73.4 (CH_2-C*C*), 48.20(N-C*H*$_2$-$(CH_2)_6$-C*H*$_2$-

N), 41.17 (N-*CH*$_2$), 28.72(N-CH$_2$-*CH*$_2$-(CH$_2$)$_4$-*CH*$_2$-CH$_2$-N), 26.76 N-(CH$_2$)$_2$-*CH*$_2$-CH$_2$-CH$_2$-*CH*$_2$-(CH$_2$)$_2$-N, 25.89 (N-(CH$_2$)$_2$-CH$_2$-*CH*$_2$-*CH*$_2$-CH$_2$-(CH$_2$)$_2$-N).

Ion exchange

Completely dissolve 1g of ionic liquid in 20mL deionized water. To a 45mL centrifuge tube contain 20mL deionized water, add 2g of Bis(trifluoromethane)sulfonimide Lithium, (3g for Bis-(perfluoroethane)sulfonimide) Lithium. Mixture two solutions and shake well. Centrifuge to get the bottom layer and washed twice with 10mL deionized water. Clear liquid with moderate mobility was achieved.

Carbonization of TSILs was carried out in a nitrogen protected atmosphere (100mL min^{-1}). A 0.5 g of ionic liquid was put into a porcelain crucible, calcined in a horizontal alumina tube furnace. In a constant heating rate (10℃ min^{-1}), the sample was heated to 500℃ and 800℃, and stay for an additional 2 hours.

In a typical surface measurement test, approximately 40 mg of materials were loaded into a quartz tube and degassed in flowing N_2 at 150℃ for 2 h without a transfer of container before gas adsorption measurement.

Nitrogen adsorption isotherms were recorded on a Micromeritics TriStar analyzer at 77K (Liquid Nitrogen). The specific surface areas were calculated using the Brunauer– Emmett–Teller (BET) method from the nitrogen adsorption data in the relative range (p/p_0) of 0.06–0.20. External surface areas and micropore contents were calculated

from an S-plots and using a standard adsorption isotherm for a non-graphitized Cabot BP 280, a non-graphitized carbon black, as the reference. CO_2 and N_2 adsorption were measured at 298K and 273K using an Intelligent Gravimetric Analyzer (Hiden Analytical Limited, UK)

Summary

In this work, we investigated the behavior of triple bonds under thermal treatment. Triple bonds underwent a polymerization process in a similar way as nitrile groups. Propargylic ionic liquids had a lower content of nitrogen than nitrile ionic liquids. However, it exhibited a better CO_2 capacity. This revealed that pore architectures played an important role in the CO_2 capture. The surface area of carbon materials greatly depends on the selection of anions and pyrolysis temperature. Ionic liquids bearing Beti anion produced carbon with the higher surface area than those bearing TSFI, and chloride ionic liquid yielded carbon with no surface area. In addition, the fraction of micropores is disproportional to the length of carbon bridge.

Abbreviates

TSILs Task-specific ionic liquid

DMSO Dimethyl sulfoxide

SEM Scanning electron microscope

TGA Thermogravimetric analysis

References

146. G. T. Rochelle, *Science*, 2009, **325**, 1652-1654.
147. X. Wang, J. S. Lee, Q. Zhu, J. Liu, Y. Wang and S. Dai, *Chemistry of Materials*, 2010, **22**, 2178-2180.
148. E. Frackowiak and F. Béguin, *Carbon*, 2001, **39**, 937-950.
149. S. M. Mahurin, J. S. Lee, X. Wang and S. Dai, *Journal of Membrane Science*, 2011, **368**, 41-47.
150. R. Ryoo, S. H. Joo, M. Kruk and M. Jaroniec, *Advanced Materials*, 2001, **13**, 677-681.
151. R. Ryoo, S. H. Joo and S. Jun, *The Journal of Physical Chemistry B*, 1999, **103**, 7743-7746.
152. M. Li and J. Xue, *The Journal of Physical Chemistry C*, 2014, **118**, 2507-2517.
153. P. Kuhn, A. Forget, D. Su, A. Thomas and M. Antonietti, *Journal of the American Chemical Society*, 2008, **130**, 13333-13337.
154. K. Huang, S.-H. Chai, R. T. Mayes, G. M. Veith, K. L. Browning, M. A. Sakwa-Novak, M. E. Potter, C. W. Jones, Y.-T. Wu and S. Dai, *Chemical Communications*, 2015, **51**, 17261-17264.
155. J. S. Wilkes, *Green Chemistry*, 2002, **4**, 73-80.
156. J. H. Davis Jr, *Chemistry Letters*, 2004, **33**, 1072-1077.
157. X. Zhu, P. C. Hillesheim, S. M. Mahurin, C. Wang, C. Tian, S. Brown, H. Luo, G. M. Veith, K. S. Han, E. W. Hagaman, H. Liu and S. Dai, *ChemSusChem*, 2012, **5**, 1912-1917.
158. J. S. Lee, X. Wang, H. Luo, G. A. Baker and S. Dai, *Journal of the American Chemical Society*, 2009, **131**, 4596-4597.
159. S. M. Mahurin, P. F. Fulvio, P. C. Hillesheim, K. M. Nelson, G. M. Veith and S. Dai, *ChemSusChem*, 2014, **7**, 3284-3289.
160. T. Shirasaki, A. Derré, M. Ménétrier, A. Tressaud and S. Flandrois, *Carbon*, 2000, **38**, 1461-1467.
161. W. Yang, X. Yue, X. Liu, J. Zhai and J. Jia, *Nanoscale*, 2015, **7**, 11956-11961.
162. M. C. R. Bertholet, *Held. Seances Acad. Sci.* , 1866.
163. J. Yang and J. G. Verkade, *Journal of the American Chemical Society*, 1998, **120**, 6834-6835.
164. S. L. Buchwald and R. B. Nielsen, *Journal of the American Chemical Society*, 1989, **111**, 2870-2874.
165. J. S. Lee, X. Wang, H. Luo and S. Dai, *Advanced Materials*, 2010, **22**, 1004-1007.
166. J. Warnan, Y. Pellegrin, E. Blart and F. Odobel, *Chemical Communications*, 2012, **48**, 675-677.

Chapter 9 Linear Crystalline Porous Organic Polymer

Abstract

In this chapter, an unprecedented porous polymer was found with the properties of both linearity and crystallinity, and surface area is up to 268 m^2/g. Solubility can be tuned by adjusting solvent amount during reactions. Meanwhile, the molecular weight was tunable. The soluble polymers were obtained in the diluted solvent yielding a soluble polymer with surface areas up to 98.08 m^2/g. An important application of PIMs is the usage as membrane precursor. However, this soluble polymer was unable to be cast as a membrane. The crystal structure of the polymer was unable to be obtained and measured by the SCXRD directly. Herein, the single crystal of model molecule was grown, and a possible structure was proposed.

Introduction

Porous organic polymers (POPs) such as covalent organic frameworks (COFs)[109, 166, 167] and polymers of intrinsic microporosity (PIMs)[168] are of great importance in gas storage[169-171], separation[172], adsorption[173] and heterogeneous catalysis[174, 175]. In the past decades, massive efforts have been devoted to the study of PIMs.

The microporous materials, with pore sizes below 2nm, are believed to have promising properties toward gas capture or separation. Microporous materials can be classified as inorganic materials (e.g., zeolites[176, 177], silicas[178], and carbon[179-181]) or organic-inorganic hybridized materials (e.g., Yaghi's metal organic frameworks[182, 183]), or pure organic materials (e.g., covalent organic frameworks[167], polymers of intrinsic microporosity[168]).

Uniform micropore is desirable for separation of some specific chemicals[184] or heterogeneous catalyzed reactions, which can be found in covalent organic frameworks. The preparation of ordered microporous materials can be achieved by assembling organic building blocks via metal-ligands[182], hydrogen-bonds[185], and covalent bonds[166]. However, more techniques and time are required for the synthesis of ordered microporous materials. However, uniform micropores are not always necessary for all applications. Polymers of intrinsic microporosity as emerging microporous materials which fit those applications, which only requires micropores.

PIMs are linear polymers with relatively rigid backbones compared with the covalent organic frameworks. Unlike conventional linear polymers, its contorted structure plays a crucial role in pore architectures. Therefore, PIMs cannot crystallize as regular linear polymers. For most PIMs, pore sizes range from 0.2-1nm.[186] The distribution of micropore can be analyzed by Horvath-Kawazoe (HK)[187] method in very low pressure of nitrogen adsorption area.

To prevent the collapse of micropores without the support of solvent, linking groups with no significant freedom of rotation are required[168]. The reason can be ascribed to the freedom of rotation, which has a significant impact on pore structure.

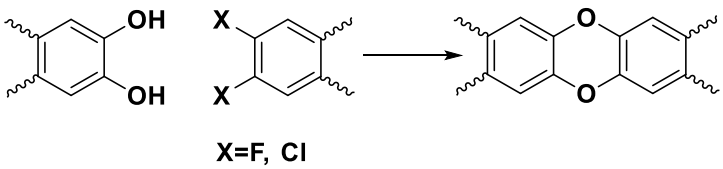

Scheme 9.1 Dibenzodioxane condensation

Dibenzodioxane condensation[188] (Scheme **9.1**) is the most common reaction to connect two building blocks (e.g., the reaction between orth-dihalo and catechol). The reaction forms a 6-membered ring that is rigid and non-rotatable. Imide and amide formation is another two methods for connecting building blocks. Amides have relatively higher freedom of rotation than imides, which explains the corresponding lower surface area for amides[189] (156m^2/g) than imides[190] (470-683 m^2/g)(Scheme **9.2**). However, imine formation method has not drawn any attention so far, which is wildly used in making covalent organic frameworks (COFs).

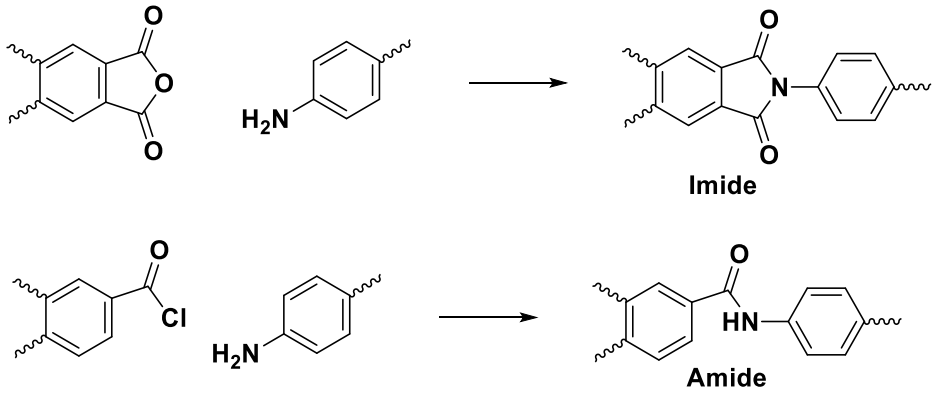

Scheme 9.2 Amide condensation and imide condensation in synthesizing PIMs.

Crystallinity was found in many linear polymers. The crystallinity has dramatically changed physical properties of polymers in terms of strength and toughness[191]. A few chains can be stacked together in an area by an approximate parallel orientation[192]. Small crystalline areas are randomly distributed in the solid and surrounded by the amorphous region. With the development of electron microscopy, recent studies showed polymers by folding chains to form a lamellar structure.

For the most crystalline polymers, its soft backbone results in the highly efficient stacking of chain, which corresponds to the nonporous structures. For non-crystalline polymers, void space is termed as free volume, which is typically less than 2.5% in the glassy state by the Williams–Landel–Ferry (WLF) equation[193] and has no significant contribution to the surface area.

In this work, we present a new synthetic route in which monomers are polymerized by imine condensation (Scheme **9.3**). Also, the property of crystallinity was discovered in this polymer.

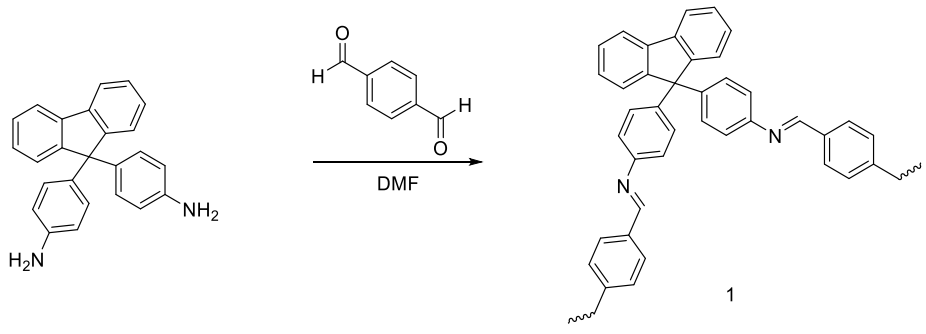

Scheme 9.3 Synthetic route for the polymer.

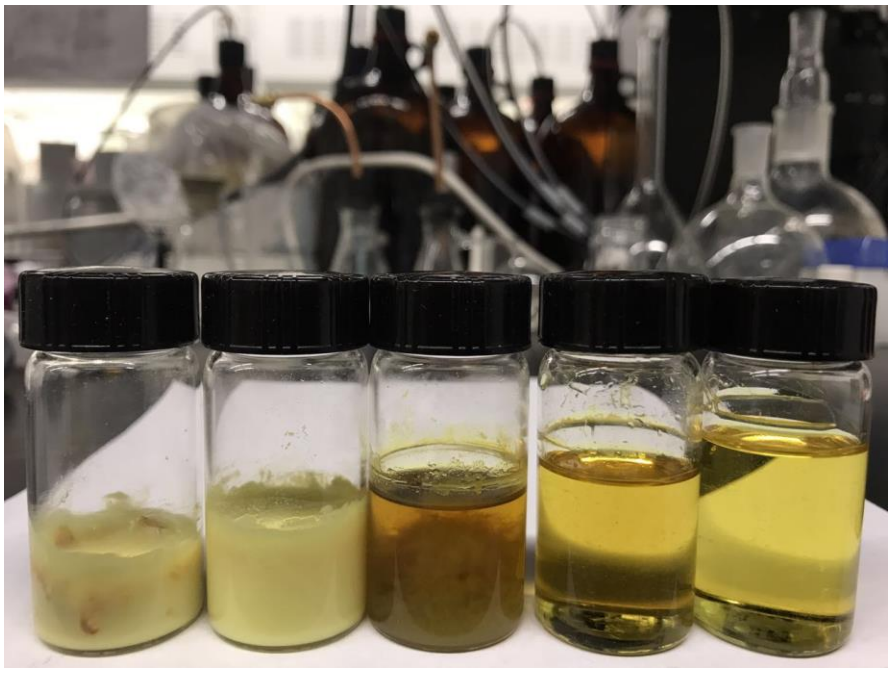

Figure 9.1 Polymerization occurred in DMF solvent (1mmol 4,4'-(9-fluorenylidene)dianiline with 1mmol terephthalaldehyde per trial)

Results and discussion

Results showed soluble polymer was produced only when the solvent amount is over 8mL (Figure **9.1**). For those soluble samples, we poured reaction mixture into 100mL methanol with stirring vigorously; then solids were collected by a centrifuge separation process. Those polymers exhibit great solubility in polar aprotic solvents such as DMF, DCM, THF. Besides, the surface area of these soluble polymers is disproportionate to the molecular weight (Table 9.1).

Measured surface areas of these polymers ranged from 10 to 268 m^2/g. However, the way polymer precipitates out is another factor, which greatly affects its surface area.

Table 9.1 Surface area of Polymer.

Entry	Solvent	Surface area	Mn	Mw/Mn	Solubility
1	DMF/3mL	197.75	N/A	N/A	No
2	DMF/5mL	110.25	N/A	N/A	No
3	DMF/8mL	268.08	N/A	N/A	No
4	DMF/8mL	98.08	1174	2.63	Yes
5	DMF/10mL	62.26	1242	2.66	Yes
6	DMF/12mL	11.81	1540	2.76	Yes

When compared with adding methanol into polymer solutions, pouring polymer solution into enough methanol will achieve solid with the higher surface area as to what we want. The degree of polymerization alone with the chaosity of the stack of polymer chains determines the surface area. Thermal analysis of each polymer shows no melting point and glass transition point below decomposition temperature which is 450℃.

Correspondingly, a small peak in liquid ^{1}H-NMR (Figure **9.2**) of the soluble polymer, at 10ppm, is attributed to residual aldehyde hydrogen. The imine hydrogen has a peak in 8.5ppm. All others are aromatic protons.

An IR spectrum showed only a weak C=O stretch absorption in the polymer at 1701cm^{-1}, which was much stronger in terephthalaldehyde (Figure **9.4**), and the appearance of imine C=N stretch absorption was at 1620cm^{-1}. Interestingly, the powder X-ray diffraction was supposed to have no peaks, because structures for all PIMs and POPs, which COFs were excluded, were disordered. However, powder X-ray diffraction analysis of the insoluble polymers showed several strong peaks, which confirmed its good crystallinity. All polymers have been washed with THF in the Soxhlet extractor overnight, and XRD pattern showed a significant difference from starting materials (Figure **9.3**). showed needle-like crystal polymer (Figure **9.5**).

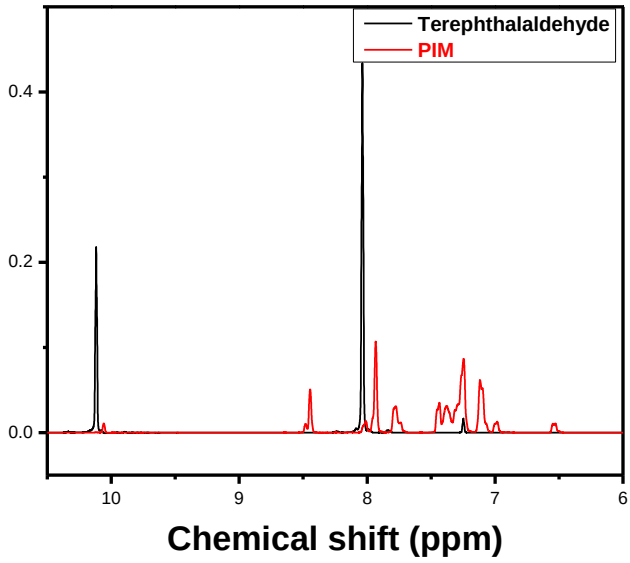

Figure 9.2 ^{1}H-NMR of the soluble polymer and terephthalaldehyde

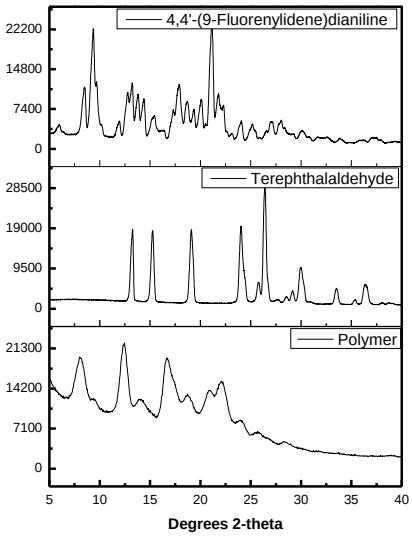

Figure 9.3 XRD pattern of starting materials and non-soluble polymer.

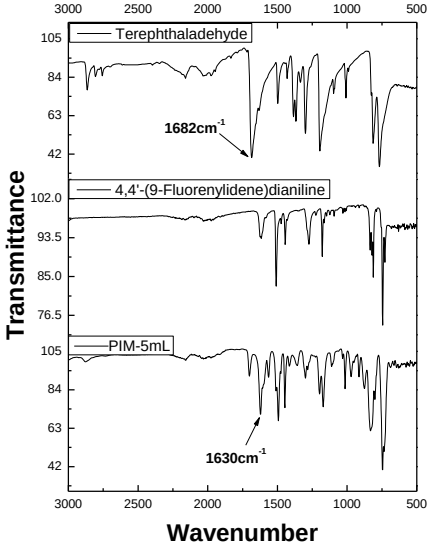

Figure 9.4 FTIR of starting materials and polymer

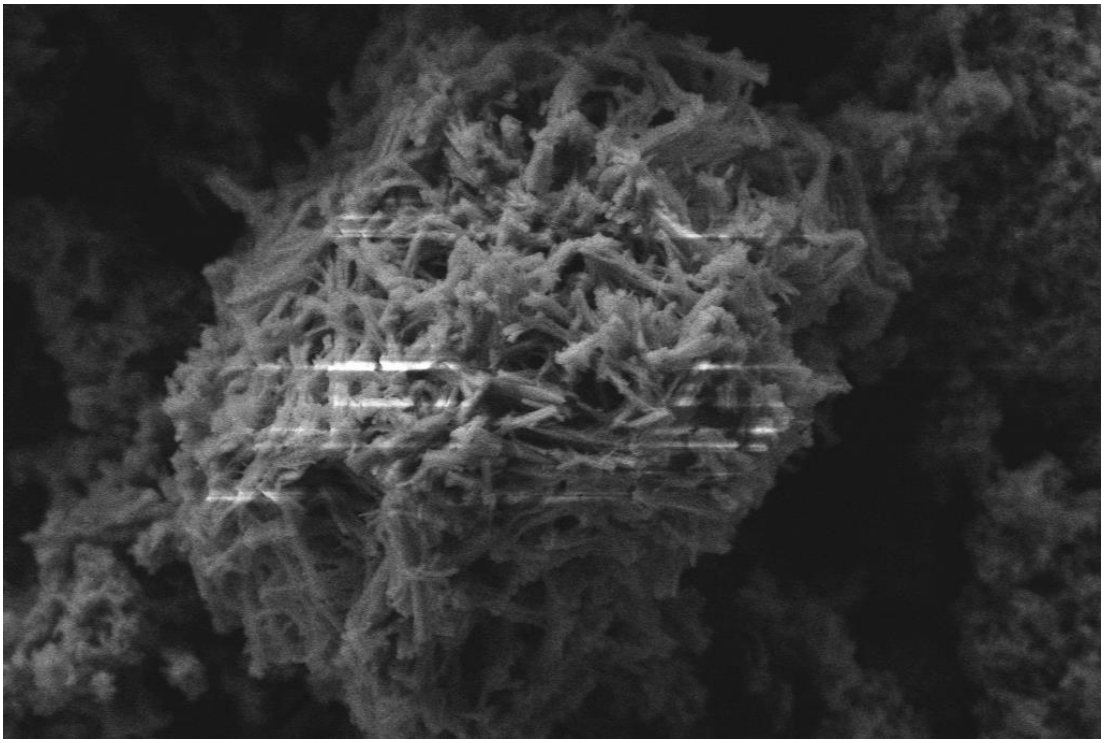

Figure 9.5 SEM of the polymer

Future work

We were unable to get a single crystal of this polymer, the single crystal structure of model molecule helps in mimicking polymer structure. In this case, model molecular was synthesized (Scheme **9.4**). The next step is to use the single crystal structure (Figure **9.6**) to match XRD pattern, which is beyond our knowledge.

Experimental

Chemicals and reagents

4,4'-(9-Fluorenylidene)dianiline (98%, Sigma Aldrich), Terephthalaldehyde(98%, Alfa Aesar), benzaldehyde(99%, Sigma Aldrich). All other solvents of A.C.S. grades were purchased from Fisher Scientific company without any further purification.

Based on the condensation of an aromatic amine and aromatic aldehyde, polymers with various molecular weight was synthesized. The molecule scaffold is derived from the condensation of 4,4'-(9-Fluorenylidene)dianiline and terephthalaldehyde

Synthesis of polyimine

The reaction was carried out in a mild condition, to investigate the effect of solvent, parallel experiments were carried out by adjusting the amount of solvent. 3mL, 5mL, 8mL, 10mL, 12mL of DMF have been applied to test the effect of the solvent amount on the degree of polymerization.

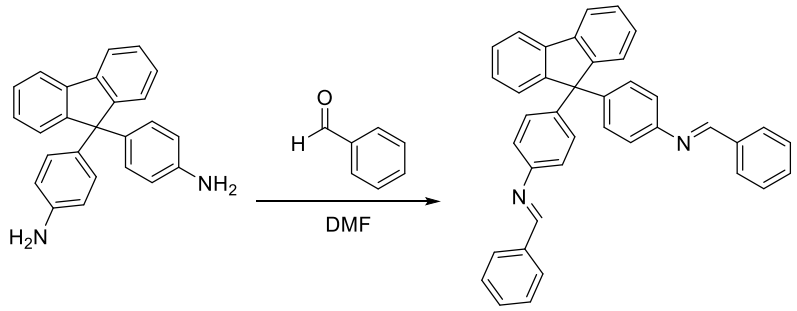

Scheme 9.4 Synthetic route for model molecular.

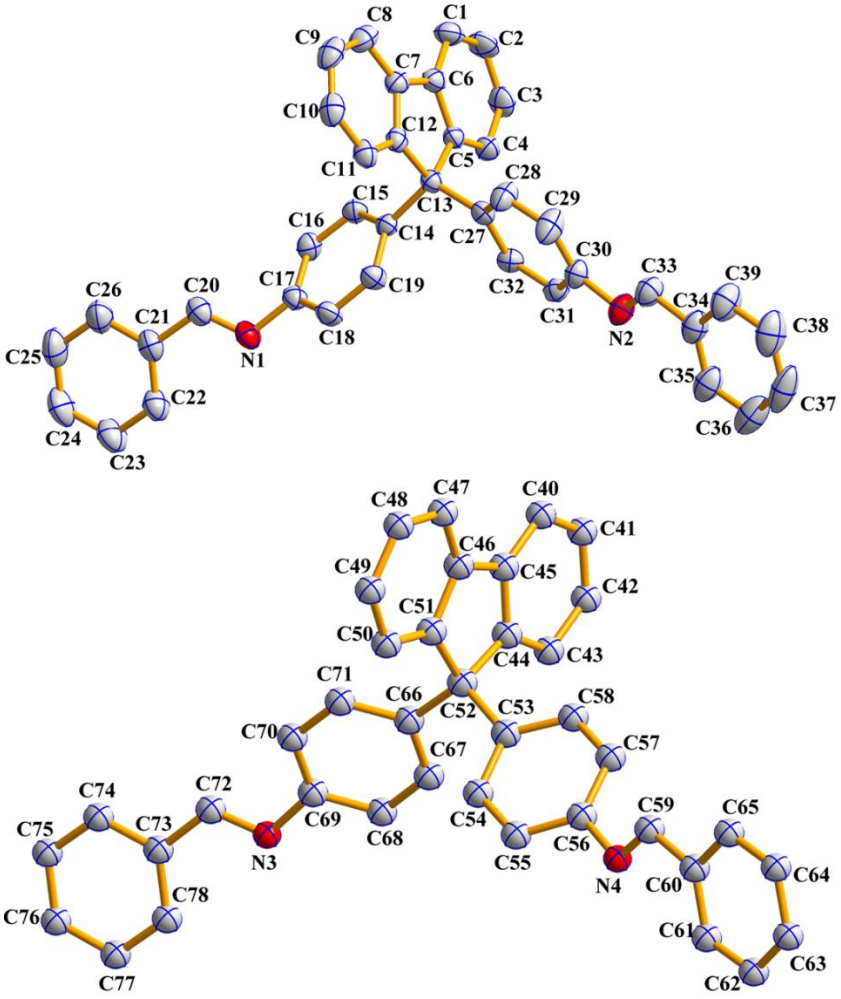

Figure 9.6 Single crystal structure of the model molecule.

To 5 labeled vials with full capacity of 20mL, add 0.348g (0.001mol) of 4,4'-(9-fluorenylidene)dianiline and 0.134g of terephthalaldehyde add 3mL, 5mL, 8 mL,10mL,15mL DMF separately. Afterward, raise the temperature to 60℃ and keep stirring for 6 hours. Then raise the temperature to 120℃, stirring for three days. After done, the yellow mixture in 3mL and 5mL vial was washed with THF in Soxhlet extractor overnight to wash out unreacted starting materials and oligomers. Solid was then dried in the vacuum oven prior to use. (0.34g, 70% from 3mL vial. 0.27g, 49% in 5mL vial)

A moderated amount of solid appears in the 8mL vial (0.09g, 18%). Solid has filtrated away. The solvent was carefully added to 25mL of ethanol. Fluffy solid was obtained by washing three times with ethanol (0.35g, 73%). No solid was found in 10mL and 12mL. Fluffy solid was obtained by pouring solution into 25mL ethanol. (0. 43g, 89% in 10mL vial. 0. 39g, 81% in 12mL vial)

In a typical experiment, approximately 40 mg of materials were loaded into a quartz tube and degassed in flowing N_2 at 80℃ for 2 h without a transfer of container prior to gas adsorption measurement.

Nitrogen adsorption isotherms were recorded on a Micromeritics TriStar analyzer at 77K (Liquid Nitrogen). The specific surface areas were calculated using the Brunauer– Emmett–Teller (BET) method from the nitrogen adsorption data in the relative range (p/p_0) of 0.06–0.20. External surface areas and micropore contents were calculated from an S-plots and using a standard adsorption isotherm for a non-graphitized Cabot BP 280, a non-graphitized carbon black, as a reference.[194]

Summary

In this work, soluble polyimides were synthesized in different solvent conditions. This offered the possibility that imine condensation method can be employed as a strategy in the synthesis of PIMs. The terephthalaldehyde and 4,4'-(9-fluorenylidene)dianiline were used as building blocks. The molecular weight of polymers was low, which can be ascribed to the presence of water. In addition, by changing solvent volumes, insoluble polymers were produced. These insoluble polymers were found to have good crystallinity, which has never been found in other porous linear polymers. The determination of crystalline structure is in progress starting from the designed model compound.

Abbreviates

BET Brunauer– Emmett–Teller

COFs Covalent organic frameworks

DCM Dichloromethane

DMF Dimethylformamide

PIMs Polymers of intrinsic microporosity

POPs Porous organic polymers

SCXRD Single Crystal X-ray Diffraction

PXRD Power X-ray Diffraction

References

168. X. Feng, X. Ding and D. Jiang, *Chemical Society Reviews*, 2012, **41**, 6010-6022.
169. A. P. Cote, A. I. Benin, N. W. Ockwig, M. O'keeffe, A. J. Matzger and O. M. Yaghi, *Science*, 2005, **310**, 1166-1170.
170. N. B. McKeown and P. M. Budd, *Chemical Society Reviews*, 2006, **35**, 675-683.
171. A. Modak, M. Nandi, J. Mondal and A. Bhaumik, *Chemical Communications*, 2012, **48**, 248-250.
172. W.-C. Song, X.-K. Xu, Q. Chen, Z.-Z. Zhuang and X.-H. Bu, *Polymer Chemistry*, 2013, **4**, 4690-4696.
173. D. Yuan, W. Lu, D. Zhao and H. C. Zhou, *Advanced Materials*, 2011, **23**, 3723-3725.
174. J. S. Seo, D. Whang, H. Lee, S. Im Jun, J. Oh, Y. J. Jeon and K. Kim, *Nature*, 2000, **404**, 982.
175. R. Dawson, E. Stöckel, J. R. Holst, D. J. Adams and A. I. Cooper, *Energy & Environmental Science*, 2011, **4**, 4239-4245.
176. Y. Zhang and S. N. Riduan, *Chemical Society Reviews*, 2012, **41**, 2083-2094.
177. A. M. Shultz, O. K. Farha, J. T. Hupp and S. T. Nguyen, *Chemical Science*, 2011, **2**, 686-689.
178. D. W. Breck, *Zeolite molecular sieves: structure, chemistry and use*, Krieger, 1984.
179. C. Baerlocher, L. B. McCusker and D. H. Olson, *Atlas of zeolite framework types*, Elsevier, 2007.
180. O. Velev, T. Jede, R. Lobo and A. Lenhoff, *Nature*, 1997, **389**, 447.
181. C. Liang, K. Hong, G. A. Guiochon, J. W. Mays and S. Dai, *Angewandte Chemie International Edition*, 2004, **43**, 5785-5789.
182. Y. Zhai, Y. Dou, D. Zhao, P. F. Fulvio, R. T. Mayes and S. Dai, *Advanced Materials*, 2011, **23**, 4828-4850.
183. C. Liang and S. Dai, *Journal of the American Chemical Society*, 2006, **128**, 5316-5317.
184. S. S. Kaye, A. Dailly, O. M. Yaghi and J. R. Long, *Journal of the American Chemical Society*, 2007, **129**, 14176-14177.
185. J. R. Long and O. M. Yaghi, *Chemical Society Reviews*, 2009, **38**, 1213-1214.
186. G. Li and Z. Wang, *Macromolecules*, 2013, **46**, 3058-3066.
187. S. Kandambeth, D. B. Shinde, M. K. Panda, B. Lukose, T. Heine and R. Banerjee, *Angewandte Chemie*, 2013, **125**, 13290-13294.
188. K. S. W. Sing and F. Schüth, in *Handbook of Porous Solids*, Wiley-VCH Verlag GmbH, 2008, DOI: 10.1002/9783527618286.ch2, pp. 24-33.
189. G. Horvarth and K. Kawazoe, *J. Chem. Eng. Jpn*, 1983, **16**, 470-475.

190. P. M. Budd, N. B. McKeown, B. S. Ghanem, K. J. Msayib, D. Fritsch, L. Starannikova, N. Belov, O. Sanfirova, Y. Yampolskii and V. Shantarovich, *Journal of Membrane Science*, 2008, **325**, 851-860.
191. J. Weber, Q. Su, M. Antonietti and A. Thomas, *Macromolecular Rapid Communications*, 2007, **28**, 1871-1876.
192. B. S. Ghanem, N. B. McKeown, P. M. Budd, N. M. Al-Harbi, D. Fritsch, K. Heinrich, L. Starannikova, A. Tokarev and Y. Yampolskii, *Macromolecules*, 2009, **42**, 7881-7888.
194. A. Galeski, *Progress in Polymer Science*, 2003, **28**, 1643-1699.
195. S. Kavesh and J. M. Schultz, *Polymer Engineering & Science*, 1969, **9**, 452-460.
196. M. L. Williams, R. F. Landel and J. D. Ferry, *Journal of the American Chemical Society*, 1955, **77**, 3701-3707.

Chapter 10 Conclusions

In summary, this dissertation focuses on the design and synthesis of functionalized ionic liquids for CO_2 capture, catalysis, and as precursors for porous materials.

α-Oximehydrazone functionalized ionic liquid

In this work, we demonstrated a synthetic route for α-oximehydrazone zwitterion-type ionic liquid with an overall yield up to 86%. An equimolar CO_2 capture was achieved. A possible conjugation effect caused a thermal decomposition of this ionic liquid at 80℃. However, the success of this ionic liquid in capturing CO_2 proved the possibility that the existence of a nine-members-ring structure in the IL-CO_2 adduct. A single crystal structure of the ILs-CO_2 adduct is needed in the future work because the structure will give solid evidence to prove the member-ring mediated mechanism. This mechanism has a profound meaning in designing ionic liquids for equimolar CO_2 capture.

Guanidine tethered ionic liquids

In this work, guanidine functionalized ionic liquids were successfully synthesized. The synthesis of these ionic liquids was attempted in three ways. It is clear that guanidine-imidazole intermediate molecules were unable to be purified through conventional purification methods. The most effective way is to start from haloalkyl amine, by reacting with the Vilsmeier's reagent to form a haloalkyl guanidine intermediate compound. Although the guanidine functionalized ionic liquids were unable to capture CO_2, the synthetic method of this ionic liquid is

important. The applications of guanidine ionic liquids are useful in the extraction of metals such as gold(III),[195] and copper(II).[196] Once guanidine and the ionic liquid was combined in one molecule, it can realize the biphase extraction of metal ions. So, in the future, synthetic routes of multi-substituted guanidine ionic liquids need to be investigated.

Amidine functionalized ionic liquids

In this work, an amidine functionalized ionic liquid was successfully synthesized through a basic strategy. The synthesis of this ionic liquid was complete by a modified Pinner reaction. It turned out the basic strategy, by utilizing sodium methoxide and ethylenediamine was an effective way of synthesizing this ionic liquid. The ammonia was used and turned out no reactions because of the weak nucleophilicity. An acidic strategy was also tried by utilizing *tert*-butanol as a reagent and was failed in the size effect caused by the *tert*-butyl group. The amidine ionic liquid was obtained with good purity. However, this ionic liquid cannot capture CO_2. Similar to guanidines, amidines can chelate with even more metal ions such as Nb(IV),[197] Au(III),[198] Bi(III),[199] Tl(III).[200] In the future, to synthesize symmetric or asymmetric amidines with a various substituent group, other amines need to be tested.

Ultra-pure ionic liquid as electrolyte

In this work, a novel graphitization process was illustrated for the preparation of flake graphite. In this process, the long-range rearrangement of carbon atoms was observed. The oxygen atoms at the surface of carbon greatly affect the graphitization yield. Compared

to another graphitization method, this method is more versatile, the graphitization of activated carbons, carbon fibers, and graphitizable cokes have been tested. The graphite derived from this method showed a much better rate capability than commercial graphite. In addition, an ultra-pure ionic liquid -(N-butyl-N-methylpyrrolidinium bis-trifluoromethanesulfonylimide) was synthesized and purified in a bi-solvent system, and all tests were conducted in this ionic liquid. It has an electro-window up to 5.5V, and the high-purity quality enabled the observation of any subtle changes such as the oxygen effect.

Heterogenous viologen catalysts for metal-free and selective oxidations.

In this work, a metal-free ionic catalyst was introduced to have high activities in selectively oxidizing thioanisoles and benzyl alcohols to sulfoxides and benzaldehydes, respectively. In addition, activity moieties were polymerized together, which enabled it to work in a heterogeneous style. Abundant viologen moieties embedded in the solid backbone was the essential point of PIN-1, which was determined through activity tests by testing all possible moieties. However, it suffered from a fast-decay of the activity, which might be caused by the collapse of the congested structure. The investigation of the decrease in activities will be future extended work.

Mesoporous carbon derived from propargylic ionic liquids

In this work, the behavior of triple bonds under thermal treatment was investigated. Similarly, as nitrile groups, triple bonds underwent an oligomerization process, then yielded porous carbon materials. Carbon materials derived from propargylic ionic liquids have a higher capacity toward CO_2 than those from nitrile ionic liquids, which revealed that the pore architecture played a critical role in capturing CO_2. The surface areas of carbon materials greatly relied on the counter ion and pyrolysis temperature. Ionic liquids bearing Beti anion produced the carbon with higher surface areas than those bearing TSFI, and the chloride ionic liquid yielded carbon with no surface area. In addition, the fraction of micropore is disproportional to the length of carbon bridge. Porous materials are important supports in the heterogeneous catalysis. Carbon materials with good stability and chemical inertness have drawn many attentions from scientists. The alkyne group chelates with many translation metals were reported. By pyrolyzing the mixture of the metal-ionic complex with the matrix of propargylic ionic liquid, porous carbon anchoring metal nanoparticles can be expected. It might be a versatile method for making porous metal-based catalysts.

Linear crystalline porous organic polymer

In this work, a new PIM was synthesized through the imine condensation, with surface areas up to 99 m^2/g. The terephthalaldehyde and 4,4'-(9-fluorenylidene)dianiline were used as building blocks. Because the high freedom of rotation of the imine

bond, the surface areas of imine-PIMs are lower than amide- and imide-PIMs. Meanwhile, the molecular weight was disproportional to the solvent amount. Once the monomer concentration is greater than 1mmol per 8 mL, insoluble polymers will be produced. These insoluble polymers with surface areas up to 288 m^2/g, and have good crystallinity, which has never been found in other porous linear polymers. This PIM was originally designed for membrane separation, but the low molecular weight made it unable to be cast as a membrane. The low molecular weight can be ascribed to the presence of water. So, in the future, a dehydrating agent will be added to exclude the hydrolysis effect.

References

197. G. A. Kordosky, J. M. Sierakoski, M. J. Virnig and P. L. Mattison, *Hydrometallurgy*, 1992, **30**, 291-305.
198. F. Xie and D. B. Dreisinger, *Transactions of Nonferrous Metals Society of China*, 2010, **20**, 1136-1140.
199. K. Patel and K. Lieser, *Analytical Chemistry*, 1986, **58**, 192-194.
200. K. Patel and K. Lieser, *Analytical Chemistry*, 1986, **58**, 1547-1551.
201. G. Alpana, P. K. Singh and M. R. Kumar, *Bulletin of the Chemical Society of Japan*, 1989, **62**, 3675-3678.
202. K. S. Patel and N. Agarwal, *International Journal of Environmental Analytical Chemistry*, 1992, **46**, 63-70.

Vita

Nanqing Chen was born in Yangzhou, China. He obtained his Bachelor of Science degree in Applied Chemistry from the Nanjing University of Technology. He joined the graduate program in Chemistry Department of University of Tennessee in August 2013 and pursued his doctoral degree in Organic Chemistry with the guidance of Dr. Sheng Dai. His major research focuses on the design and synthesizes functional ionic liquids for gas sorption.